Reduced reaction kinetics model for CO_2 dissociation in non-thermal microwave discharges

A non-equilibrium distribution averaged kinetic model for multidimensional simulations

S.H. Moreno Wandurraga

Faculty Mechanical, Maritime and Materials Engineering

TU Delft Delft University of Technology

Challenge the future

REDUCED REACTION KINETICS MODEL FOR CO_2 DISSOCIATION IN NON-THERMAL MICROWAVE DISCHARGES

A NON-EQUILIBRIUM DISTRIBUTION AVERAGED KINETIC MODEL FOR MULTIDIMENSIONAL SIMULATIONS

by

S.H. Moreno Wandurraga

in partial fulfillment of the requirements for the degree of

Master of Science
in Mechanical Engineering

at the Delft University of Technology,
Process & Energy, Faculty 3mE
Intensified Reactions & Separation Systems
November, 2015

Supervisor:	Dr. ir. G. D. Stefanidis	
Thesis committee:	Prof. dr. ir. A. I. Stankiewicz,	TU Delft
	Prof. dr. D. J. E. M. Roekaerts,	TU Delft
	Dr. ir. G. D. Stefanidis,	TU Delft

An electronic version of this thesis is available at http://repository.tudelft.nl/.

TU Delft Delft University of Technology

ABSTRACT

In the context of CO_2 utilization, the electricity surplus from renewable energies can be used in a non-thermal microwave plasma reactor to reduce CO_2 and produce chemical fuels. The chemical processes in non-thermal plasma are extremely complex due to the large number of excited species, radicals and ions that are present. Energy stored inside these energetic species can initiate reactions that in thermal chemistry are difficult to achieve. In the case of non-thermal CO_2 microwave plasma, the energy stored in the vibrational modes can effectively stimulate dissociation reactions.

Numeric models are being developed to get insights into this process and predict the performance of reactors under different conditions. However, the most recent kinetic model for CO_2 dissociation in this type of plasma is highly complex and not suitable for multidimensional simulations. It considers +100 species and +10000 reactions.

A reduced kinetic model is developed by only including dominant reactions and by grouping the asymmetric vibrationally excited states of CO_2 into a fictitious species. The kinetic model is then reduced to 44 reactions and 13 species. Its validation is done in a 2D reactor model with computation times lower than 25 minutes. The results are in good agreement with those reported in the detailed kinetic model. Furthermore, it is shown that the reduced kinetic model can be adjusted to experimental results.

Prospectives are given regarding the next steps in the development of self-consistent multidimensional models. The proposed kinetic model is intended for multidimensional simulations of non-thermal plasma reactors and facilitate the design and operation of these in industrial applications.

CONTENTS

1

INTRODUCTION

The environmental consequences of CO_2 emissions have been of common knowledge for decades as well as the long-lasting efforts to track its concentration and reduce emissions. Historically, most of the research has been done on technologies to reduce, capture and storage CO_2, whereas research on CO_2 utilization had been lagging behind, mostly because of the entanglements of breaking such a stable molecule in an energy efficient way, i.e. carbon negative or neutral process.

More recently, with the continuing growth of renewable energy sources in the electricity supply share, a new concept for CO_2 utilization is under development. In this process, electricity surplus from renewable energies can be used to obtain H_2 from water, feed it to a novel catalytic reactor to reduce CO_2 and produce chemical fuels, in such a way that CO_2 is recycled and excess electricity is stored as a fuel [1].

Different technologies have been considered for the design of such reactor and among these, non-thermal plasma stands out [2]. The characteristics of non-equilibrium plasma are particularly favorable for the dissociation and utilization of CO_2 [3, 4], and for that reason the scientific community has once again turned its attention onto it. CO_2 conversion into chemical fuels is possible through different reaction pathways [5], in which by CO_2 hydrogenation, hydrocarbons are obtained.

Chemical processes in non-thermal plasma are extremely complicated since a large number of excited species, radicals and ions are present in this type of discharges. Reactions involving these energetic species are the reason behind the potential of non-thermal plasma, as the energy stored inside the internal modes of atoms and molecules can initiate reactions that in ordinary chemical mechanisms are difficult or even impossible to achieve [6]. Overall, non-thermal plasma is a very promising technology for chemical process intensification [7]. The effectiveness of intra- and intermolecular processes is maximized and the driving forces from electron to molecule scales can be optimized.

In a non-thermal microwave discharge, the energy stored in the vibrational modes of molecules can decrease the activation energy of endothermic reactions, such as CO_2 dissociation [3]. However, the mechanism of CO_2 dissociation in non-thermal microwave discharges is still not fully understood and numeric models are being developed to get insights into the dissociation process and predict the performance of a non-thermal plasma reactor under different conditions [8].

In this regard, the PLASMANT group of the University of Antwerp developed a reaction kinetics model for CO_2 dissociation in non-thermal microwave plasma [8, 9]. This kinetic model was the first to include all the relevant processes that are involved in the CO_2 dissociation process. Its latest version considers +100 species and +10000 reactions, and besides its great level of detail, it is still a zero dimensional qualitative model. Due to its complexity its implementation in multidimensional models is prohibitive.

The aim of this work is to develop a reduced kinetic model suitable for multidimensional simulations of CO_2 dissociation in a non-thermal microwave plasma reactor. The reduced kinetic model will be used to qualitatively predict the influence of different parameters in the dissociation process. Relevant processes taking place in the discharge must be preserved in the reduced kinetic model, so that it can be implemented in future self-consistent models. Undoubtedly, these models will be of great help for the design of non-thermal microwave plasma reactors.

2

BRIEF INTRODUCTION TO PLASMA CHEMISTRY

The main plasma chemistry concepts are introduced in this chapter. Only basic and concise descriptions of these fundamentals are given, mostly related to their specific application in the work herein presented. Extensive discussions of these concepts are found elsewhere [3, 6, 10–12] and the reader is referred to these for further details.

2.1. BASIC DEFINITIONS

Plasma is an ionized gas, usually regarded as the fourth state of the matter. As temperature increases, the molecules and atoms in a solid state matter gain energy, increasing their vibration and movement until eventually the transition to the liquid phase takes place. If temperature is further increased, the transition to the gas phase and ultimately to the plasma phase takes place.

In a plasma, molecules dissociate into atoms and radicals, and the electrons of atoms and molecules loose their bonds, forming ions in the process. Hence, a plasma is a mixture of neutrals, ions and electrons moving randomly. It is electrically neutral or quasi-neutral, but its electrical properties are affected by the large number of charged particles [6].

A plasma can be produced in a gas by applying a constant or oscillating electric field. This must be sufficiently high to generate the electric breakdown and produce an electron avalanche. Thus, in these gas discharges, the plasma initiates when an unbounded electron gain enough energy from the electric field to produce additional electrons by collision processes, see Figure 2.1. The plasma is sustained as long as additional electrons are produced to replace those that diffuse to the walls or are lost in collisions. When the plasma cease to exists, recombination processes take place and the gas phase is obtained again.

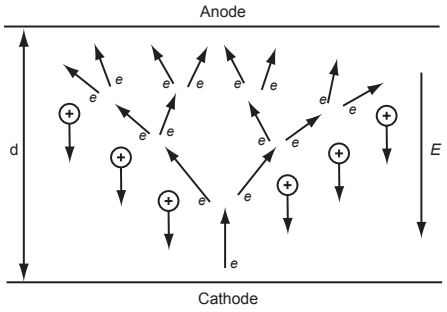

Figure 2.1: Electron avalanche in a gap. Taken from [3].

.

Plasma can be found in nature, for instance lightning, aurora borealis, solar corona and solar wind occur spontaneously in nature. There are also artificial plasmas, so-called gas discharges and are used for different applications, such as artificial lightning, fabrication of microelectronics, ozone production, wounds treatment, plasma televisions and materials treatment and processing, among others [6].

The most common artificial plasmas are the glow discharge, corona discharge, dielectric barrier discharge, microwave discharge and the gliding arc discharge. Each of these has its own characteristics, which makes it more suitable for specific applications, being chemicals processing one the most promising applications.

In this regard, plasma has unique characteristics that make it attractive for the intensification of chemical processes. The temperatures and energy densities in a plasma can significantly exceed those of conventional chemical processing technologies, indeed, high concentrations of energetic and chemically active species are produced in a plasma. Furthermore, some discharges can be far from thermodynamic equilibrium, making possible high temperature chemistry at low temperatures [13]. In brief, these characteristics allow plasma to initiate reactions that in ordinary chemical mechanisms are difficult or even impossible to achieve [3].

Plasmas are also divided in thermal and non-thermal plasmas. The former is a quasi-equilibrium plasma in which the local thermodynamic equilibrium conditions are met. Thus, the thermal plasma is in chemical equilibrium and can be characterized by a single temperature at every point in space. The chemical processes taking place in a thermal plasma are mostly determined by this single temperature [3].

On the other hand, the non-thermal plasma, also called non-equilibrium or cold plasma, can be far from thermodynamic equilibrium. It is characterized by multiple temperatures, which are related to different species and their excited states. The chemical processes can be determined by other temperatures different than the gas temperature. For instance, electron collision reactions are determined by the electron temperature T_e.

This multiple temperature characteristic is usually presented as $T_e > T_v > T_r \approx T_i \approx T_0$, where the electron temperature T_e is the highest temperature, followed by the vibrational temperature T_v and the rotational temperature T_r. The latter is usually very close to the ions temperature T_i and the gas temperature T_g, which is also called the translational temperature and is the lowest of all temperatures [3]. To understand this concept is important to keep in mind the molecular degrees of freedom (translational, rotational, vibrational and electronic) and their energy levels, as well as the definition of temperature from the kinetic theory.

The highest temperatures reached in thermal and non-thermal plasmas are usually in the same order of magnitude, in the first case it corresponds to T_g, while in the second to T_e. Non-thermal plasmas are usually obtained at low pressures, low powers or pulsed discharges. They are also more selective, since the energy is used for obtaining a high number of excited species instead of being used in heating the bulk gas. On the other hand, thermal plasmas are more powerful and are mainly used in high temperature applications [3].

Some important variables needed for the study of plasma are the following

- Electron density, n_e [1/m^3]: Number of electrons per unit of volume, at a specific point in space.
- Electron energy density, n_ε [eV/m^3]: Energy of the electrons per unit of volume, at a specific point. It is useful to relate this value to the kinetic energy of the electrons.
- Mean electron energy, $\bar{\varepsilon}$ [eV]: Mean value of the electrons energy, at a specific point in space. It is computed from n_ε / n_e. It is also the mean value of the electron energy distribution function (EEDF).
- Electron temperature, T_e [K]: It is defined according to the kinetic theory, represents the average kinetic energy of the electrons. It is computed from $\bar{\varepsilon} * 2/3$. (1 [eV] ≈11605 [K]).
- Ionization degree [1]: Gives an indication of the fraction of neutrals that have been ionized in the discharge. It can also be seen as the number of electrons per neutrals. It is computed from n_e / n_n, where n_n is the total number density of neutral species.

Artificial plasmas of practical relevance have typical electron densities in the range between 10^6 and 10^{18} [1/cm^3] and electron temperatures in the range between 1 and 20 [eV], being mostly in the lower limit for chemical process applications, in which the ionization degrees are also in the range between 10^{-7} and 10^{-4}.

In the specific case of microwave discharges, the electron temperature is much higher than the gas temperature ($T_e >> T_g$), this means that a highly non-equilibrium plasma can be generated. In this, the energy of the electrons is transferred to the molecules by selectively exciting their vibrational modes. This energy is subsequently used in endothermic reactions, therefore, less bulk gas heating and high energy efficiencies are obtained. Microwave discharges are characterized by high electron densities $n_e \approx 10^{12-14}$ [1/cm^3], low electron temperatures $T_e \approx 1-2$ [eV] and ionization degrees around 10^{-5}, besides, they are usually generated at low pressures, between 100 and 300 [Torr] [3, 8, 14].

2.2. ELECTRON ENERGY DISTRIBUTION FUNCTION (EEDF)

The study of non-equilibrium plasma requires the consideration of the microscopic processes taking place in the discharge. Detailed descriptions of collisions between different species are needed, specially the collisions involving electrons, which are the driving force of the plasma. In this context, statistical mechanics, kinetic and scattering theories are needed to describe and understand the plasma microkinetics.

The Electron energy distribution function (EEDF) f(ε) is the probability density for an electron to have an specific energy ε [3]. This distribution function is needed for the computation of electron impact reactions rates and the transport properties of electrons in the plasma. The EEDF can be computed from the Boltzmann equation, which gives the time evolution of the electron distribution in the six-dimensional phase space ($\mathbf{r}$,$\mathbf{v}$) [10]. For electrons in the plasma the Boltzmann equation takes the following vectorial form [10, 15]

$$\frac{\partial f}{\partial t} + \mathbf{v}\cdot\nabla_{\mathbf{r}} f - \frac{e}{m}\mathbf{E}\cdot\nabla_{\mathbf{v}} f = \left.\frac{\partial f}{\partial t}\right|_c \tag{2.1}$$

Where f is the electron distribution in the six-dimensional phase space, $\mathbf{v}$ is the velocity, e is the elementary charge, m the electron mass, $\mathbf{E}$ the electric field, $\nabla_{\mathbf{r}}$ is the position-gradient operator $\partial/\partial x_i$, $\nabla_{\mathbf{v}}$ is the velocity-gradient operator $\partial/\partial u_i$ and the term on the right is the collision term, which gives the rate of change of f due to collisions. The derivation of this equation is found in [10].

No analytic solution has been found for the Boltzmann equation. The well-known two-term approximation is commonly used as the solution approach [15] and good results are expected for the reduced electric field values at which the plasma discharges are generated. The EEDF can also be computed with the Fokker-Plank equation, as discussed in [3].

For some specific cases the EEDF can be easily obtained. The most common solution is the quasi-equilibrium Maxwellian distribution. This distribution is obtained assuming that the electron-neutral collision frequency is constant and the elastic collisions dominate the electron energy losses [3]. Likewise, assuming that the electrons are in thermodynamic equilibrium among them, at the electron temperature T_e, the distribution is computed from the following expression

$$f(\varepsilon) = 2\sqrt{\frac{\varepsilon}{\pi T_e^3}}\exp\left(\frac{-\varepsilon}{T_e}\right) \tag{2.2}$$

where ε is the electron energy and T_e is the electron temperature, both in [eV]. Figure 2.2 shows the Maxwellian EEDF for different values of the electron temperature T_e. Although this distribution is based on equilibrium conditions, it can give good results for non-equilibrium discharges under certain conditions, as will be shown in Chapter 5.

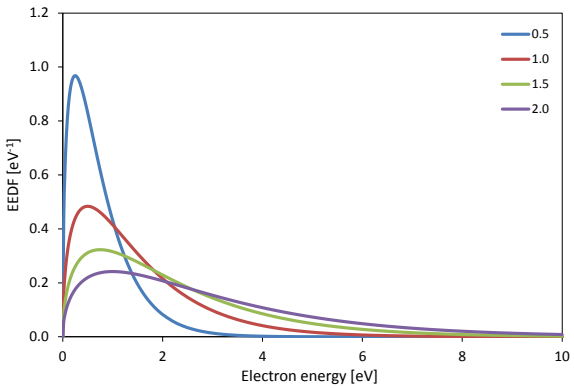

Figure 2.2: Maxwellian EEDF for selected values of the electron temperature T_e in [eV].

2.3. COLLISIONAL CROSS SECTIONS

When an electron collides with another species several processes can take place. This depends upon the collision energy (kinetic energy of the electron) and the collisional cross section data of the species. The former is given by the mean electron energy (or the electron temperature) and the EEDF.

For a collision between particles A and B, the cross section σ of an elementary reaction can be considered as the area of an imaginary circle moving together with one of the particles. If the center of the other particle enters this imaginary circle, the reaction takes place [3]. This is simplest definition of the cross section, the three dimensional form and the quantum mechanical treatment can be found in [10, 12].

The processes that take place in a collisions between an electron and a molecule are the following, which for sake of simplicity are shown for a diatomic molecule AB [12].

- Elastic scattering: $e + AB \rightarrow e + AB$
- Rotational transition: $e + AB(J) \rightarrow e + AB(J')$

  where J and J' are the initial and final rotational quantum numbers.
- Vibrational transition: $e + AB(v) \rightarrow e + AB(v')$

  where v and v' are the initial and final vibrational quantum numbers.
- Electronic excitation: $e + AB \rightarrow e + AB^*$
- Dissociation: $e + AB \rightarrow e + A + B^{(*)}$
- Ionization: $e + AB \rightarrow e + e + AB^{+(*)}$
- Dissociative ionization: $e + AB \rightarrow e + e + A + B^{+(*)}$
- Electron attachment: $e + AB \rightarrow A + B^-$ or $e + AB + M \rightarrow AB^- + M$

In these definitions, * is the short hand notation for an eletronically excited state. (*) denotes that the species can be either in the ground state or in an electronically excited state. Atomic and molecular term symbols are commonly used for specifying the electronic states, a brief description of these symbols is given in [6]. M represents an additional neutral molecule which acts as a third body in the electron attachment collision.

For a triatomic molecule, like CO_2, the collision processes are more complicated, considering the additional degrees of freedom for rotation and vibration. Moreover, the dissociation processes can give different products, i.e. AB + C, A + BC, AC + B or A + B + C, and each of these species may also be in an excited state. On the other hand, the collision processes for atoms are more simple since some processes are not present, e.g rotational and vibrational excitation and dissociation.

Each of these collision processes is characterized by a cross section, which is a function of the collision's energy. For instance, Figure 5.8 shows the cross sections for some electron collision processes with CO_2. Besides the cross sections of the aforementioned collision processes the following cross sections are also relevant [12]

- Momentum transfer cross section (also called effective cross section): Accounts for the total momentum transfer by elastic and inelastic collision processes between the same colliding particles. Useful for determining the transport coefficients for electrons.
- Emission cross section: Accounts for the excitation to an electronically excited states and its subsequent radiative transition to a lower state. It is not necessarily equal to the electronic excitation cross section.
- Total scattering cross section: Accounts for all collision processes. It is the sum of the elastic scattering cross section and the inelastic scattering cross section. The latter is the sum of the cross sections of all processes, excluding the elastic scattering.
- Stopping cross section: Accounts for the energy transferred in the collision processes. Indicates how much the incoming electron loses its energy.

The rate constant for an electron collision process is computed by integrating the product of its cross section and the EEDF. The following expression can be used [3, 16]

$$k = \gamma \int_0^\infty \varepsilon \sigma(\varepsilon) f(\varepsilon) \mathrm{d}\varepsilon \tag{2.3}$$

where ε is the electron energy, $\sigma(\varepsilon)$ is the cross section of the collision process, $f(\varepsilon)$ is the EEDF and γ is a conversion units constant. It is to be noted that the convolution of the cross section and the EEDF must be computed to obtain the rate constant of the collision process for a range of mean electron energies. Indeed, for a Maxwellian distribution it is possible to compute this convolution and fit an algebraic equation to obtain the rate constant as a function of the electron temperature. Additional information about collision processes is found in [3, 6, 12].

2.4. BOLTZMANN EQUILIBRIUM DISTRIBUTION

In thermal equilibrium conditions, the number of particles n_i in a specific quantum state with energy E_i, is proportional to $\exp(-E_i/T)$, where T is the equilibrium temperature related to the mean energy of the particles in the system [6]. Thus, with the same units for E_i and T this is written as

$$n_i \propto \exp\left(-\frac{E_i}{T}\right) \tag{2.4}$$

This relation can be derived by statistical mechanics and is called the Boltzmann distribution function. It indicates the maximum thermodynamic probability of finding a particle in the specific state (energy level) and must be corrected with the statistical weight g_i if the energy level is degenerate, i.e. multiple states with the same energy. The statistical weight or degeneracy, is the number of states with the same energy level.

The Boltzmann distribution can also be used to compute relative population densities. The following expression is easily derived and can be used for this purpose

$$n_i = n_j \frac{g_i}{g_j} \exp\left(-\frac{E_{ij}}{T}\right) \tag{2.5}$$

where n_i is the population density of the state i, g_i is the statistical weight of the state i, and E_{ij} is the energy of the state i with respect to the energy of the state j. This practical equation is mostly used with the ground state $j = 0$, although in the the detailed balancing principle is used as presented.

2.5. TREANOR NON-EQUILIBRIUM DISTRIBUTION

In thermal equilibrium conditions the population of vibrationally excited states (vibrational distribution) follow the Boltzmann distribution. On the contrary, in non-equilibrium conditions the vibrational distribution can be far from the Boltzmann distribution, with populations that usually exceed the equilibrium ones.

In some specific cases the VV relaxation is much faster than the VT relaxation and an overequilibrium population of high vibrational levels is obtained. For diatomic molecules the vibrational distribution in these cases can be computed from the Treanor distribution [18]

$$n_v = n_0 \exp\left(-\frac{vE_1}{T_v} + \frac{vE_1 - E_v}{T_g}\right) \tag{2.6}$$

where n_v is the population density and E_v the energy in [eV] of the vibrational level v. T_g and T_v are the translational and vibrational temperatures, both in [eV]. The vibrational temperature in the previous equation is based in the population density of the first vibrational level and it is computed as follows

$$T_v = \frac{E_1}{\ln(n_0/n_1)} \tag{2.7}$$

In non-equilibrium conditions the vibrational temperature can significantly exceed the translational temperature. This is a consequence of an overequilibirum population of the first vibrational level n_1 due to high vibrational excitation rates. In equilibrium conditions n_1 is computed from the Boltzmann distribution, thus, $T_v = T_g$. See Figure 2.3 for a comparison of the Treanor and Boltzmann distributions.

The Treanor distribution is derived by neglecting the VT relaxation and only considering VV relaxation, which is only valid for low vibrational levels. High populations are obtained for high vibrational levels as a consequence of the anharmonicity of the energy levels. The energy difference for consecutive energy levels reduces as the levels increase, therefore, the energy is more easily transferred from lower vibrational levels to higher vibrational levels. If the molecules are considered harmonic oscillators the energy levels are equally spaced and the Treanor distribution reduces to the Boltzmann distribution (even if $T_v > T_g$) [6].

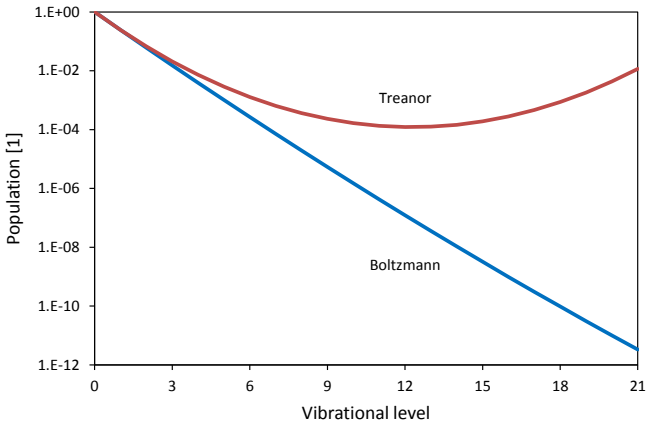

Figure 2.3: Comparison of the Treanor non-equilibrium distribution and the Boltzmann equilibrium distribution.

The vibrational energy is stored in high vibrational levels as a consequence of the Treanor distribution. High efficiencies and reaction rates are obtained when this energy is used in endothermic reactions. However, the Treanor distribution is a theoretical approximation and the unlimited growth predicted for the populations of high vibrational levels is not physically realistic. At high vibrational levels the VT relaxation rate is high enough to produce a decline in the vibrational distribution [6].

3

CO_2 DISSOCIATION IN NON-THERMAL MICROWAVE DISCHARGES

3.1. CURRENT STATE OF THE TECHNOLOGY

The CO_2 dissociation in moderate pressure non-thermal microwave discharges was intensively studied nearly 40 years ago. At that time, the highest energy efficiencies for CO_2 dissociation in this type of discharges were experimentally obtained. For subsonic flow, a maximum energy efficiency of 80% was attained, while for supersonic flow the energy efficiency reached 90%. In both cases the CO_2 conversion ranged between ~10% and ~20% [3]. The importance of vibrational excitation for obtaining high energy efficiencies in the dissociation process was also known at that time [19]. More recently, different configurations, conditions and gas mixtures were investigated [14, 20–25]. The highest energy efficiency was reported to be around 45%, with a CO_2 conversion around 25%.

The renewed interest in developing this technology is due to the possibility of using electricity surplus from renewable sources to power a novel reactor and utilize the CO_2 in a carbon negative (or neutral) process [1]. In this context, the characteristics of non-equilibrium microwave discharges make this technology an excellent candidate for the reactor design, even though its research is still at laboratory scale.

In general, non-thermal plasma is a very promising technology for chemical process intensification [7]. It maximizes the effectiveness of intra- and intermolecular processes, stimulating endothermic reactions by vibrational excitation. In optimum conditions it nearly gives the same processing experience to each molecule when the driving forces in the microscales (electrons collisions) are maximized. The four domains of process intensification can also be used to optimize the conversions and efficiencies, e.g. RF discharges, plasma catalysis and pulsed discharges.

Yet, there is still a long trail ahead for large scale industrial applications of non-thermal microwave reactors, since some technological challenges still need to be addressed [26]. Due to its complexity, all the chemical processes taking place in a non-equilibrium discharge are not fully understood [8]. The simultaneous attainment of high conversions and high energy efficiencies is known to be a very difficult task [20, 25]. Instabilities arise when increasing the pressure to near atmospheric values, while attempting to maintain the non-equilibrium characteristics [3, 25]. Not to mention the scaling up, which is perhaps the most challenging task. Recent works addressing these challenges were presented in the 22^{nd} International Symposium on Plasma Chemistry, ISPC 22 [25].

For the specific case of CO_2 dissociation most of the research has been done experimentally, by building complicated and expensive setups that not always give the expected results. In this regard, numerical models can be exceptional tools for getting insights into the processes before building setups, saving time and money. However, the modeling was hindered by the complexity of the chemical processes and indeed, no reaction kinetics model involving all the relevant processes was available until very recently.

In 2014, the PLASMANT group of the University of Antwerp published a reaction kinetics model for CO_2 dissociation in non-equilibrium plasmas [9]. This kinetic model was the first to include all the relevant physics that take place in the discharge and are involved in the CO_2 dissociation process. It was updated in a subsequent publication [8], in its latest version includes +100 species and +10000 reactions and besides its great level of detail, it is still a qualitative model. Naturally, due to its large number of variables it is a zero

dimensional kinetic model, whose implementation in multidimensional models is prohibitive.

It is therefore required to reduce this kinetic model to make it suitable for its implementation in multidimensional models. These models can be used to better understand the effects of gradients and to parameterize the design of reactors.

In line with this necessity, a reduced kinetic model suitable for multidimensional simulations is developed in this work. This reduced kinetic model is based on the kinetic model of the PLASMANT group, hence, it can be used to qualitatively predict the influence of different parameters in the process. It preserves the relevant processes taking place in the discharge and therefore it can be used in self-consistent models, under the conditions for which it is developed.

3.2. THE CO_2 MOLECULE

The CO_2 molecule is a triatomic linear molecule in its ground state, its dissociation energy is ~5.5 [eV] and its ionization energy ~13.8 [eV] [12]. In this section the vibrational degree of freedom is briefly discussed, due to its importance in the dissociation process in non-equilibrium microwave discharges. Details on the rotational and electronic degrees of freedom are also found in [12].

The CO_2 molecule has three vibrational modes, the symmetric stretching (υ_1), the symmetric bending (υ_2) and the asymmetric stretching (υ_3), see Figure 3.1. The symmetric bending is doubly degenerate, which means that for each energy level there are two vibrational states with the same energy (different bending plane).

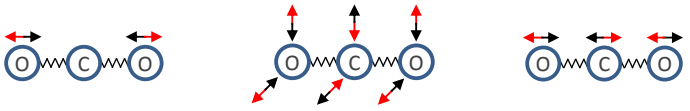

(a) υ_1: symmetric stretching (b) υ_2: symmetric bending (c) υ_3: asymmetric stretching

Figure 3.1: CO_2 Vibrational modes.

The energies of the vibrational levels can be computed from the triatomic anharmonic oscillator model, the expression to the second order of approximation is [27]

$$\frac{E_{(\upsilon_1\ \upsilon_2\ \upsilon_3)}}{hc} = \sum_i \omega_i \left(\upsilon_i + d_i/2\right) + \sum_{j\geq i} x_{ij} \left(\upsilon_i + d_i/2\right)\left(\upsilon_j + d_j/2\right) + x_{l_2 l_2} l_2^2 \tag{3.1}$$

where h is the Planck constant, c the speed of light, υ_i and d_i the vibrational quantum number and the degeneracy of the vibrational mode i, respectively. The spectroscopic constants for CO_2 are given in Table 3.1 [27].

Table 3.1: Spectroscopic constants for computing the vibratoinal energy levels of CO_2. Taken from [27].

Constant	Value [1/cm]
ω_1	1354.31
ω_2	672.85
ω_3	2396.32
x_{11}	–2.93
x_{12}	–4.61
x_{13}	–19.82
x_{22}	1.35
x_{23}	–12.31
x_{33}	–12.47
$x_{l_2 l_2}$	–0.97

The vibrational state of the CO_2 molecule is specified by the vibrational quantum numbers of the three modes, ($\upsilon_1\ \upsilon_2\ \upsilon_3$). For simplicity, the special quantum number for the angular momentum of the quasi-rotation around the principal axis l_2 is neglected. This rotation results from the summation of the symmetric

bendings in perpendicular planes [6]. The error induced by this assumption is very small (~0.01%) considering the relatively small value of $x_{l_2 l_2}$ and the low symmetric levels considered in this work.

The symmetric modes are also coupled by the Fermi resonance. i.e. the energies of the vibrational levels (v_1 v_2 v_3) and ((v_1-1) (v_2+2) v_3) are very close and the states resonate [9]. For simplicity, only one of these states is referred in this report. The vibrational levels considered in this work are listed in Table 3.2, where the notation used in [9] is adopted and energy levels are computed from equation 3.1.

Table 3.2: Vibrational levels considered in this work. Symmetric levels are denoted by letters and asymmetric levels are denoted by numbers.

Notation	Vibrational state	Energy [eV]
CO_2	(0 0 0)	0.000
$CO_2\,v_a$	(0 1 0)	0.083
$CO_2\,v_b$	(1 0 0)	0.166
$CO_2\,v_c$	(0 3 0)	0.250
$CO_2\,v_1$	(0 0 1)	0.291
$CO_2\,v_2$	(0 0 2)	0.579
$CO_2\,v_3$	(0 0 3)	0.864
$CO_2\,v_4$	(0 0 4)	1.146
$CO_2\,v_5$	(0 0 5)	1.425
$CO_2\,v_6$	(0 0 6)	1.701
$CO_2\,v_7$	(0 0 7)	1.974
$CO_2\,v_8$	(0 0 8)	2.243
$CO_2\,v_9$	(0 0 9)	2.510
$CO_2\,v_{10}$	(0 0 10)	2.773
$CO_2\,v_{11}$	(0 0 11)	3.034
$CO_2\,v_{12}$	(0 0 12)	3.291
$CO_2\,v_{13}$	(0 0 13)	3.545
$CO_2\,v_{14}$	(0 0 14)	3.796
$CO_2\,v_{15}$	(0 0 15)	4.044
$CO_2\,v_{16}$	(0 0 16)	4.289
$CO_2\,v_{17}$	(0 0 17)	4.531
$CO_2\,v_{18}$	(0 0 18)	4.770
$CO_2\,v_{19}$	(0 0 19)	5.005
$CO_2\,v_{20}$	(0 0 20)	5.238
$CO_2\,v_{21}$	(0 0 21)	5.467

The energy diagram of the vibrational levels is shown in Figure 3.2 [9], where it is seen that the highest considered asymmetric vibrational level $CO_2\,v_{21}$ is in the dissociation limit. The symmetric sublevels (0 n v) used for scaling the rate constants of the VT and VV' relaxation processes are shown in grey lines (see Chapter 5).

The CO_2 molecule, as other molecules like N_2, CO and H_2, are capable of storing vibrational energy for relatively long times. This is caused by the big difference between vibrational excitation and vibrational relaxation rates, thus, they are easy to activate and difficult to deactivate. The stored vibrational energy can be effectively used to stimulate endothermic reactions, leading to high reaction rates and energy efficiencies [6]. This important characteristic of the CO_2 molecule makes it an excellent candidate for developing non-equilibrium chemical processes based on microwave discharges.

The elementary processes for vibrational energy transfer (relaxation) are extensively discussed in [3, 6, 11]. In the following, only short definitions of these processes are provided. Additional details needed for the development of the reduced kinetic model are introduced in Chapters 4 and 5. For a thorough description of the relaxation processes the aforementioned sources are recommended.

- VV Relaxation: In this relaxation process the vibrational energy is transferred between vibrationally excited states in the same vibrational mode. Through this process the vibrational energy is transferred to higher vibrational levels, increasing their population. For instance, in a collision between two vibrationally excited states $CO_2\,v_1$, vibrational energy is transferred from one excited state to the other. The

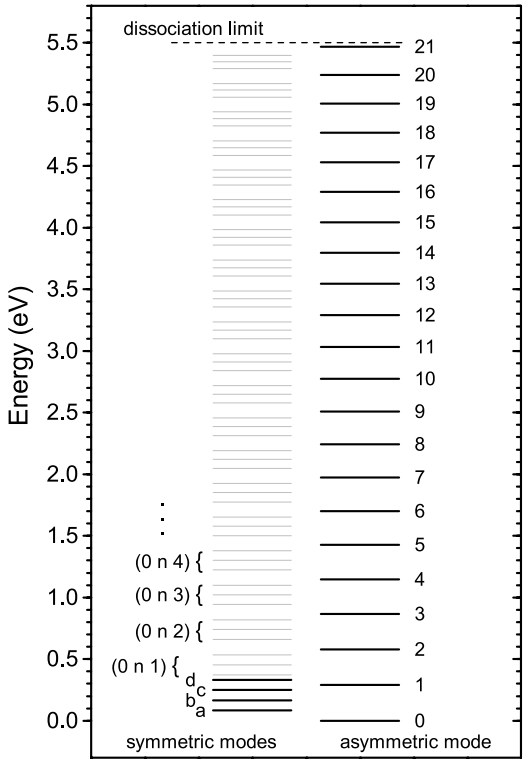

Figure 3.2: Energy diagram of the CO_2 vibrational levels considered in this work. Taken from [9].

result, for a single quantum transition, is that one excited state decreases its vibrational level in 1 and the other increases its vibrational level also in 1. The reaction is

$$CO_2\,v_1 + CO_2\,v_1 \rightarrow CO_2 + CO_2\,v_2$$

Multiquantum transitions ($\Delta v > 1$) are also possible although their rate is usually orders of magnitude smaller than the single quantum transition, therefore, they are usually neglected.

- VT Relaxation: In this relaxation process the vibrational energy is transferred to the translational degree of freedom, it is "lost" in heating the bulk gas. For instance in a collision between a vibrationally excited state $CO_2\,v_a$ and a groundstate O_2 molecule, the former loses its vibrational energy and the kinetic energy of the colliding species is increased. The reaction is

$$CO_2\,v_a + O_2 \rightarrow CO_2 + O_2$$

This reaction can also take place in the asymmetric vibrational mode. Multiquantum transitions are also possible and at higher temperatures their may become relevant.

- VV' Relaxation: In this relaxation process the vibrational energy is transferred between different molecules (or different vibrational modes [9], see Chapters 4 and 5). For instance, in a collision between vibrationally excited states of CO_2 and CO the following process, similar to VV relaxation, can occur

$$CO_2\,v_2 + CO\,v_1 \rightarrow CO_2\,v_1 + CO\,v_2$$

Multiquantum transitions are also possible and their rates depend on the colliding species and their vibrational energy levels.

3.3. CO_2 DISSOCIATION MECHANISM IN MICROWAVE DISCHARGES

The plasma conditions of moderate pressure microwave discharges are known to be in the optimum range to obtain the highest energy efficiency for the CO_2 dissociation. These are, low electron temperatures $T_e \approx 1-2$

[eV], high electron densities $n_e \approx 10^{12-14}$ [1/cm^3], sufficiently high ionization degrees $n_e/n_n > 10^{-6}$, high vibrational temperatures $T_v > 1000$ [K] and low bulk gas temperatures $T_g <\sim 1000$ [K]. They are generated at moderate pressures $p \approx 100-300$ [Torr] and values of the reduced electric field $E/n_n <\sim 100$ [Td] [3, 8]. Yet, the simultaneous achievement of these conditions is very difficult.

At electron temperatures in the mentioned range, most of the energy given to the plasma is transferred from the electrons to the vibrational modes of the CO_2 molecule, specially to the asymmetric vibrational mode, see Figure 3.3 and Chapter 5. At low bulk gas temperatures the VV relaxation of this vibrational mode is much faster than the VV relaxation of the symmetric modes, also, the VT relaxation is much slower than the same of the symmetric modes [3]. In other words, at low bulk gas temperatures, the vibrational energy of the lower asymmetric levels is rapidly transfer to higher asymmetric levels, where it is used to stimulate endothermic reactions.

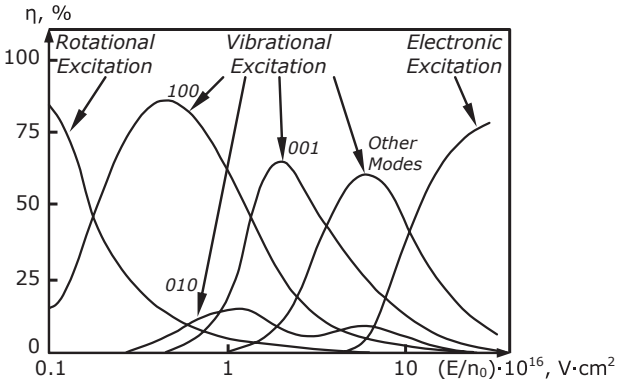

Figure 3.3: Fractions of the energy transferred to different channels of the CO_2 molecule in non-thermal discharges, as a function of the reduced electric field E/n_n (1 [Td] = 10^{-17} [V cm^2]). Taken from [3].

The CO_2 dissociation in non-thermal plasma is achieved by different mechanisms: electronic excitation, dissociative electron attachment and vibrational excitation. Among these, the vibrational excitation is the most efficient mechanism, for which efficiencies as high as 80% and 90% have been reported. The reasons for its high efficiency are summarized as follows [3]:

1. For electron temperatures values between $1-3$ [eV] up to 95% of the energy can be transferred to the vibrational modes of CO_2, specially to the asymmetric vibrational mode.

2. The vibrational energy is the most efficient means for the stimulation of endothermic reactions, such as those of CO_2 dissociation (see below). The activation energy of these reactions is effectively lowered by the vibrational energy.

3. The vibrational energy used in the CO_2 dissociation is equal to the energy of the CO=O bond, 5.5 [eV]. This is the minimum energy required for the process and is lower than the energy required by the other dissociation mechanisms, e.g. ~7 [eV] for direct dissociation through electronic excitation.

The details of the CO_2 dissociation by vibrational excitation are discussed in [3]. The mechanism involves a non-adiabatic (fast) electronic transition from the ground state ($^1\Sigma^+$) to a triple electronic state ($^3B_2$), which takes place in the intersection of the potential curves and includes a change in the spin of an electron. The result of this transition is that only 5.5 [eV] are required for the following dissociation reaction to take place

$$CO_2\,v + M \rightarrow CO + O + M$$

where $CO_2\,v$ is a vibrationally excited CO_2 molecule and M is a neutral molecule, such as CO, O_2 or CO_2 itself. The produced O atom can also react with another vibrationally excited CO_2 molecule, producing a second CO molecule

$$CO_2\,v + O \rightarrow CO + O_2$$

This reaction requires an energy of just 0.3 [eV] and is faster than the three-body O recombination for sufficiently high vibrational temperatures, $T_v \geqslant 0.1$ [eV].

In this two-step process, two CO_2 molecules are dissociated and one O_2 molecule is formed. Therefore, it can be represented by the following single process, for which an energy of 2.93 [eV] is required per molecule

$$CO_2 \rightarrow CO + \frac{1}{2}O_2$$

Theoretically, this is the most efficient reaction for CO_2 dissociation in a gas discharge and its energy requirement is used to compute the energy efficiencies of actual CO_2 dissociation processes, as follows [9]

$$\eta = X\frac{2.93}{\text{SEI}} \tag{3.2}$$

Where X is the CO_2 conversion (dissociation) and SEI is the Specific Energy Input in [eV/molecule], which indicates the average energy transferred per molecule in the active zone of the discharge. This is computed from the total power absorbed by the plasma in [W] and the flow of molecules in the active zone in [1/s], e is the elementary charge.

$$\text{SEI} = \frac{P}{eQ_N} \tag{3.3}$$

4

CO_2 KINETIC MODELS FOR NON-EQUILIBRIUM MICROWAVE DISCHARGES

4.1. COMPLETE CO_2 KINETIC MODEL

As mentioned before, the dissociation of the CO_2 molecule in non-thermal microwaves discharges was thoroughly researched some decades ago [19] and although at that time the main characteristics of the dissociation mechanism were identified, a reaction kinetics model with all the relevant physics required to describe the process was not reported until very recently.

The latter is the result of the work done at the University of Antwerp by the PLASMANT group, where a numeric model for CO_2 dissociation in non-equilibrium plasmas was developed. For the specific case of microwave discharges, they proposed a kinetic model which includes the relevant physics involved in the dissociation process [9]. This kinetic model is an extension of the simpler set of reactions developed by the same group to study the influence of vibrationally excited states on the CO_2 dissociation in Dielectric Barrier Discharges [28]. This 0-dimensional kinetic model considers homogeneous plasma properties in the discharge zone and includes electron impact reactions, reactions of neutrals, reactions involving charged species and vibrational energy transfer reactions.

Improvements to this kinetic model were introduced in subsequent publications of the same group. In [29], all charged species but CO_2^+ were omitted since their influence on the kinetics of neutrals is negligible, although electron impact reactions involving charged species were still included in the Boltzmann Equation solver to calculate the EEDF. More recently [8], further modifications were done, being the most important the addition of 53 vibrational levels of CO, which greatly increased the complexity of the model. Furthermore, the existing set of reactions was slightly modified and an energy conservation equation was included to study the efficiency of the dissociation process.

The latest kinetic model comprises a total of 110 species and more than 10000 reactions, including electron impact reactions, reactions of neutrals and vibrational energy transfer reactions. As in their first update, charged species reactions are only included to calculate the EEDF, which is then used to compute the rate coefficients of electron impact reactions. It is important to remark that this kinetic model provides a good qualitative matching between theoretical and experimental results, but it does not accurately reproduce any specific experimental results.

Despite the great work and results achieved by the PLASMANT group, the large number of species and reactions makes it computationally expensive and not suitable for 2D and 3D models. Different reduction techniques, such as the Principal Component Analysis [29], are being explored by the scientific community to simplify this kinetic model. Nevertheless, a practical kinetic model for 2D simulations has not been reported yet.

The species considered in the kinetic model are listed in Table 4.1. A complete description of the CO_2 kinetic model is found in [8, 9] and is not reproduced here, only a brief explanation of the reactions is provided in the following subsections.

Table 4.1: Chemical species included in the CO_2 kinetic model [8]

Type	Species
Neutral ground states	CO_2, CO, O_2, O_3, O, C_2O, C, C_2
Vibrationally excited states	$CO_2\upsilon_a$,..., $CO_2\upsilon_d$, $CO_2\upsilon_1$,..., $CO_2\upsilon_{21}$, $CO\upsilon_1$,..., $CO\upsilon_{63}$, $O_2\upsilon_1$,..., $O_2\upsilon_4$
Electronically excited states	CO_2e_1, CO_2e_2, COe_1,..., COe_4, O_2e_1, O_2e_2
Charged species	CO_2^+, e

4.1.1. ELECTRON IMPACT REACTIONS

For non-Maxwellian EEDF, cross section data is usually preferred over analytic expressions for computing rate constants of electron impact reactions. These rate constants are computed by first solving the Boltzmann equation to obtain the EEDF, which is multiplied by a cross section and then integrated to yield the respective constant rate (see equation 2.3).

The kinetic model comprises the electron impact reactions listed in Table 4.2. Cross sections are included for collisions between electron and neutral ground species, which are also used for computing the cross sections of electron collisions with vibrationally excited states of CO_2, CO and O_2. All listed reactions are used for computing the EEDF, although, as explained before, electron impact reactions producing charged species others than CO_2^+ are not considered for computing the population densities of species.

Although included in the first kinetic model [9], electron collisions with charged species are no longer considered, since they were specified by analytic expressions and not cross sections. The sources for the cross section data are found in [8] and the scaling laws specified in the notes are explained in detail in Chapter 5.

Table 4.2: Electron impact reactions specified by cross sections [8].

No.	Reaction	Note	No.	Reaction	Note
(X1)	$e + CO_2 \rightarrow e + CO_2$	a	(X24)	$e + CO\upsilon_i \rightarrow e + CO\upsilon_j$	d
(X2)	$e + CO_2 \rightarrow e + e + CO_2^+$	a	(X25)	$e + C \rightarrow e + C$	
(X3)	$e + CO_2 \rightarrow e + e + CO^+ + O$	b	(X26)	$e + C \rightarrow e + e + C^+$	
(X4)	$e + CO_2 \rightarrow e + e + C^+ + O_2$	b	(X27)	$e + C_2 \rightarrow e + C_2$	
(X5)	$e + CO_2 \rightarrow e + e + O^+ + CO$	b	(X28)	$e + C_2 \rightarrow e + C + C$	
(X6)	$e + CO_2 \rightarrow O^- + CO$	b	(X29)	$e + C_2 \rightarrow e + e + C_2^+$	
(X7)	$e + CO_2 \rightarrow e + CO + O$	b	(X30)	$e + O_2 \rightarrow e + O_2$	a
(X8)	$e + CO_2 \rightarrow e + CO_2e_1$	a	(X31)	$e + O_2 \rightarrow e + O + O$	b
(X9)	$e + CO_2 \rightarrow e + CO_2e_2$	a	(X32)	$e + O_2 \rightarrow e + e + O_2^+$	a
(X10)	$e + CO_2 \rightarrow e + CO_2\upsilon_a$		(X33)	$e + O_2 \rightarrow e + e + O + O^+$	b
(X11)	$e + CO_2 \rightarrow e + CO_2\upsilon_b$		(X34)	$e + O_2 \rightarrow O^- + O$	b
(X12)	$e + CO_2 \rightarrow e + CO_2\upsilon_c$		(X35)	$e + O_2 \rightarrow e + O_2\upsilon_i$	
(X13)	$e + CO_2 \rightarrow e + CO_2\upsilon_d$		(X36)	$e + O_2 \rightarrow e + O_2e_1$	
(X14)	$e + CO_2\upsilon_i \rightarrow e + CO_2\upsilon_j$	c	(X37)	$e + O_2 \rightarrow e + O_2e_2$	
(X15)	$e + CO \rightarrow e + CO$	a	(X38)	$e + O_3 \rightarrow e + O_3$	
(X16)	$e + CO \rightarrow e + e + CO^+$	a	(X39)	$e + O_3 \rightarrow e + O_2 + O$	
(X17)	$e + CO \rightarrow e + e + C^+ + O$	b	(X40)	$e + O_3 \rightarrow e + e + O_2^+ + O$	
(X18)	$e + CO \rightarrow e + e + C + O^+$	b	(X41)	$e + O_3 \rightarrow e + O^+ + O^- + O$	
(X19)	$e + CO \rightarrow C + O^-$	b	(X42)	$e + O_3 \rightarrow O^- + O_2$	
(X20)	$e + CO \rightarrow e + CO_2e_1$	a	(X43)	$e + O_3 \rightarrow O + O_2^-$	
(X21)	$e + CO \rightarrow e + CO_2e_2$	a	(X44)	$e + O \rightarrow e + O$	
(X22)	$e + CO \rightarrow e + CO_2e_3$	a	(X45)	$e + O \rightarrow e + e + O^+$	
(X23)	$e + CO \rightarrow e + CO_2e_4$	a			

[a] Same cross section is used for analogous reactions involving vibrationally excited states $CO_2\upsilon_i$, $CO\upsilon_i$ and $O_2\upsilon_i$.

[b] The energy threshold of the cross section is reduced by the vibrational level's energy for analogous reactions involving vibrationally excited states $CO_2\upsilon_i$, $CO\upsilon_i$ and $O_2\upsilon_i$, .

[c] Cross section for $i = 0$ and $j = 1$ is shifted and scaled by using Fridman's approximation [3].

[d] Cross sections for $i = 0$ and $j = 1, \ldots, 10$ are shifted and scaled by using Fridman's approximation [3].

4.1.2. REACTIONS OF NEUTRAL SPECIES

The reactions of neutral species are listed in Table 4.3. These reactions are also applicable to vibrationally excited states of CO_2, CO and O_2 by using the Fridman-Macheret α-model [3], for which the α values are also given. Each of these values is a representation of the effectiveness of the vibrational energy in overcoming the activation energy barrier of the reaction. The Fridman-Macheret α-model is used in Chapter 5, where a brief description is also given. The sources of these reactions are found in [8].

Table 4.3: Reactions of neutrals included in the kinetic model, M = CO_2, CO and O_2. Gas temperature T_g in [K] and rate constants in [cm^3/s] and [cm^6/s] for binary and ternary reactions, respectively [8].

No.	Reaction	Rate constant	α
(N1)	$CO_2 + M \rightarrow CO + O + M$	$4.39 \times 10^{-7} \exp(-65000/T_g)$	1.0
(N2)	$CO_2 + O \rightarrow CO + O_2$	$7.77 \times 10^{-12} \exp(-16600/T_g)$	0.5
(N3)	$CO + O + M \rightarrow CO_2 + M$	$8.2 \times 10^{-34} \exp(-1510/T_g)$	0.0
(N4)	$O_2 + CO \rightarrow CO_2 + O$	$1.23 \times 10^{-12} \exp(-12800/T_g)$	0.5
(N5)	$CO_2 + C \rightarrow CO + CO$	1.0×10^{-15}	
(N6)	$CO + O_3 \rightarrow CO_2 + O_2$	4.0×10^{-25}	
(N7)	$CO + C + M \rightarrow C_2O + M$	6.5×10^{-32}	
(N8)	$O_2 + C \rightarrow CO + O$	3.0×10^{-11}	
(N9)	$CO + M \rightarrow O + C + M$	$1.52 \times 10^{-4} (T_g/298)^{-3.1} \exp(-129000/T_g)$	1.0
(N10)	$O + C + M \rightarrow CO + M$	$2.14 \times 10^{-29} (T_g/300)^{-3.08} \exp(-2114/T_g)$	
(N11)	$O + C_2O \rightarrow CO + CO$	5.0×10^{-11}	
(N12)	$O_2 + C_2O \rightarrow CO_2 + CO$	3.3×10^{-13}	
(N13)	$O + O_3 \rightarrow O_2 + O_2$	$3.1 \times 10^{-14} T_g^{0.75} \exp(-1575/T_g)$	
(N14)	$O_3 + M \rightarrow O_2 + O + M$	$4.12 \times 10^{-10} \exp(-11430/T_g)$	
(N15)	$O + O_2 + M \rightarrow O_3 + M$	$6.11 \times 10^{-34} (T_g/300)^{-2.6}$	
(N16)	$O + O + M \rightarrow O_2 + M$	$1.27 \times 10^{-32} (T_g/300)^{-1} \exp(-170/T_g)$	

4.1.3. VIBRATIONAL ENERGY TRANSFER REACTIONS

Vibrational energy transfer reactions included in the kinetic model are given in Table 4.4. The forward rate constants are taken from [8], whereas the x_e values and the notes are taken from [9] since they are not given in the former. There are some differences between the reactions given in those publications, specially in the VT relaxation of CO and O_2, reactions (V3) and (V4), respectively. Therefore, the multipliers 0.001 and 1.0 for M = O_2 in reactions (V3) and (V4) (see Notes c and d) are assumed to match the specific reactions given for these processes in [9]. Nevertheless, these reactions are not further used in this work and they are given here for completion of the model.

The rate constants are given for the forward reactions and for specific vibrational levels, $i = 1$ and $j = 0, 1$. These rate constants are scaled to reactions involving higher vibrational levels by using expressions derived from the SSH theory [9], the given anharmonicity coefficient x_e is used in the process. Rate constants for the reverse reactions are computed by using the detailed balancing principle [11]. The process for computing rate constants for the whole set of reactions is explained in Chapter 5.

4.2. REDUCED CO_2 KINETIC MODEL

The proposed kinetic model is based on the one developed by the PLASMANT group. Several simplifications are made to reduce such an extensive and complex model to a simpler one with a manageable number of reactions. It is important to remark that such simplifications are done at expenses of some accuracy with respect to the complete kinetic model, since the purpose here is getting trends with fair accuracy rather than accurate results. Indeed, in view of the dissimilar experimental results reported so far [14, 19–25], there is no strong interest in obtaining highly accurate results until the model can be adjusted to a specific experiment. Moreover, a simpler kinetic model that can be easily adjusted to match experimental results is preferred.

The main concept in the simplification of the kinetic model is the lumping of the asymmetric vibrational mode of the CO_2, which has been identified as the most effective channel in the dissociation of CO_2 in non-equilibrium microwave discharges [3]. For this purpose the fictitious species CO_2^* is created, which is a representation of all vibrationally excited states of the asymmetric vibrational mode. In a similar way as CO_2 can be

Table 4.4: Vibrational energy transfer reactions [8, 9], M = CO_2, CO and O_2. Gas temperature T_g in [K].

No.	Reaction	Forward rate constant, ($i = 1$) [cm^3/s]	$x_e \times 10^3$	Note
(V1)	$CO_2\,v_x + M \leftrightarrow CO_2 + M$	$7.14\times10^{-8}\exp(-177T_g^{-1/3}+451T_g^{-2/3})$	0.0	a
(V2a)	$CO_2\,v_i + M \leftrightarrow CO_2\,v_{i-1(a)} + M$	$0.43\exp(-407T_g^{-1/3}+824T_g^{-2/3})$	3.7	b
(V2b)	$CO_2\,v_i + M \leftrightarrow CO_2\,v_{i-1(b)} + M$	$0.86\exp(-404T_g^{-1/3}+1096T_g^{-2/3})$	1.0	b
(V2c)	$CO_2\,v_i + M \leftrightarrow CO_2\,v_{i-1(c)} + M$	$1.43\times10^{-5}\exp(-252T_g^{-1/3}+685T_g^{-2/3})$	-15.6	b
(V3)	$CO\,v_i + M \leftrightarrow CO\,v_{i-1} + M$	$8.84\times10^{-12}T_g\exp(-222T_g^{-1/3}+379T_g^{-2/3})$	6.13	c
(V4)	$O_2\,v_i + M \leftrightarrow O_2\,v_{i-1} + M$	$7.99\times10^{-5}\exp(-320T_g^{-1/3}+615T_g^{-2/3})$	0.0	d
(V5a)	$CO_2\,v_i + CO_2 \leftrightarrow CO_2\,v_{i-1(b)} + CO_2\,v_a$	$2.13\times10^{-5}\exp(-242T_g^{-1/3}+633T_g^{-2/3})$	2.8	
(V5b)	$CO_2\,v_i + CO_2 \leftrightarrow CO_2\,v_{i-1(a)} + CO_2\,v_b$	$2.13\times10^{-5}\exp(-242T_g^{-1/3}+633T_g^{-2/3})$	17.6	
(V6)	$CO_2\,v_i + CO_2\,v_j \leftrightarrow CO_2\,v_{i-1} + CO_2\,v_{j+1}$	$1.8\times10^{-11}\exp(24.7T_g^{-1/3}-65.7T_g^{-2/3})$	5.25	$j=1$
(V7)	$CO\,v_i + CO\,v_j \leftrightarrow CO\,v_{i-1} + CO\,v_{j+1}$	$1.5\times10^{-15}T_g\exp(1.97T_g^{-1/3}+82.3T_g^{-2/3})$	6.13	$j=1$
(V8)	$CO_2\,v_i + CO\,v_j \leftrightarrow CO_2\,v_{i-1} + CO\,v_{j+1}$	$4.8\times10^{-12}\exp(10^{-6}T_g^{-1/3}-153T_g^{-2/3})$	5.25; 6.13	$j=0$

[a] $x = a, b, c, d$. Multiply by 1.0, 0.7 and 0.7 for M = CO_2, CO and O_2, respectively.
[b] Multiply by 1.0, 0.3 and 0.4 for M = CO_2, CO and O_2, respectively.
[c] Multiply by 1.0, 1.0 and 0.001 for M = CO_2, CO and O_2, respectively.
[d] Multiply by 0.3, 1.0 and 1.0 for M = CO_2, CO and O_2, respectively.

seen as a collection of ground and excited states in thermal equilibrium with the translational temperature (gas temperature), CO_2^* can be seen as a collection of excited states in which the asymmetric vibrationally excited states are not in thermal equilibrium. This concept is further explained in Chapter 5 for the simplification process.

Besides this fictitious species CO_2^*, only the species with high populations or taking part in main processes are included in the model. In such way, the chemical species considered for the reduced kinetic model are shortened to only 13, instead of 110 considered in the complete kinetic model. They are presented in Table 4.5.

Table 4.5: Chemical species considered for the reduced kinetic model.

Type	Species
Neutral ground states	CO_2, CO, O, O_2
Vibrationally excited states	$CO_2\,v_a$, $CO_2\,v_b$, $CO_2\,v_c$, CO_2^*
Charged species	CO_2^+, CO^+, O_2^+, O^+, e

In a similar fashion, the reactions included in the reduced kinetic model are limited to the dominant reactions of the main processes. By following this principle it is possible to propose a reduced kinetic model of 44 reactions, which is depicted in the reaction pathway of Figure 4.1. The simplification process and the reactions are explained in detailed in Chapter 5, although, a short description of the reactions is given in the following subsections.

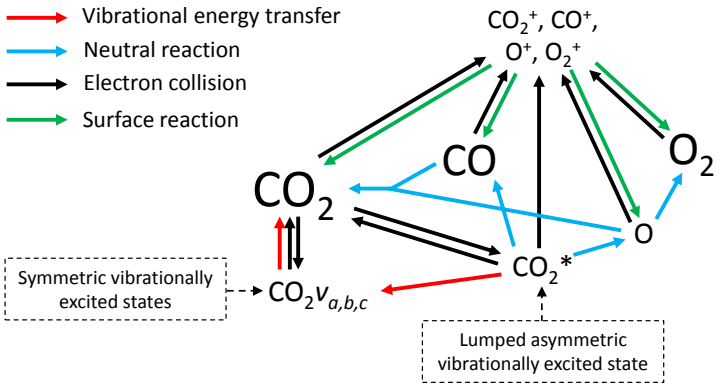

Figure 4.1: Reaction pathway of the reduced kinetic model

4.2.1. ELECTRON IMPACT REACTIONS

These reactions are the driving force of a plasma. In the case under consideration, electrons gain energy from the electromagnetic field and transfer it to other species through impact reactions. New electrons required to sustain the plasma are also produced by these reactions. Several processes can occur when an electron collides with another species (see section 2.3), however, in the reduced model only the following processes are considered

- Elastic scattering (RX1-5): This process has the largest cross sections in the range of mean electron energies for the microwave discharges under consideration (< 3[eV]). In other words, this type of electron impact reaction has the highest reaction rate of all electron collisions. Elastic scattering reactions are included for the neutral ground states and the lumped excited state CO_2^*.
- Electron impact ionization (RX6-10): Electrons are produced in this process. These are required to sustain the plasma, replacing those that are lost on the walls. Electron impact ionization reactions are included for neutral ground states and the lumped excited state CO_2^*.
- Vibrational excitation (RX11-13): Neglecting rotational excitation, this process has the second largest cross sections in the considered range of energies and has been identified as the main energy transfer channel from electrons to CO_2 in non-thermal microwave discharges. In other words, through this process the kinetic energy of electrons is transferred to the CO_2 molecule as vibrational energy. Electron impact vibrational excitation reactions are included for the first level of each symmetric vibrational mode of CO_2, as well as for the lumped asymmetric vibrational mode CO_2^*. No reactions of this type are included for other neutral ground states.

A total of 16 electron impact reactions are obtained, they are presented in Table 4.8. Reverse processes for the vibrational excitation reactions (vibrational de-excitation or superelastic collisions) are also included.

Table 4.6: Electron impact reactions considered for the reduced kinetic model.

No.	Process	Reaction
(RX1)	CO_2 Elastic scattering	$e + CO_2 \rightarrow e + CO_2$
(RX2)	CO_2^* Elastic scattering	$e + CO_2^* \rightarrow e + CO_2^*$
(RX3)	CO Elastic scattering	$e + CO \rightarrow e + CO$
(RX4)	O Elastic scattering	$e + O \rightarrow e + O$
(RX5)	O_2 Elastic scattering	$e + O_2 \rightarrow e + O_2$
(RX6)	CO_2 Ionization	$e + CO_2 \rightarrow e + e + CO_2^+$
(RX7)	CO_2 Ionization from CO_2^*	$e + CO_2^* \rightarrow e + e + CO_2^+$
(RX8)	CO Ionization	$e + CO \rightarrow e + e + CO^+$
(RX9)	O Ionization	$e + O \rightarrow e + e + O^+$
(RX10)	O_2 Ionization	$e + O_2 \rightarrow e + e + O_2^+$
(RX11)	Vibrational (de)excitation to $CO_2\,v_a$	$e + CO_2 \leftrightarrow e + CO_2\,v_a$
(RX12)	Vibrational (de)excitation to $CO_2\,v_b$	$e + CO_2 \leftrightarrow e + CO_2\,v_b$
(RX13)	Vibrational (de)excitation to CO_2^*	$e + CO_2 \leftrightarrow e + CO_2^*$

4.2.2. REACTIONS OF NEUTRAL SPECIES

At favorable conditions for the CO_2 dissociation, a fraction of the energy transferred from the electrons to the CO_2 is stored as internal energy in high vibrational levels of the asymmetric mode. The fictitious species CO_2^* is a representation of this non-equilibrium energy accumulation, which can either be used to facilitate its dissociation or be transferred to the bulk gas as heat. The former leads to the production of CO and O, which can recombine to from CO_2 again. The produced O atoms can also recombine to form the more stable O_2 molecule. These three processes are considered for the reactions of neutrals.

- CO_2 dissociation (RN1,2): It is effectively achieved in collisions between neutrals and high asymmetric vibrationally excited states of CO_2. The lumped excited state CO_2^* is therefore considered for this process and reactions for the collisions with neutral ground states are included in the reduced kinetic model.

- CO and O recombination (RN3,4): Recombination of CO and O to form CO_2 also takes place in the discharge. The reactions included for this process are the three-body recombination involving a neutral ground state and the well-known reaction between CO and O_2.
- O recombination (RN5): Oxygen atoms produced in the dissociation of CO_2^* can recombine to form the more stable O_2 molecule. This proceeds mainly through a three-body reaction between two O atoms and a neutral ground state.

A total of 11 reactions of neutrals are obtained, they are listed in Table 4.7 and can be seen as a reduced set of those included in the complete kinetic model.

Table 4.7: Reactions of neutrals considered for the reduced kinetic model. M = CO_2, CO, O_2.

No.	Process	Reaction
(RN1)	CO_2^* Dissociation by collisions with CO_2, CO and O_2	$CO_2^* + M \rightarrow CO + O + M$
(RN2)	CO_2^* Dissociation by collisions with O	$CO_2^* + O \rightarrow CO + O_2$
(RN3)	Three-body CO and O recombination	$CO + O + M \rightarrow CO_2 + M$
(RN4)	Two-body CO and O recombination	$CO + O_2 \rightarrow CO_2 + O$
(RN5)	Three-body O recombination	$O + O + M \rightarrow O_2 + M$

4.2.3. VIBRATIONAL ENERGY TRANSFER REACTIONS

As explained before, the lumped excited state CO_2^* can either dissociate through reactions of neutrals or transfer its energy to the bulk gas by vibrational relaxation. In the latter, the energy that could have been used to dissociate the molecule is lost in heating the bulk gas. The following three processes are considered for the vibrational relaxation.

- VT Relaxation of symmetric vibrationally excited states (RV1): In this process, a symmetric vibrationally excited state of CO_2 loses its vibrational energy in a collision with a neutral ground state. Reactions involving the different neutral ground states are included for each of the symmetric vibrationally excited states.
- VT Relaxation of the lumped asymmetric vibrationally excited state (RV2): This process is equivalent to the previous, although for the asymmetric vibrational mode, represented by CO_2^*. In this case, however, a fraction of the vibrational energy is transferred to the symmetric vibrational modes, which are intermediate steps towards the energy loss to the bulk gas.
- VV' Relaxation between symmetric and asymmetric vibrationally excited states (RV3): In this process, the lumped excited state CO_2^* collides with a CO_2 molecule and transfers a fraction of its vibrational energy to the symmetric modes of the CO_2 molecule. In other words, a CO_2 molecule gets vibrationally excited in a collision with the lumped excited state CO_2^*.

A total of 13 vibrational energy transfer reactions are obtained, they are listed in Table 4.8. It is to be noted that reactions (RV2) and (RV3) are "lumped" versions of the analogous reactions presented in the complete kinetic model. The derivation of these approximations is given in section 5.8.

Table 4.8: Vibrational energy transfer reactions considered for the reduced kinetic model. M = CO_2, CO, O_2.

No.	Process/Reaction
(RV1)	VT Relaxation of symmetric vibrationally excited states. $x = a, b, c$.
	$CO_2\upsilon_x + M \rightarrow CO_2 + M$
(RV2)	VT Relaxation of the lumped asymmetric vibrationally excited state.
	$CO_2^* + M \rightarrow \nu_{l2}CO_2^* + \nu_{s2}(CO_2\upsilon_a + CO_2\upsilon_b + CO_2\upsilon_c) + M$
(RV3)	VV' Relaxation between symmetric and asymmetric vibrationally excited states.
	$CO_2^* + CO_2 \rightarrow \nu_{l3}CO_2^* + \nu_{s3}(CO_2\upsilon_a + CO_2\upsilon_b)$

4.2.4. SURFACE REACTIONS

The charged species, electrons and ions, produced by electron impact ionization reactions, diffuse together to the grounded walls by effect of ambipolar diffusion. Once at the wall, they recombine and the neutral charge is restored in the ion. This surface recombination, or neutralization, is the only process considered to take place in the surface and it is required to avoid the accumulation of ions in the reactor.

Hence, one neutralization surface reaction is included for each ion, obtaining a total of 4 surface reactions, which are listed in Table 4.9. For all of them a sticking coefficient of 1 is assumed (see section 5.9).

Table 4.9: Surface reactions included in the reduced kinetic model.

No.	Process	Reaction
(RS1)	CO_2^+ Neutralization	$CO_2^+ \rightarrow CO_2$
(RS2)	CO^+ Neutralization	$CO^+ \rightarrow CO$
(RS3)	O^+ Neutralization	$O^+ \rightarrow O$
(RS4)	O_2^+ Neutralization	$O_2^+ \rightarrow O_2$

5

SIMPLIFICATION PROCESS

Conventional kinetic models are built to model processes that take place in thermal equilibrium conditions, in which the internal energy modes (rotational, vibrational and electronic) of atoms and molecules are in thermal equilibrium with the external energy mode (translational). In other words, the distribution of excited states in these degrees of freedom follows the Boltzmann distribution at the translational temperature, which, from the kinetic theory of gases, is no other than the temperature of the gas. Since the distribution of excited states is already fixed, so are the processes in which they take part, and hence, they can be neglected as well. The outcome are kinetic models whose complexity depends on the number of species with different constituents and on the reactive processes between them. The latter processes break or form chemical bonds and usually have an Arrhenius type temperature dependence.

These conventional kinetic models fail when used to model processes in non-equilibrium conditions, where the distribution of excited states can be far from the Boltzmann distribution. This implies that processes involving these excited states must be included to properly and accurately describe the reactions kinetics. The best approach to deal with the complex processes taking part in non-equilibrium conditions is building state-to-state (STS) kinetic models, where excited states are considered as separate species and their radiative and collisional processes are also included. Radiative processes are those in which electronic transitions take place by emitting or absorbing radiation, whereas collisional processes take place upon collisions of two or three particles and can have a reactive or non-reactive character. In a reactive collision chemical bonds are broken or formed, while in a non-reactive collision the energy transfer takes place without affecting the chemical bonds.

STS kinetic models, also called Collisional Radiative Models (CRM), have proved to be of great value in modeling discharges in non-equilibrium conditions. This approach has been successfully applied to accurately describe the ionization and dissociation kinetics in non-thermal plasmas, by identifying the main energy transfer channels in the discharge. However, due to its inherent complexity, the number of species can reach the hundreds and the number of reactions can easily reach the thousands. For instance, a simplified CRM of the simplest molecule H_2 may have around 40 species and 1100 reactions [30], the complete CO_2 vibrational collisional model herein considered has 110 species and more than 10000 reactions [29], and the ro-vibrational collisional model for N_2 + N can have more than 23 million reactions [31].

It is worth to mention that STS kinetic models are built for specific applications, since the main energy channels may differ from one application to another, depending on its characteristics. Hence, although they are usually tailored for each specific case, the large number of species and reactions is a common issue among them. For the previous reason this approach is computationally expensive and its application has been mostly limited to zero or one-dimensional models. Nevertheless, some processes or applications are better studied in multidimensional models, thus the need to reduce the complexity of the STS kinetic models, for which some methods have been recently proposed.

5.1. REVIEWED APPROACHES TO REDUCE STS KINETIC MODELS

In this work, several approaches to reduce the CO_2 kinetic model described in Chapter 4 were considered. Simple kinetic models were obtained in [13, 32, 33] by fitting experimental data of selected species to rate constants, for which different temperature dependence expressions were proposed. These methods were

used in Corona and Dielectric Barrier Discharges, where the vibrational kinetics play a minor role in comparison to microwave discharges [9]. In this case, the STS kinetic model is required for the application of such methods, so that a comprehensive set of results can be used to fit the rate constants. Moreover, these methods are, to some extent, decoupled from the physics involved in the process and might be inapplicable in cases where the vibrational kinetics plays the key role in the dissociation kinetics.

As in the previous approaches, the STS kinetic model is also required to calculate the macroscopic reaction rates of the Principle of Macroscopic Kinetics presented in [34]. Likewise, the application of the Principal Component Analysis also requires the STS kinetic model [29]. Although this approach is indeed a statistical procedure, it can be applied to reduce the dimension of data sets by finding the components with the highest variance, which are called Principal Components and are used to reconstruct the remaining data. The STS kinetic model is used to obtain the training data required to identify these Principal Components.

Software for reducing kinetic models are also available. In this regard, CHEMKIN-PRO has been mostly used for combustion, except some plasma applications like [33]. On the other hand, PumpKin [35] is a post-processing tool to find principal pathways in plasma chemical models, based on the algorithm proposed by [36]. This algorithm is an iterative process in which key components are identified and reactions are grouped in new reactions pathways, thus, reducing the kinetic model.

The approaches presented in [37] and [38] are more related to the case studied here. In the former, a multitemperature approach for the dissociation and recombination regimes of N_2 + N in non-equilibrium hypersonic flows is proposed. The main characteristic of this approach is that the dissociation and recombination kinetics are described by a vibrational temperature and a translational temperature, $T_v > T_g$. It further assumes that the vibrational distribution follows the Boltzmann distribution at T_v. In the latter approach, the Two-Level Distribution model is introduced as an improvement to the multitemperature model. In this approach, the population of last vibrational level is computed by using state-to-state kinetics instead of the Boltzmann distribution. Park's effective temperature model is also discussed in both publications and a brief description is also found in [3].

Recently, approaches where internal modes are divided into groups were proposed. Inside these groups, uniform and Boltzmann distributions have been assumed in [31] and [39], respectively. The schemes presented in [40] can be seen as an upgraded generalization of the former, being the main difference the variables chosen as conserved variables. It was also shown that choosing population densities related to internal partitions of the groups as conserved variables gives more accurate results, as well as keeping the lower levels of the internal energy modes as separate species. The development of more accurate schemes for reducing STS kinetic models is an ongoing research topic, as there is an imperative need for them to make possible the multidimensional modeling of non-equilibrium processes.

5.2. PROPOSED APPROACH TO REDUCE THE CO_2 KINETIC MODEL

Despite the different approaches described above, none of the them were considered convenient. Most of them require a STS kinetic model, either to fit results or to apply difficult algorithms or mathematical procedures. Indeed, it is preferred in this work to circumvent the development of the STS CO_2 kinetic model and avoid the complex task of gathering information, coding, debugging and validating a kinetic model of 110 species and +10000 reactions. Therefore, a different approach is proposed for obtaining a reduced kinetic model.

The basis of the proposed approach is the grouping of the asymmetric vibrationally excited states of CO_2, which are the most effective channel in the dissociation of CO_2 in non-equilibrium microwave discharges. The 21 levels considered in Section 3.2 are then grouped into a a single asymmetric vibrationally excited state represented by the fictitious species CO_2^*. This species is a representation of all vibrationally excited states of the asymmetric mode, which are not in thermal equilibrium with the translation energy mode.

The dissociation of CO_2 in non-equilibrium plasma is better achieved at low bulk gas temperatures [8], since VT losses are reduced and the vibrational energy is used in the dissociation process instead of being lost in bulk gas heating. At such temperatures the highest relaxation rate is the VV relaxation for most of the CO_2 asymmetric vibrational levels. Hence, once the CO_2 molecule is excited in this vibrational mode, it is more likely that it exchanges energy with other CO_2 excited molecule of the same vibrational mode. In such way the vibrational energy is distributed among the vibrational levels. Especially, the vibrational energy is transferred from low levels to high levels where it is used in the dissociation process or lost in VT relaxation.

It is assumed that inside this group, the 21 levels solely exchange energy through VV relaxation, although as a group they can either dissociate or lose energy via VT relaxation. In other words, the fictitious species CO_2^*

stores the energy transferred to the asymmetric vibrational mode. On the one hand this energy is lost when CO_2^* reacts to form either CO_2 or an excited state in the symmetric modes $CO_2\,v_{a,b,c}$, which subsequently relaxes to CO_2. On the other hand this energy is used when the CO_2^* dissociates into CO and O. The previous concept is shown in Figure 5.1, where $CO_2\,v_i$ represents the asymmetric vibrational level i.

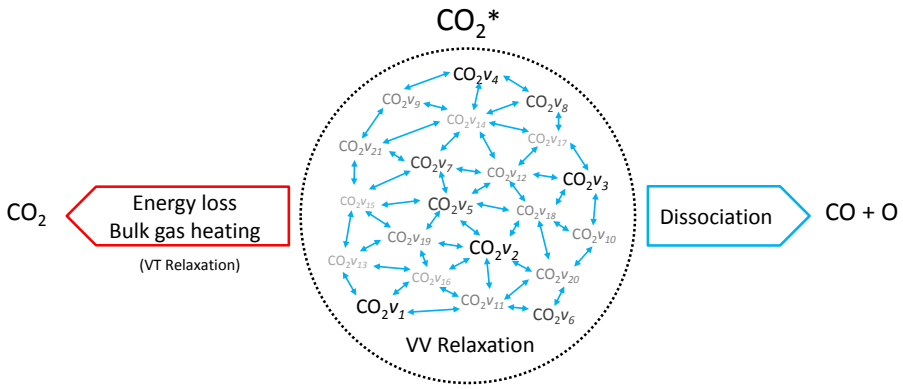

Figure 5.1: Grouping of 21 asymmetric vibrational levels in the fictitious species CO_2^*.

Since only VV relaxation is taking place inside the group, it is assumed that the excited states follow the Treanor non-equilibrium distribution (see section 2.5), in which the population of the high vibrationally excited states is higher than in a Boltzmann equilibrium distribution. Furthermore, considering that these excited states are purely asymmetric and only exchange energy between them, a good approximation is to fit their energy levels to a diatomic anharmonic oscillator model and compute an effective anharmonicity coefficient to be used in the calculation of the Treanor distribution [9].

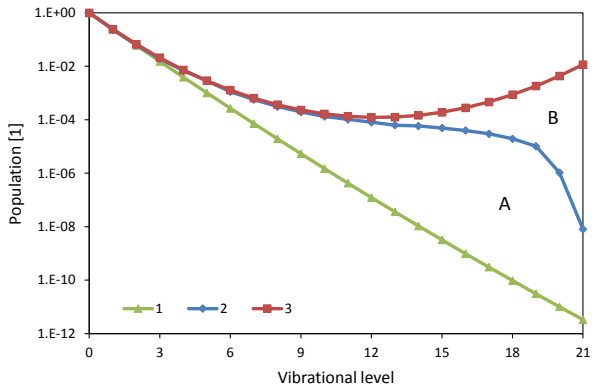

Figure 5.2: Comparison of normalized vibrational distributions for the asymmetric mode of CO_2, $T_g = 300$ [K]. 1: Boltzmann distribution, 2: STS Kinetic model [9], 3: Treanor distribution, $T_v = 2400$ [K].

Figure 5.2 shows three different vibrational distributions for a gas temperature of 300 [K]. The Boltzmann distribution is shown in the lower part and is the reference to evaluate the departure of the distributions from the thermal equilibrium. The intermediate distribution was taken from the results of [9] and corresponds to isothermal calculations of their STS kinetic model. In the higher part, the Trearon distribution for a vibrational temperature of 2400 [K] is shown.

The area between the curves represents the stored vibrational energy. For instance, in the Treanor distribution, the sum of areas A and B represents the stored energy when there are no VT losses and no other reactions, only VV relaxation. At a specific moment in time, area B denotes the VT losses and the energy used in reactions, which are greater for higher levels ($v > 12$) and cause the decline in the distribution's tail. Area A corresponds to the vibrational energy that is still to be used or to be lost. In the proposed approach, the used or lost energy is accounted as a group, rather than individually for each level, as is the case in the STS approach.

Averaged cross sections and rate constants for reactions involving the lumped excited state CO_2^* are obtained by adding the individual contributions of the vibrational levels, which are computed from their populations and individual rate constants.

5.3. FITTING ENERGY LEVELS TO A DIATOMIC ANHARMONIC OSCILLATOR MODEL

As mentioned above, the energy levels of the asymmetric vibrational mode in the CO_2 molecule can be fitted to the diatomic anharmonic oscillator model. In this way, the anharmonicity coefficient of the vibrational mode is computed, allowing the calculation of the Treanor distribution as well. The simplest expression for the diatomic anharmonic oscillator model involves only the first anharmonicity coefficient [9], this is

$$\frac{E_v}{hc} = \omega_e(v+0.5) - \omega_e x_e(v+0.5)^2 \tag{5.1}$$

where E_v is the energy of the vibrational level v, h the Planck constant, c the speed of light, ω_e the harmonic frequency and x_e the first anharmonicity coefficient. However, in this case the anharmonicity coefficient must be computed from the energy levels. Therefore, the following expression, which can be easily derived from the previous, is used

$$x_e = \frac{1-\Delta E_v/E_1}{2\times(v-\Delta E_v/E_1)}\ ,\ \Delta E_v = E_v - E_{v-1} \tag{5.2}$$

The energy of purely asymmetric vibrational levels is computed from the triatomic anharmonic oscillator model (equation 3.1), the results are shown in Table 5.1. Replacing v in the previous equation by any vibrational level $v>0$, the same value for the anharmonicity coefficient $x_e = 5.253\times10^{-3}$ is obtained.

Table 5.1: Energy levels in [eV] of the asymmetric vibrational mode (0 0 v).

Level, v	Energy, $E_{(0\ 0\ v)}$	Level, v	Energy, $E_{(0\ 0\ v)}$
0	0.0000	11	3.0338
1	0.2913	12	3.2910
2	0.5794	13	3.5452
3	0.8645	14	3.7962
4	1.1465	15	4.0442
5	1.4254	16	4.2891
6	1.7012	17	4.5309
7	1.9739	18	4.7696
8	2.2435	19	5.0052
9	2.5100	20	5.2377
10	2.7734	21	5.4671

The previous calculation can also be done to compute the anharmonicity coefficient of the energy change in vibrational relaxation reactions. This anharmonicity coefficient is used in the SSH theory to scale the vibrational relaxation reactions to higher levels, as explained in following sections.

5.4. TREANOR DISTRIBUTION AND ITS EVOLUTION WITH TEMPERATURE

Besides the anharmonicity of the energy levels, the bulk gas temperature and the vibrational temperature are also needed for the calculation of the Treanor distribution. For the latter, the original expression based on the energy of the vibrational levels (see equations 2.6 and 2.7) is preferred over the expressions based on anharmonicity coefficients [3].

The population of the first vibrational level is needed for the calculation of the vibrational temperature. However, this population is the result of a kinetic model that includes the first vibrational level as a separate species. This is not the case in the proposed kinetic model. Indeed , the vibrational temperature is used to compute the Treanor distribution, which in turn is used to compute the averaged rate constants for the lumped excited state CO_2^*.

Therefore, as a first approximation the vibrational temperature is considered as the product of the bulk gas temperature and a factor k, which represents the non-equilibrium character of the discharge. Figure 5.3 illustrates how at lower values of k, the Treanor distribution approaches the Boltzmann distribution until they match at $k=1$.

Naturally, this factor is a function of the bulk gas temperature and the pressure of the discharge. For specific conditions it is computed from results of experiments or STS kinetic models in the following way

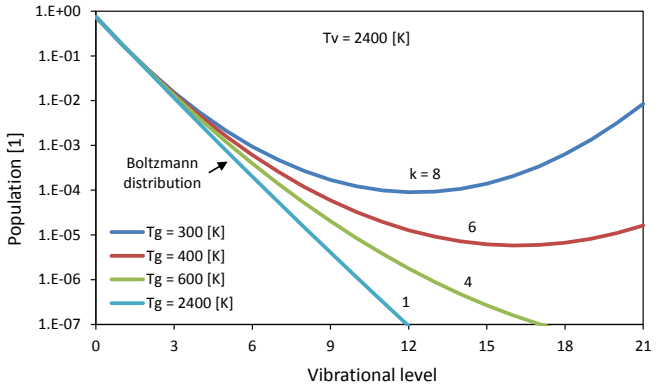

Figure 5.3: Treanor distributions for a constant vibrational temperature of 2400 [K] and different k factors.

$$k(T_g, p) = \frac{T_v}{T_g} \tag{5.3}$$

Since the purpose of this work is getting a reduced kinetic model of the one proposed in [8, 9], their results are used for computing the k factor. Thus, from the specific results of [8] it is seen that k is in the approximate range between 5.2 and 7, for a constant gas pressure of 100 [Torr] and bulk gas temperatures of 300 and 320 [K], respectively. The lower limit corresponds to the point where the bulk gas temperature starts increasing, indicating that VT relaxation is taking place, which does not imply that the maximum vibrational energy has been transferred to the asymmetric vibrational mode of the initial system. The upper limit corresponds to the point where the CO_2 dissociation becomes noticeable, indicating that the highest vibrational level has been excited and fewer CO_2 molecules of the initial system are remaining. Therefore, in between these values the maximum vibrational energy is stored in the initial system.

Additionally, the gas temperature dependence of the k factor is needed to estimate how the vibrational temperature evolves as the VT relaxation proceeds. This is very difficult to estimate beforehand and it is a result of the whole vibrational kinetics. In this regard, the following observations are made

- The bulk gas temperature increases as a consequence of VT relaxation and this increase leads to higher VT relaxation rates. This combined effect causes an exponential growth of the bulk gas temperature [3] and it is caused by the strong exponential dependence on the temperature (Landau-Teller temperature dependence). This can also be seen in the rate constants of VT relaxation reactions (V2a,b,c) of Table 4.4, where $T_g^{-1/3}$ dominates over $T_g^{-2/3}$.
- At high bulk gas temperatures, all the processes favoring the energy loss dominate the vibrational kinetics. In the rate constants of reactions (V1), (V2a,b,c) and (5a,b) of Table 4.4 the Landau-Teller temperature dependence dominates.

Therefore, as a rough approximation it is assumed that the k factor also follows the Landau-Teller temperature dependence, the following expression is then proposed

$$k = a \exp\left(\frac{b}{T_g^{1/3}}\right) \times \frac{1}{T_g} \tag{5.4}$$

Where a and b are coefficients that are determined by fitting this function to known values of k. At least one k value for low temperatures and another for high temperatures are required for doing such fitting. However, the value for the high temperatures can be assumed to be 1, if temperatures are much higher than the characteristic vibrational temperature, which is the energy of the first vibrational level in [K]. At these high temperatures, VV and VT relaxations become approximately equal, even for the lowest transitions at the lowest vibrational levels [18].

In other words, as the bulk gas temperature increases, T_g and T_v approach each other and at highly enough temperatures the discharge is thermalized by VT relaxation. Thus, the discharge is considered in equilibrium, $T_v = T_g$ and $k = 1$. With this assumption it is expected to obtain a fair approximation of the evolution of k for low bulk gas temperatures (lower than $\sim$ 1000 [K]), which is indeed the temperature range of interest for CO_2 dissociation.

For the reduction of the CO_2 STS kinetic model, it is assumed that $k = 6.0$ for a gas temperature of 300 [K] and $k = 1$ for a gas temperature of 5070 [K]. This temperature is 1.5 times the characteristic vibrational temperature of CO_2, which is 3380 [K]. The result of the fitting is shown in Figure 5.4, where it is seen how k approaches 1 as T_g increases.

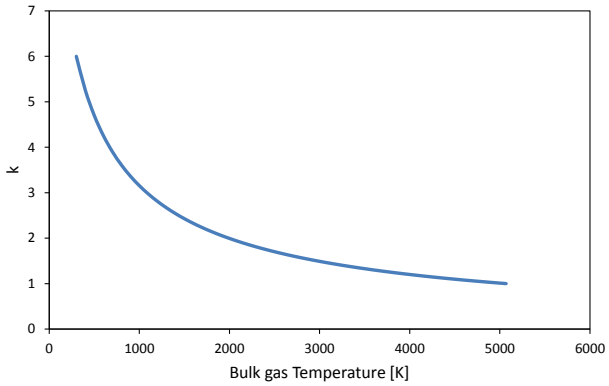

Figure 5.4: k factor for the reduction of the CO_2 STS kinetic model.

The equation for computing k is

$$k = 10936.7 \exp\left(\frac{-12.05}{T_g^{1/3}}\right) \times \frac{1}{T_g} \tag{5.5}$$

With this fitting the Treanor distribution becomes exclusively a function of T_g. The next step in the process is to compute the Treanor distributions in the temperature range between 300 and 1500 [K]. This is done in steps of 100 [K] by first computing the k factor, then the vibrational temperature and finally the Treanor distribution. The results for selected temperatures are shown in Figure 5.5, where the evolution of the initial Treanor distribution to a Boltzmann distribution is observed.

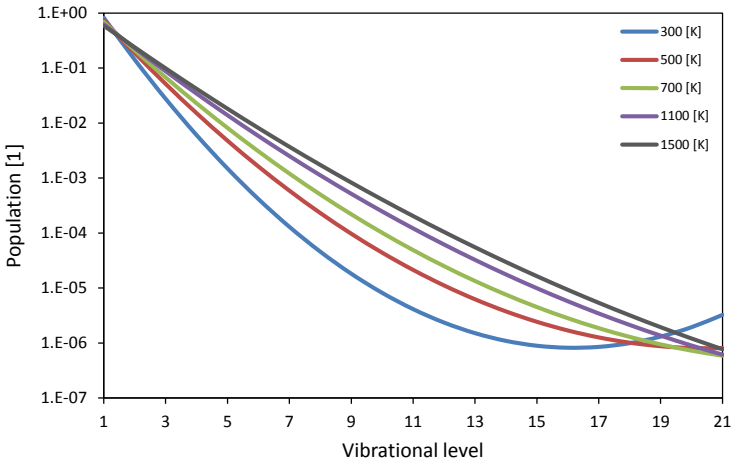

Figure 5.5: Treanor distributions for the reduction of the CO_2 STS kinetic model, $T_g = 300, 500, 700, 1100, 1500$ [K].

These distributions are used to compute averaged cross sections and constants rates for the reactions involving CO_2^*. The simplification process for each type of reaction is explained next.

5.5. ELECTRON ENERGY DISTRIBUTION FUNCTION

One of the most important simplifications in the reduced kinetic model is the assumption that the EEDF is Maxwellian, hence, it does not depend on the cross section data and is only a function of the mean electron energy. This assumption is also done in [14], where a comparison between a Maxwellian EEDF and a non-equilibrium EEDF is made for a mean electron temperature of $T_e = 1$ [eV].

The reason behind this assumption is that for mean electron temperatures between 0.5 and 2.0 [eV], which are typical for microwave discharges, the Maxwellian EEDF is similar to the non-equilibrium EEDF obtained by solving the Boltzmann equation. This is evident when comparing the Maxwellian EEDF of Figure 5.6a and the non-equilibrium EEDF of Figure 5.6b. Both were computed for the same process conditions and cross section database (Morgan database) by using the online BOLSIG+ solver [15], available at `www.lxcat.net`.

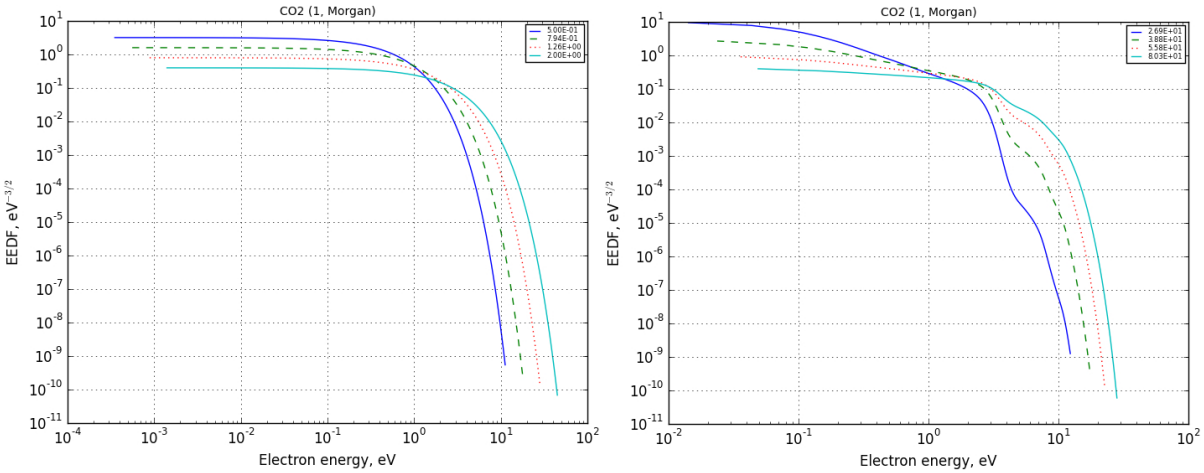

(a) Maxwellian EEDF

(b) Non-equilibrium EEDF

Figure 5.6: Electron energy distribution functions for $T_e = 0.5, 0.8, 1.3, 2.0$ [eV] ($E/N = 26.9, 38.8, 55.8, 80.3$ [Td], respectively), obtained with BOLSIG+ solver [15] at `www.lxcat.net`.

Furthermore, it is seen that the EEDF are very similar in the electron energy range of interest, i.e. between 0.1 and 10 [eV], where vibrational excitation of CO_2 takes place. This is better seen in Figures 5.7 and 5.8. In the former, both EEDFs are shown in the same scale and in the latter, the recommended cross sections for electron collisions with CO_2 are shown [17].

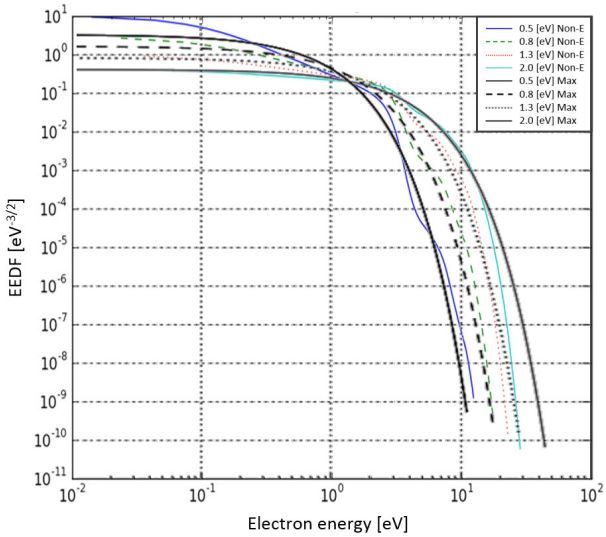

Figure 5.7: Comparison of Maxwellian and non-equilibrium EEDF for $T_e = 0.5, 0.8, 1.3, 2.0$ [eV].

With this assumption it is not required to include the complete set of cross sections to compute the EEDF, hence, the only cross sections to include in the reduced kinetic model are those with an important influence in the CO_2 dissociation kinetics.

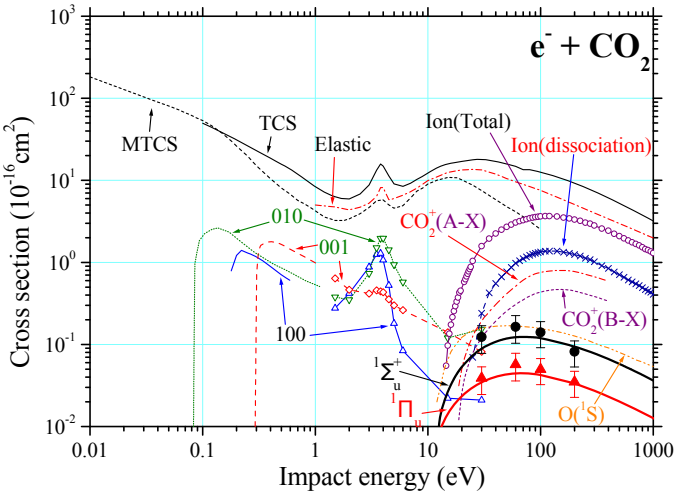

Figure 5.8: Cross sections for electron collisions with CO_2. Taken from [17].

5.6. ELECTRON IMPACT REACTIONS

As stated before, these reactions are the driving force of a plasma. In the case of microwave discharges, electrons gain energy from the electromagnetic field and transfer it to other species through collision processes. When these collisions take place, different reactions occur and the next step in the simplification process is to only include the collisions relevant to the CO_2 dissociation in non-thermal microwave discharges.

In these discharges the mean electron energies are lower than 3 [eV], i.e. mean electron temperatures lower than $T_e = 3 \times 2/3 = 2$ [eV], therefore, the Maxwellian distributions peak at electron energy values lower than 10 [eV] (see Figure 5.6a). For instance, in a Maxwellian distribution with a mean electron temperature of 2 [eV], 98% of the electrons have an energy lower than 10 [eV]. This means that almost all the electrons are in the range where elastic scattering and vibrational excitation take place (see Figure 5.8). It is important to remark than in this low energy range also rotational excitation takes place, however, as in [9], this energy mode is disregarded. The latter is a common practice for the gas temperatures considered here (300 - 1500 [K]), as it can be assumed that the rotational energy mode is in thermal equilibrium with the translational energy mode [3].

High reaction rates are expected for elastic scattering and vibrational excitation since the EEDF and the cross sections have large values at low electron energies. At higher electron energies the EEDF is considerably smaller and although the cross sections for some processes are large, their rate constants are orders of magnitude smaller than those in the low energy range. Therefore, in the high electron energy range only large cross sections are considered.

For electron energies higher than 10 [eV], it is seen in Figure 5.8 that besides the elastic scattering, the largest cross section is the total ionization cross section, which is the sum of all the collision processes that produce an additional electron. From all these processes, the single charge ionization of CO_2 has the largest cross section and the lowest energy threshold [41], which is the minimum energy required by the ionization process. This implies that higher ionization rates are obtained for the single charge ionization process when compared to dissociative ionization or multiple charge ionization processes. Indeed, for the range of mean electron energies considered here, the total ionization rate due to dissociative ionization or multiple charge ionization is at least two orders of magnitude smaller than the rate of ionization through single charge ionization, i.e. more than 98% of the electrons are produced by the non-dissociative single charge ionization process, see Figure 5.9. The other collision processes in the high energy range have smaller cross sections or don't have influence in the dissociation kinetics of CO_2. For these reasons, other electron collisions with CO_2 considered in [8] are not included here.

The outcome of the previous analysis is that elastic scattering, vibrational excitation and non-dissociative single charge ionization (hereafter ionization for simplicity) are the only collision processes of CO_2 to be included in the reduced kinetic model. The next step is to repeat this analysis in the remaining species of the reduced kinetic model, which are species with high population densities or species that participate in relevant processes.

According to the results of [8], CO, O, O_2 and O_3 are the main neutral products of CO_2 dissociation. Nev-

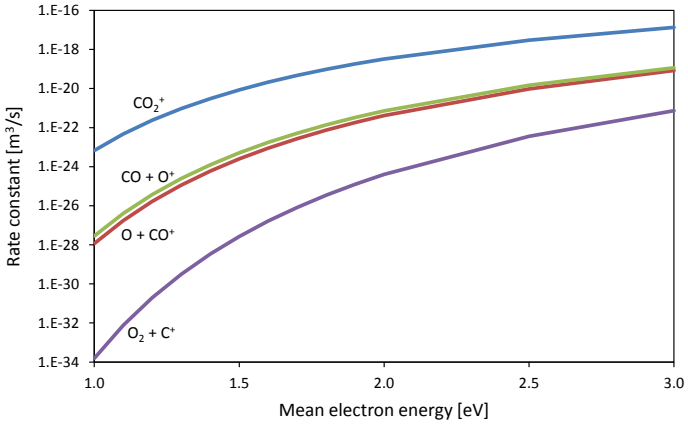

Figure 5.9: Rate constants of the main products in the electron impact ionization of CO_2 for a Maxwellian EEDF. Computed with COMSOL Multiphysics, using the Boltzmann equation two-term approximation Interface.

ertheless, the population density of O_3 is at least two orders of magnitude less than that of O_2 and at least three orders of magnitude less than the one CO_2, therefore it is no included in the kinetic model. One can argue that at some point its population density is comparable to that of O, however, O_3 has no influence in the CO_2 dissociation kinetics (it is mostly formed in the afterglow), whereas O plays a crucial role in the CO_2 dissociation kinetics (see section 5.7).

By carefully analyzing the cross section data of CO, O_2 and O, given in [17, 42–46], together with the electron impact reactions included in [8], the same relevant processes are obtained. In other words, elastic scattering, vibrational excitation and ionization processes should be also considered for these species in the reduced model. Further simplifications are possible, thus, each of these processes is evaluated for each of the species.

It is important to remark that the electronic excitation process is also neglected for CO, O_2 and O, even though it has lower energy thresholds than for CO_2. Electronically excited species have no influence in the CO_2 dissociation kinetics at the lower mean electron energies considered here, therefore, they are not included in the reduced kinetic model. In [8], this process was included to account for its effect in the EEDF, however, it is assumed here that the EEDF is mainly determined by CO_2 and it is approximated to a Maxwellian EEDF.

Assuming a quasi-neutral discharge with an ionization degree around 10^{-5} [8], the mass fractions of charged species are at least 5 orders of magnitude smaller than neutrals, therefore, electron impact reactions of charged species are not considered. In the case of electron collisions with vibrationally excited states, the same approach of [8] is used. Accordingly, electron impact reactions are only considered for the asymmetric vibrationally excited states $CO_2\,v_i$, here represented by CO_2^*. No reason is given on why this was done, but presumably it is based on the fact that even for the lowest symmetric levels, the VT relaxation rates are comparable to the electron impact vibrational excitation rates and therefore short lifetimes are expected.

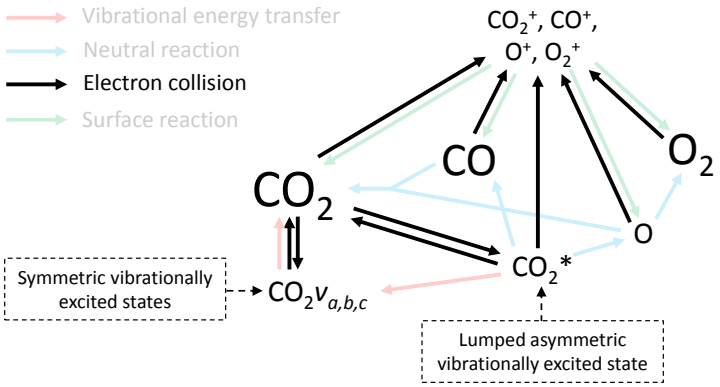

Figure 5.10: Schematic of the electron impact reactions included in the reduced kinetic model.

Figure 5.10 shows the electron impact reactions included in the reduced kinetic model. In summary, the processes and the additional simplifications are:

- Elastic scattering (RX1-5): No additional simplifications are possible. One elastic scattering reaction is included for each of CO_2, CO, O, O_2 and CO_2^*. As in [8], for the asymmetric levels, here represented by CO_2^*, the same cross section of CO_2 is assumed.

- Electron impact ionization (RX6-10): The electrons required to sustain the plasma are produced in this process. Electron impact reactions are included for CO_2, CO, O, O_2 and CO_2^*. As in [8], the same cross section of CO_2 is assumed for CO_2^*.

- Vibrational excitation (RX11-13): This is the main energy transfer channel from electrons to the CO_2 molecule in the considered range of mean energies (see Figure 3.3). Vibrational excitation reactions are only included for CO_2, as it has been reported that the energy transfer to vibrational modes of other neutrals is considerably small [8]. Therefore, it is concluded that the internal energy modes are only considered for CO_2.

  Electron impact vibrational excitation reactions are included for the first level of each symmetric vibrational mode of CO_2 ($CO_2\,v_a$ and $CO_2\,v_b$), as well as for the lumped asymmetric vibrational mode CO_2^*. For the latter, a lumped cross section is computed in subsection 5.6.1. As opposed to [8], electron impact vibrational excitation reactions for higher symmetric levels ($CO_2\,v_c$ and $CO_2\,v_d$, see Figure 3.2) are not included here, since the cross sections for multiquantum vibrational jumps are smaller than for single quantum vibrational jumps.

  The reverse process of the vibrational excitation (vibrational de-excitation or superelastic collision) is also included in the reduced kinetic model. The cross sections for this process are computed by using the detailed balancing principle [12]

$$g_1\varepsilon_1\sigma_{12}(\varepsilon_1) = g_2\varepsilon_2\sigma_{21}(\varepsilon_2) \tag{5.6}$$

  where g_1 and g_2 are the statistical weights of states 1 and 2 (also called degeneracies), σ_{12} is the cross section for the excitation from the state 1 to state 2, σ_{21} the cross section for the reverse process (superelastic collision), ε_1 and ε_2 are the electron energies before and after the excitation process. These are related by $\varepsilon_1 = \varepsilon_2 - \Delta\varepsilon_{12}$, where $\Delta\varepsilon_{12}$ is the energy lost by the electron in the process (energy threshold).

A total of 16 electron impact reactions are included, they are presented in Table 5.2 together with the sources for their cross sections.

Table 5.2: Electron impact reactions included in the reduced kinetic model.

No.	Process	Reaction	Cross section
(RX1)	CO_2 Elastic scattering	$e + CO_2 \rightarrow e + CO_2$	[41]
(RX2)	CO_2^* Elastic scattering	$e + CO_2^* \rightarrow e + CO_2^*$	Same as (RX1)
(RX3)	CO Elastic scattering	$e + CO \rightarrow e + CO$	[42, 43]
(RX4)	O Elastic scattering	$e + O \rightarrow e + O$	[43]
(RX5)	O_2 Elastic scattering	$e + O_2 \rightarrow e + O_2$	[45]
(RX6)	CO_2 Ionization	$e + CO_2 \rightarrow e + e + CO_2^+$	[41]
(RX7)	CO_2 Ionization from CO_2^*	$e + CO_2^* \rightarrow e + e + CO_2^+$	Same as (RX6)
(RX8)	CO Ionization	$e + CO \rightarrow e + e + CO^+$	[42]
(RX9)	O Ionization	$e + O \rightarrow e + e + O^+$	[44]
(RX10)	O_2 Ionization	$e + O_2 \rightarrow e + e + O_2^+$	[45]
(RX11)	Vibrational (de)excitation to $CO_2\,v_a$	$e + CO_2 \leftrightarrow e + CO_2\,v_a$	[41]
(RX12)	Vibrational (de)excitation to $CO_2\,v_b$	$e + CO_2 \leftrightarrow e + CO_2\,v_b$	[41]
(RX13)	Vibrational (de)excitation to CO_2^*	$e + CO_2 \leftrightarrow e + CO_2^*$	Subsection 5.6.1

5.6.1. CROSS SECTION FOR THE VIBRATIONAL EXCITATION FROM CO_2 TO CO_2^*

The cross section for the vibrational excitation from CO_2 to CO_2^* must include all the vibrational excitation processes in the asymmetric vibrational mode, from a lower to a higher level, including level 0 (CO_2). Thus, the cross section considers all the vibrational excitation processes that increase the energy or population of CO_2^*. Vibrational de-excitation cross sections are not computed for each specific transition, instead, an averaged de-excitation cross section is computed from the averaged vibrational excitation cross section by using the detailed balancing principle (equation 5.6).

The calculation of the cross section for the vibrational excitation from CO_2 to CO_2^* starts by considering the total electron impact vibrational excitation rate from a level i to a level j, this is

$$k_{i,i+1} n_i n_e + \ldots + k_{i,21} n_i n_e = n_i n_e \sum_{j=i+1}^{21} k_{i,j} \tag{5.7}$$

where n_i is the population density of vibrational level i, n_e is the population density of electrons and $k_{i,j}$ is the rate coefficient for the vibrational excitation from level i to level j, which is computed from the cross section with equation 2.3. Therefore, the total electron impact vibrational excitation rate from a level i to a level j reduces to a sum of the cross sections

$$n_i n_e \sum_{j=i+1}^{21} k_{i,j} = n_i n_e \gamma \int_0^\infty \varepsilon \sigma_{iv}(\varepsilon) f(\varepsilon) \mathrm{d}\varepsilon \tag{5.8}$$

with

$$\sigma_{iv}(\varepsilon) = \sum_{j=i+1}^{21} \sigma_{i,j}(\varepsilon) \tag{5.9}$$

All the cross sections for the excitation from any level i to a higher level j are not available, hence, they are computed by using the Fridman's approximation [3]. In this approximation, the cross section of the lowest transition, from level 0 to level 1, is scaled to higher transitions by using the following expression

$$\sigma_{i,j}(\varepsilon + E_{i,j} - E_{0,1}) = \sigma_{0,1}(\varepsilon) \exp\left(\frac{-\alpha\left(j - i - 1\right)}{1 + \beta i}\right) \tag{5.10}$$

where $E_{i,j} = E_j - E_i$ is the energy difference between levels j and i, α and β are scaling factors. For the specific case of CO_2 the former takes the value of 0.5 and the latter is assumed to be 0 [3, 9]. This approximation is used to compute all the transitions from level i, which are subsequently added to obtain σ_{iv}. Figure 5.11 shows the result for the specific case of $i = 0$. The cross section's magnitude increases as a consequence of adding the cross sections of multiquantum vibrational jumps, while the discrete energy levels explain the presence of multiple peaks. The values of $\sigma_{0,1}(\varepsilon)$ used in the calculations are taken from [41].

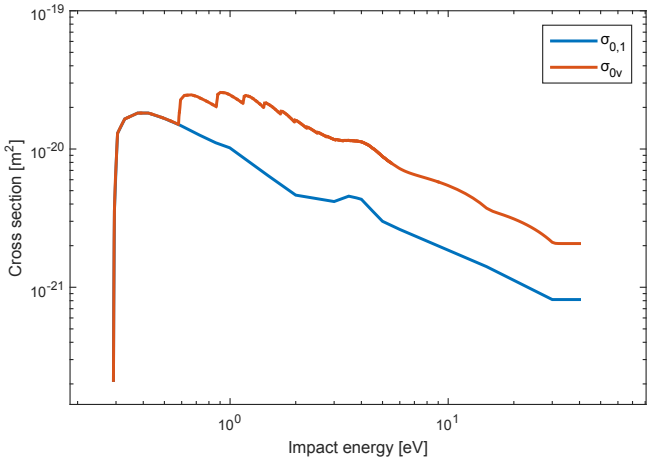

Figure 5.11: Total cross section for purely asymmetric vibrational excitation from level 0.

The total electron impact vibrational excitation rate is a sum of the vibrational excitation rates of all levels (equation 5.8), thus

$$\sum_{i=0}^{20}\left(n_i n_e \sum_{j=i+1}^{21} k_{i,j}\right) = n_e\gamma \sum_{i=0}^{20}\int_0^{\infty} \varepsilon n_i \sigma_{iv}(\varepsilon) f(\varepsilon)\mathrm{d}\varepsilon \tag{5.11}$$

It is also possible to express the previous equation in terms of relative populations n_i/n_0 and calculate the total cross section for the vibrational excitation processes

$$\sum_{i=0}^{20}\left(n_i n_e \sum_{j=i+1}^{21} k_{i,j}\right) = n_0 n_e\gamma \int_0^{\infty} \varepsilon \sigma_V(\varepsilon) f(\varepsilon)\mathrm{d}\varepsilon \tag{5.12}$$

where $\sigma_V(\varepsilon)$ is the cross section for the excitation from CO_2 to CO_2^*, reaction (RX13) of table 5.2, and is computed as follows

$$\sigma_V(\varepsilon) = \sum_{i=0}^{20} \frac{n_i}{n_0}\sigma_{iv}(\varepsilon) \tag{5.13}$$

where $\sigma_{iv}(\varepsilon)$ are computed from equation 5.9 and the populations of the vibrational levels are computed from the Treanor distribution, equation 2.6. These populations are functions of T_v, which through equations 5.3 and 5.5 is assumed to be a function of the bulk gas temperature T_g, and therefore, the cross section $\sigma_{iv}(\varepsilon)$ is also a function of T_g.

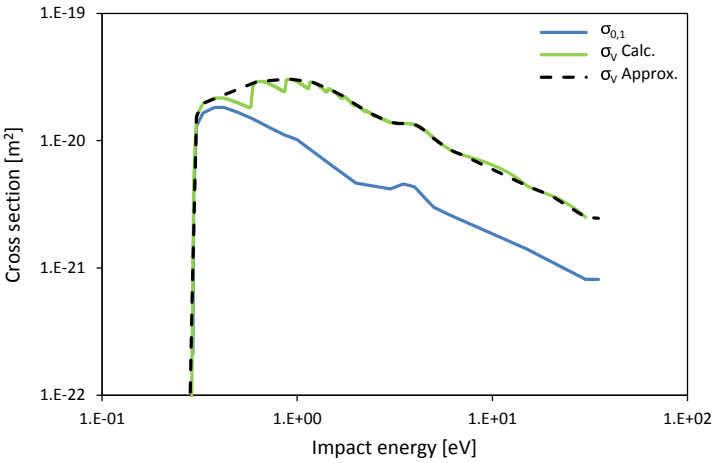

Figure 5.12: Cross section for the vibrational excitation from CO_2 to CO_2^*, for $T_g = 300$ [K].

A MATLAB script was developed to perform the calculations, the result for $T_g = 300$ [K] is shown in Figure 5.12. By comparing this figure with Figure 5.11 is it seen that σ_V is larger than σ_{0v}, although the difference is not large. The peaks don't vanish in the summation process and are clearly visible. For simplicity, the cross section used in the kinetic model is the envelope of the calculated σ_V. This is mainly done to keep a limited number of points to describe the cross section and to preserve the same shape of the specific levels transitions. Besides, the cross section area included by this approximation is a small value of the total cross section's area, hence, no big impact in the rate of vibrational excitation is expected. The minimum energy difference between consecutive levels is assumed to be the energy threshold of the process, which in this case takes the value of $E_{21} - E_{20} = 0.23$ [eV].

The calculations are repeated for selected temperatures in the range between 300 to 1500 [K], the results are shown in Figure 5.13. It is seen in this figure that by increasing T_g the cross sections increase in magnitude, albeit keeping the same shape and energy threshold. Therefore, it is possible to compute the cross sections for higher temperatures from the cross section of the lowest temperature 300 [K]. A scaling factor ϕ is computed from the MATLAB results and is used in the following expression to compute the approximated cross section (envelope) for higher bulk gas temperatures

$$\sigma_V(T_g) = \phi(T_g)\sigma_V(300) \tag{5.14}$$

The ϕ values used in the calculations are given in Table 5.3 and the scaled cross sections are shown in Figure 5.13, where the good agreement between these and the MATLAB results is evident.

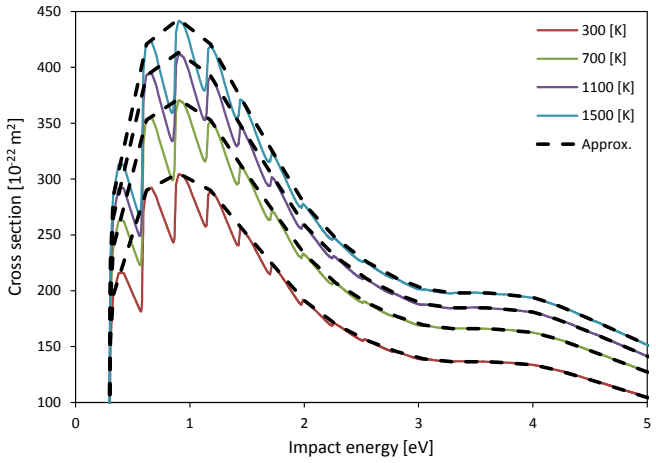

Figure 5.13: Cross section for the vibrational excitation from CO_2 to CO_2^*, for $T_g = 300, 700, 1100, 1500$ [K].

The evolution of ϕ with the bulk gas temperature is shown in Figure 5.14. Although a fit of this function seems reasonable, it is not proposed in this kinetic model. The reason for not doing so relies in the software used for the validation of the reduced kinetic model, as it does not allow variable cross sections. Nonetheless, in Chapter 6 it will be shown that the impact of this scaling factor is small for bulk gas temperature changes around 200 [K]. An average factor for the discharge is used instead.

Table 5.3: Values of the scaling factor ϕ for different bulk gas temperatures.

T_g [K]	300	500	700	900	1100	1300	1500
ϕ	1.00	1.12	1.22	1.29	1.35	1.41	1.45

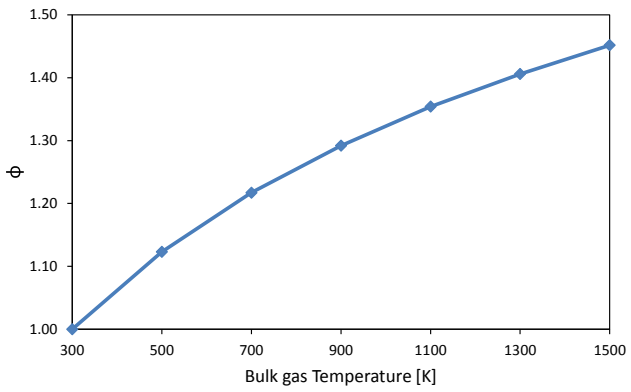

Figure 5.14: ϕ as a function of the bulk gas temperature.

5.7. REACTIONS OF NEUTRAL SPECIES

The energy transferred from the electrons to the lumped excited state CO_2^* can either be used to facilitate its dissociation or be transferred to the bulk gas as heat. The former leads to the production of CO and O, which can recombine to form CO_2 again. In addition, the produced O atoms can also recombine to form O_2. These three are the main processes considered for the reactions of neutrals.

The STS kinetic model [8] includes additional processes (see Table 4.3), which involve C, C_2O and O_3. The reasons for neglecting these processes are the very low population density of these species and the low rates of the reactions in which they take part. Furthermore, these species have practically no influence in the dissociation kinetics of CO_2, as pointed out for O_3 in section 5.6.

The results of [8] suggest that the population densities of C and C_2O are at least 5 orders of magnitude smaller than the same of CO_2 and this can be easily explained by the low rates at which these species are produced. C atom is only produced by dissociative ionization electron collisions (see Table 4.2) and CO dissociation by neutrals collisions (see Table 4.3). The arguments for not including the former are given in section 5.6, whereas for the latter an easy calculation gives a reaction rate around 20 orders of magnitude smaller than an included reaction involving the same reactants (comparing (N4) and (N9) of Table 4.3 at T_g = 800 [K]). These neutrals collisions were included in [8] to account for the reduction of its activation energy by effect of vibrationally excited CO, however, this was not considered in the reduced kinetic model. Lastly, the C atom is also the precursor of C_2O (see Table 4.3), thus, this is not included either.

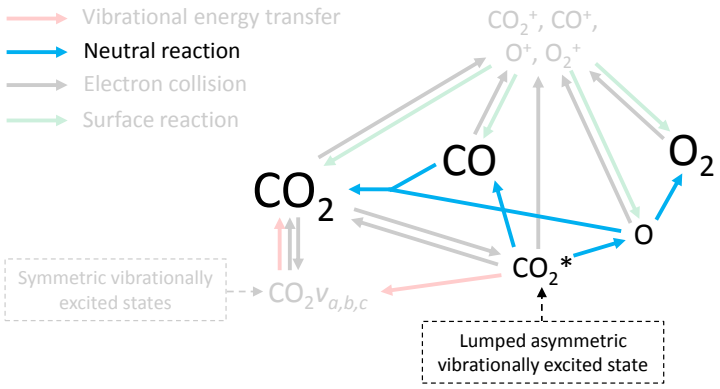

Figure 5.15: Schematic of the reactions of neutrals included in the reduced kinetic model.

The reactions of neutrals are then limited to the ones involving CO_2, CO, O and O_2, this is depicted in Figure 5.15. In summary, the included processes are:

- CO_2 dissociation (RN1,2): Effectively achieved in collisions between neutrals and high asymmetric vibrationally excited states of CO_2. The lumped excited state CO_2^* is therefore considered for this process and reactions for the collisions with CO_2, CO, O_2 and O are included. CO_2 dissociation reactions from its vibrational ground state ($v = 0$) are not included since their activation energies are high, giving very low reaction rates in comparison with those of CO_2 dissociation through the lumped excited state CO_2^*.
- CO and O recombination (RN3,4): Recombination of CO and O to form CO_2. The reactions included for this process are the three-body recombination involving CO_2, CO or O_2 as the third body, and the reaction between CO and O_2. In [8] these reactions are enhanced by the vibrational excitation of CO, however, this is neglected here and the rate constants for the vibrational ground state are used.
- O recombination (RN5): Oxygen atoms produced in the dissociation of CO_2^* can recombine to form the more stable O_2 molecule. This is attained through a three-body reaction between two O atoms and CO_2, CO or O_2 as the third body.

The rate constant of each dissociation reaction is determined by first computing the rate constant for each asymmetric vibrational level at a defined bulk gas temperature. As in [8], the Fridman-Macheret α-Model is used to estimate the efficiency in the reduction of the activation energy due to vibrational excitation. The rate constants are then multiplied by the corresponding population densities, computed from the Treanor distribution at the same bulk gas temperature, and added to find an averaged rate constant.

This process is repeated for the whole temperature range of interest, 300 - 1500 [K], and the results are fitted to a modified Arrhenius type equation to find a single temperature dependent expression for the rate constant of the CO_2^* dissociation reaction. There is, however, a small difference in the calculation of rate constants for reaction (RN1) and (RN2).

A total of 11 reactions of neutrals are included, they are presented in Table 5.4 together with their rate constants.

5.7.1. RATE CONSTANT FOR REACTION (RN1)

The calculation process for this rate constant starts by computing the rate constant for each vibrationally excited state within CO_2^*, at a specific temperature T_g. For this purpose the following expression is used [47]

Table 5.4: Reactions of neutrals included in the reduced kinetic model. M = CO_2, CO, O_2. Gas temperature T_g in [K] and rate constants in [cm^3/s] and [cm^6/s] for binary and ternary reactions, respectively.

No.	Process/Reaction	Rate constant
(RN1)	CO_2^* Dissociation by collisions with CO_2, CO and O_2	
	$CO_2^* + M \rightarrow CO + O + M$	$9.59 \times 10^{-16}\ (T_g/300)^{2.921}\ \exp(639/T_g)$
(RN2)	CO_2^* Dissociation by collisions with O	
	$CO_2^* + O \rightarrow CO + O_2$	$3.35 \times 10^{-14}\ (T_g/300)^{1.465}\ \exp(-271/T_g)$
(RN3)	Three-body CO and O recombination	
	$CO + O + M \rightarrow CO_2 + M$	$8.2 \times 10^{-34}\ \exp(-1510/T_g)$
(RN4)	Two-body CO and O recombination	
	$CO + O_2 \rightarrow CO_2 + O$	$1.23 \times 10^{-12}\ \exp(-12800/T_g)$
(RN5)	Three-body O recombination	
	$O + O + M \rightarrow O_2 + M$	$1.27 \times 10^{-32}(T_g/300)^{-1}\ \exp(-170/T_g)$

$$k_v(E_v, T_g) = A\ \exp\left(-\frac{E_a - \alpha E_v}{T_g}\right) \tag{5.15}$$

where A is the conventional pre-exponential factor, E_a is the activation energy of the reaction in [K], E_v is the vibrational energy of level v in [K], T_g is the bulk gas temperature in [K] and α is the efficiency of the vibrational energy in reducing the activation energy. The α values are taken from [9] (see Table 4.3), which were estimated by the Fridman-Macheret α-Model [3].

The energy levels in [K] of the asymmetric vibrational mode are listed in Table 5.5. For reaction (RN1), the pre-exponential factor is 4.39×10^{-7} [cm^3/s], the activation energy is $E_a = 65000$ [K] and α takes the value of 1.0 (see Table 4.3). Figure 5.16 shows the rate constant as a function of the vibrational level, at bulk gas temperatures of 300, 700 and 1100 [K]. The large variation of the rate constant with the vibrational level is evident, for instance, at 300 [K] the rate constant for level 0 (CO_2) is more than 80 orders of magnitude smaller than for level 21. Although for high temperatures the difference becomes smaller, at 1500 [K] it is still of ~20 orders of magnitude, hence, the dissociation from level 0 (CO_2) is neglected.

Table 5.5: Energy levels in [K] of the asymmetric vibrational mode (0 0 v)

Level, v	Energy, E_v	Level, v	Energy, E_v
0	0	11	35205
1	3380	12	38191
2	6724	13	41140
3	10032	14	44053
4	13304	15	46931
5	16541	16	49773
6	19741	17	52578
7	22906	18	55348
8	26035	19	58082
9	29127	20	60780
10	32184	21	63443

The averaged rate constant for CO_2^* at a specific bulk gas temperature is computed by adding the individual contributions of the lumped vibrational levels ($v = 1-21$), which are computed from their individual rate constants and populations. The latter are computed from the Treanor distribution at the same bulk gas temperature T_g.

$$k(T_g) = \sum_{v=1}^{21} n_v(T_g) k_v(E_v, T_g) \tag{5.16}$$

This calculation is repeated for the whole temperature range in steps of 100 [K], $T_g = 300, 400, \ldots, 1500$ [K], and the results are shown in Figure 5.17. By comparing this figure with Figure 5.16 it is seen that the averaged

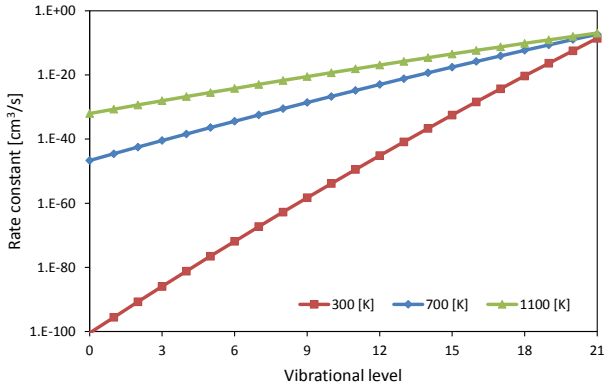

Figure 5.16: Rate constant of CO_2 dissociation through collisions with CO_2, CO and O_2, as a function of the asymmetric vibrational level, at bulk gas temperatures of $T_g = 300, 700, 1100$ [K].

rate constants are closer to the individual rate constants of the highest levels, as a consequence of their high population in the Treanor distribution. The results are also fitted to a modified Arrhenius equation to obtain the expression given in Table 5.4, which is only a function of the bulk gas temperature.

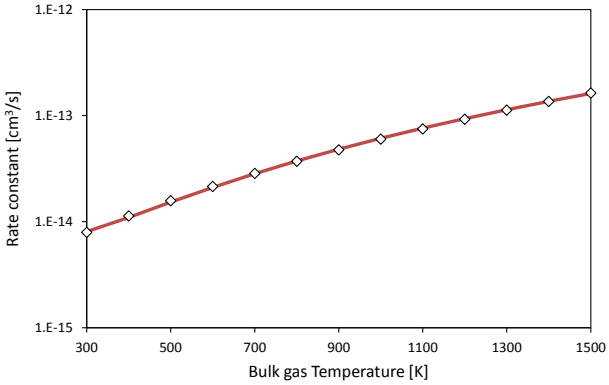

Figure 5.17: Rate constant of reaction (RN1) as a function of the bulk gas temperature.

5.7.2. RATE CONSTANT FOR REACTION (RN2)

The rate constant for this reaction is computed in a similar way as done for reaction (RN1), however, due to a difference in the value of α a correction is needed at the end of the process. Equation 5.15 is also used for the calculation of the individual rate constants at specific bulk gas temperatures, although in this case the pre-exponential factor is 7.77×10^{-12} [cm^3/s], the activation energy is $E_a = 16600$ [K] and α takes the value of 0.5 (see Table 4.3).

Figure 5.18 shows the rate constant as a function of the vibrational level, at bulk gas temperatures of 300, 700 and 1100 [K]. In this reaction the difference in rate constants between level 0 and higher levels is smaller than in (RN1), however it is still large at the low bulk gas temperatures where efficient dissociation takes place (<700 [K]) [8]. Hence, the dissociation from level 0 (CO_2) is also neglected for this reaction.

By comparing Figures 5.16 and 5.18 a difference is noticed in the rate constant variation of reactions (RN1) and (RN2) as the vibrational level increases. Reaction (RN1) is an endothermic reaction with a high activation energy, which is not completely reduced even for the highest vibrational level, whereas reaction (RN2) is a thermoneutral reaction with an activation energy that vanishes at vibrational levels higher than 10. This characteristic clearly divides the behavior of the rate constant into two groups. In the first one ($0 < v \leq 10$) the rate constant increases exponentially with the vibrational level, while in the second ($10 < v \leq 21$) the rate constant remains constant. To deal with this difference the following correction is proposed for the calculation of the averaged rate constant for CO_2^* at a specific bulk gas temperature

$$\ln k(T_g) = \frac{v_1}{v_2} \ln k_1(T_g) + \frac{v_2 - v_1}{v_2} \ln k_2 \tag{5.17}$$

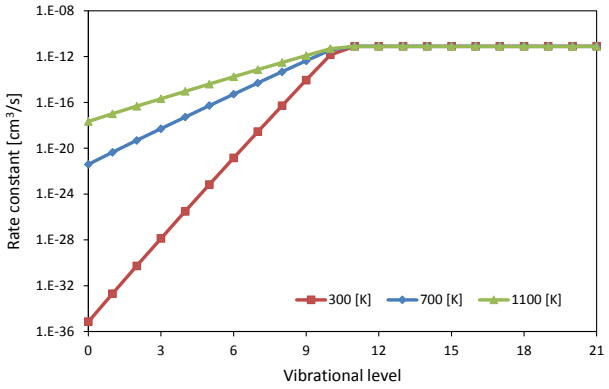

Figure 5.18: Rate constant of CO_2 dissociation through collision with O, as a function of the asymmetric vibrational level, at bulk gas temperatures of $T_g = 300, 700, 1100$ [K].

where k_1 is the averaged rate constant of the first group ($0 < v \leq v_1$) and k_2 is the rate constant of the second group ($v_1 < v \leq v_2$). The former is computed as in equation 5.16, although with v_1 as the upper summation bound. The later reduces to the the pre-exponential factor 7.77×10^{-12} [cm^3/s] and is not a function of T_g.

The calculation is repeated for the whole temperature range in steps of 100 [K], $T_g = 300, 400, \ldots, 1500$ [K], the results are shown in Figure 5.19, where k_1 and k_2 are also shown for reference. It is seen in the figure that the averaged rate constants are between the rate constants of the groups k_1 and k_2. The values of k are also comparable to the averaged rate constants of reaction (RN1) and are closer to the individual rate constants of the highest levels, as expected. The results are also fitted to a modified Arrhenius equation to obtain the expression given in Table 5.4.

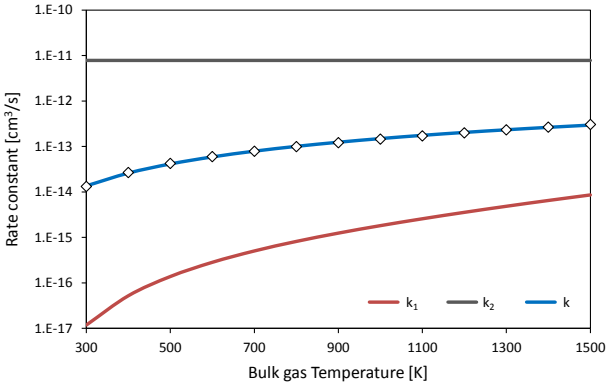

Figure 5.19: Rate constant of reaction (RN2) as a function of the bulk gas temperature. Rate constants k_1 and k_2 are also shown for reference.

5.8. VIBRATIONAL ENERGY TRANSFER REACTIONS

Vibrationally excited states of species different than CO_2 are not considered in the reduced kinetic model, since the energy transfer to their vibrational modes is considerably small [8]. Hence, the vibrational energy transfer reactions are limited to reactions involving solely CO_2, $CO_2\,v_i$ and the excited states of the symmetric vibrational modes, $CO_2\,v_{a,b,c}$. The higher symmetric level $CO_2\,v_d$ is also included as a separate species in [8], although it does not take part in any of their vibrational energy transfer reactions. It is indeed, for this reason, that this species is not included in the reduced kinetic model.

In the CO_2 STS kinetic model the VT, VV' and VV relaxation processes of $CO_2\,v_i$ and $CO_2\,v_{a,b,c}$ are accounted for in reactions (V1), (V2a,b,c), (V5a,b) and (V6) of Table 4.4. However, the asymmetric vibrationally excited states $CO_2\,v_i$ are lumped into CO_2^* and their distribution is assumed to follow the Treanor distribution, hence, there is no need and no interest in including the VV relaxation process. The VT and VV' relaxation processes are included to account for the transfer of vibrational energy from the asymmetric mode to the symmetric and translational modes.

Thus, the lumped excited state CO_2^* can either dissociate through reactions of neutrals or transfer its vibrational energy through VT and VV' relaxation. Most of this energy is first transferred to the symmetric vibrationally excited states, which subsequently transfer the energy to the translational mode. In any case, the energy is ultimately transferred to the CO_2 and instead of being used in the dissociation process it is lost in heating the bulk gas.

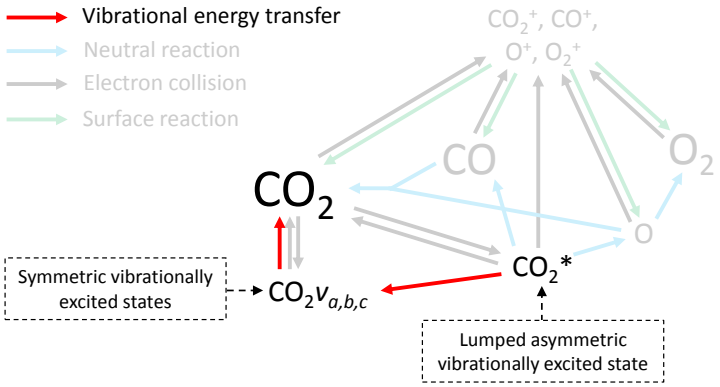

Figure 5.20: Schematic of the vibrational energy transfer reactions included in the reduced kinetic model.

Figure 5.20 shows the vibrational energy transfer reactions included in the reduced kinetic model. It is evident that the outcome of these processes is the energy loss from the lumped excited state to the bulk gas. In summary, the included processes are:

- VT Relaxation of symmetric vibrationally excited states (RV1): In this process, a symmetric vibrationally excited state $CO_2\,v_{a,b,c}$ loses its vibrational energy in a collision with a neutral ground state. Reactions involving CO_2, CO and O_2 as the collision partner are included for each of the symmetric vibrationally excited states. The rate constants are taken from [8] and the reverse reactions are not considered, as was also the case in [9]. The symmetric vibrationally excited states are mostly produced by electron collisions and vibrational energy transfer reactions of CO_2^*, rather than the reverse process of this reaction.

- VT Relaxation of the lumped asymmetric vibrationally excited state (RV2): This process is equivalent to the previous, although for the asymmetric vibrational mode, represented by CO_2^*. In this case, however, a fraction of the vibrational energy is transferred to the symmetric vibrational modes $CO_2\,v_{a,b,c}$. Reactions are included for CO_2, CO and O_2 as the collision partner and the rate constants are computed in subsection 5.8.1.

  These reactions are "lumped" reactions of the analogous (V2a,b,c) of Table 4.4. The reverse reactions are not included, since in this process an asymmetric vibrational level $v > 1$ relaxes to an asymmetric level with a symmetric sublevel, e.g. (0 0 6) → (0 1 5), which is assumed to subsequently relax its symmetric vibrational energy to obtain a purely asymmetric level, e.g. (0 1 5) → (0 0 5) [9]. The rate constants for reactions (V2a,b,c) are given for the combined process, e.g. (0 0 6) → (0 0 5), which is not a direct process and therefore the detailed balancing principle is not applicable.

  Furthermore, for the non-equilibrium conditions assumed inside CO_2^*, the forward reaction is faster than the reverse reaction. This process is taking these vibrationally excited states back to thermal equilibrium, instead of moving them further away from it.

- VV' Relaxation between symmetric and asymmetric vibrationally excited states (RV3): In this process, the lumped excited state CO_2^* collides with a CO_2 molecule and transfers a fraction of its vibrational energy to the symmetric modes of the CO_2 molecule. In other words, a CO_2 molecule gets vibrationally excited to $CO_2\,v_{a,b}$ in a collision with the lumped excited state CO_2^*. One single reaction is included for this process and its rate constant is computed in subsection 5.8.2.

  This reaction is the "lumped" reaction of the analogous (V5a,b) of Table 4.4. As in the previous case, an asymmetric vibrational level $v > 1$ relaxes to an asymmetric level with a symmetric sublevel, which subsequently relaxes its symmetric vibrational energy. The rate constants for reactions (V5a,b) are given

for the combined process, hence, the detailed balancing principle is not applicable and the reverse reactions are not included.

A total of 13 vibrational energy transfer reactions are included, they are presented in Table 4.8 together with their rate constants.

Table 5.6: Vibrational energy transfer reactions included in the reduced kinetic model. M = CO_2, CO, O_2. Gas temperature T_g in [K].

No.	Process/Reaction	Rate constant [cm^3/s]
(RV1)	VT Relaxation of symmetric vibrationally excited states. $x = a, b, c$.	
	$CO_2\,v_x + M \rightarrow CO_2 + M$	$7.14\times10^{-8}\exp(-177\,T_g^{-1/3} + 451\,T_g^{-2/3})$
	$M = CO_2$	$\times 1$
	$M = CO, O_2$	$\times 0.7$
(RV2)	VT Relaxation of the lumped asymmetric vibrationally excited state.	
	$CO_2^* + M \rightarrow \nu_{l2}CO_2^* + \nu_{s2}(CO_2\,v_a + CO_2\,v_b + CO_2\,v_c) + M$	
	$M = CO_2$	$4.72\times10^{-17}\,(T_g/300)^{6.547}\exp(1289/T_g)$
	$M = CO$	$1.47\times10^{-17}\,(T_g/300)^{6.531}\exp(1282/T_g)$
	$M = O_2$	$1.95\times10^{-17}\,(T_g/300)^{6.532}\exp(1282/T_g)$
(RV3)	VV' Relaxation between symmetric and asymmetric vibrationally excited states.	
	$CO_2^* + CO_2 \rightarrow \nu_{l3}CO_2^* + \nu_{s3}(CO_2\,v_a + CO_2\,v_b)$	$3.99\times10^{-15}\,(T_g/300)^{4.462}\exp(398/T_g)$

The rate constants of reactions (RV2) and (RV3) are determined in a similar fashion as done for the reactions of neutrals. The energy change in reactions (V2a,b,c) and (V5a,b) are fitted to diatomic anharmonic oscillator models and the anharmonicity coefficients are computed. These are needed to scale the rate constants of the lowest transitions to higher transitions at specific bulk gas temperatures.

Finally, the results for different temperature values in the range between 300 and 1500 [K], are fitted to modified Arrhenius type equations. A particular characteristic of these reactions is that the stoichiometric coefficients also depend on the Treanor distribution, which in turn depends on the bulk gas temperature.

5.8.1. RATE CONSTANT FOR REACTION (RV2)

The calculation process for this rate constant starts by computing the rate constant of reactions (V2a,b,c) for each vibrationally excited state within CO_2^*, for a specific temperature T_g. For this purpose, the approach used in [9] is adopted here. It is required first to understand how these reactions scale to higher vibrational levels, as well as the assumptions made to simplify this relaxation process.

Reactions (V2a,b,c) are the VT relaxation of a purely asymmetric vibrational level v into an lower asymmetric vibrational level $v-1$ with a symmetric sublevel a, b, c, respectively (see Figure 3.2). This is,

$$\begin{aligned} CO_2(0\,0\,v) + M &\rightarrow CO_2(0\,1\,v-1) + M \quad \text{(V2a)} \\ &\rightarrow CO_2(0\,2\,v-1) + M \quad \text{(V2b)} \\ &\rightarrow CO_2(0\,3\,v-1) + M \quad \text{(V2c)} \end{aligned}$$

However, it is assumed that these symmetric sublevels are rapidly relaxed through additional VT relaxation and become in thermal equilibrium with $(0\,0\,v)$ [9]. Thus, although for an asymmetric vibrational level $v > 1$ the reactions (V2a,b,c) are scaled as reactions of purely asymmetric vibrational levels

$$CO_2(0\,0\,v) + M \rightarrow CO_2(0\,0\,v-1) + M \quad \text{(V2a,b,c)}$$

These are not direct processes and consist of multiple VT relaxation reactions, in which the first process is assumed to be the rate limiting step [48]

$$\left.\begin{aligned} CO_2(0\,0\,v) + M &\rightarrow CO_2(0\,1\,v-1) + M \\ &\rightarrow CO_2(0\,2\,v-1) + M \\ &\rightarrow CO_2(0\,3\,v-1) + M \end{aligned}\right\} \xrightarrow{\text{VT Relaxation}} CO_2(0\,0\,v-1) + M \quad \begin{aligned} &\text{(V2a)} \\ &\text{(V2b)} \\ &\text{(V2c)} \end{aligned}$$

This implies that the symmetric sublevels must be considered when computing the change of energy in the reactions, even if it is assumed for simplicity that the reactions for $v > 1$ solely involve asymmetric levels

[48]. For the sake of brevity, the rate constant calculation is only explained for reaction (V2a), although it also applies to the other reactions.

The rate constants are scaled by using expressions derived from the SSH theory [49, 50], which was developed for the collision of diatomic anharmonic oscillators. Therefore, as an approximation, this expression is used for scaling the reaction rates of CO_2 by fitting the change of energy in the reaction to a diatomic anharmonic oscillator model.

In the case of reaction (V2a) this is done by computing the difference in energy between levels (0 0 v) and (0 1 $v-1$) from equation 3.1. Table 5.7 shows the energy of the vibrational level before the collision $E_{(0\ 0\ v)}$, after the collision $E_{(0\ 1\ v-1)}$ and the vibrational energy lost in the collision ΔE_v.

Table 5.7: Energy levels in [K] of the vibrational sates (0 0 v) and (0 1 $v-1$), and their difference ΔE_v.

Level, v	$E_{(0\ 0\ v)}$	$E_{(0\ 1\ v-1)}$	ΔE_v
1	3380	962	2418
2	6724	4324	2400
3	10032	7650	2382
4	13304	10941	2364
5	16541	14195	2345
6	19741	17414	2327
7	22906	20597	2309
8	26035	23744	2291
9	29127	26855	2273
10	32184	29930	2255
11	35205	32969	2236
12	38191	35972	2218
13	41140	38940	2200
14	44053	41871	2182
15	46931	44767	2164
16	49773	47627	2146
17	52578	50451	2127
18	55348	53239	2109
19	58082	55991	2091
20	60780	58708	2073
21	63443	61388	2055

The values in the first and last columns of Table 5.7 are used in equation 5.2 to compute the anhamonicity coefficient of the energy change in reaction (V2a). The obtained value is $x_e = 3.7 \times 10^{-3}$, which is the the same value given in [9], see Table 4.4.

The rate constants are scaled with the same expressions used in [9], which are taken from different sources presenting the SSH theory. The rate constants of reactions involving higher vibrational levels $v > 1$ are computed from the rate constant of the reaction involving the lowest levels (from $v = 1$ to $v = 0$) by using the following expressions [11]

$$k_{v,v-1} = k_{1,0} Z_v \frac{F(\gamma_v)}{F(\gamma_1)} \tag{5.18}$$

where $k_{v,v-1}$ is the rate constant for the VT Relaxation from level v to level $v-1$, $k_{1,0}$ is given in Table 4.4 and depends on the collisions partner M, Z_v is a function of the vibrational level and the anharmonicity of the energy levels

$$Z_v = v \frac{1 - x_e}{1 - v x_e} \tag{5.19}$$

The adiabacity function $F(\gamma_v)$ is computed by the following approximation [51]

$$F(\gamma_v) = \frac{1}{2}\left[3 - \exp\left(-\frac{2}{3}\gamma_v\right)\right] \exp\left(-\frac{2}{3}\gamma_v\right) \tag{5.20}$$

where the adiabatic factor γ_v, is the Massey parameter for the vibrational relaxation from level v to level $v-1$ and is computed from [3]

$$\gamma_v = \frac{0.32\Delta E_v}{\alpha}\sqrt{\frac{\mu}{T_g}} \tag{5.21}$$

in which ΔE_v is the change of energy in the reaction in [K], T_g is the bulk gas temperature in [K], α is a measure of the effective extend of the mutual repulsive potential in the colliding species and for CO_2 can be computed by the following approximation [51]

$$\alpha = \frac{17.5}{r_0} \tag{5.22}$$

where r_0 is the radius parameter of the Lennard-Jones potential in [Å]. The values for r_0 are taken from [9] and are 3.94, 3.69 and 3.47 [Å] for CO_2, CO and O_2, respectively. For collisions of different species the average value of r_0 is used in the calculations. Finally, μ is the reduced mass of the colliding species and is expressed as

$$\mu = \frac{m_1 m_2}{m_1 + m_2} \tag{5.23}$$

where m_i is the mass, in atomic mass units, of the colliding species i. For CO_2, CO and O_2 it takes the value of 44, 28 and 32, respectively.

By using the previous expressions with the values of Table 5.7, the rate constants of reaction (V2a) are computed for all the asymmetric vibrationally excited states. Figure 5.21 shows the results of the calculations, where it is seen that VT Relaxation increases with the vibrational level and the bulk gas temperature. The rate constants for 300 [K] are in agreement with those reported in [9].

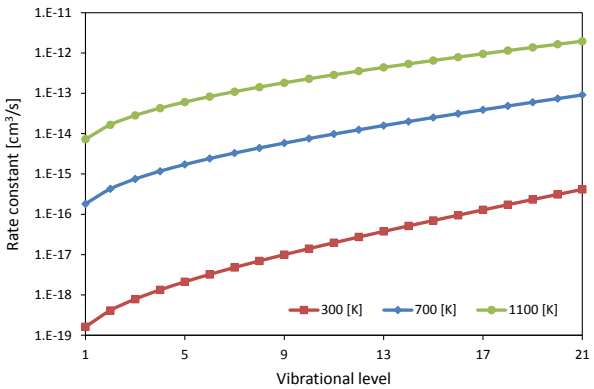

Figure 5.21: Rate constant of reaction (V2a) with M = CO_2, as a function of the asymmetric vibrational level, at bulk gas temperatures of $T_g = 300, 700, 1100$ [K].

At a specific bulk gas temperature T_g and collision partner M, the averaged rate constant of reaction (V2a) for CO_2^*, is computed in the same way as done for the reactions of neutrals, this is 5.16

$$k_{M,a}(T_g) = \sum_{v=1}^{21} n_v(T_g) k_{M,v}(v, \Delta E_v, T_g) \tag{5.24}$$

It is important though, to take a look at the resulting reaction when averaging in this form. The (V2a) reactions of the asymmetric vibrational levels within CO_2^* are

$$\begin{aligned}
n_{21}CO_2\,v_{21} + n_{21}M &\rightarrow n_{21}CO_2\,v_{20} + n_{21}M \\
n_{20}CO_2\,v_{20} + n_{20}M &\rightarrow n_{20}CO_2\,v_{19} + n_{20}M \\
\vdots \qquad\qquad & \qquad\qquad \vdots \\
n_2CO_2\,v_2 + n_2M &\rightarrow n_2CO_2\,v_1 + n_2M \\
n_1CO_2\,v_1 + n_1M &\rightarrow n_1CO_2\,v_a + n_1M
\end{aligned}$$

whose sum can be written as

$$\sum_{i=1}^{21}(n_i CO_2 v_i + n_i M) \rightarrow \sum_{i=2}^{21}(n_i CO_2 v_{i-1} + n_i M) + n_1 CO_2 v_a + n_1 M \tag{5.25}$$

and simplified to

$$CO_2^* + M \rightarrow (1-n_1)CO_2^* + n_1 CO_2 v_a + M \tag{5.26}$$

assuming

$$\sum_{i=2}^{21} n_i CO_2 v_{i-1} \approx (1-n_1)CO_2^* \tag{5.27}$$

Hence, it is possible to write a more general "lumped" reaction, applicable to reactions (V2a,b,c)

$$CO_2^* + M \rightarrow (1-n_1)CO_2^* + n_1 CO_2 v_{a,b,c} + M \tag{5.28}$$

which can be further expanded for the same collision partner M to obtain convenient reactions that are included in the reduced kinetic model, i.e.

$$CO_2^* + M \rightarrow \nu_{l2} CO_2^* + \nu_{s2}(CO_2 v_a + CO_2 v_b + CO_2 v_c) + M \tag{5.29}$$

where ν_{l2} and ν_{s2} are the stoichiometric coefficients of the lumped excited state and the symmetric levels a, b, c, respectively. These are functions of the first asymmetric vibrational level population density n_1, which is in turn a function of the bulk gas temperature

$$\nu_{l2}(T_g) = 1 - n_1(T_g)\,, \quad \nu_{s2}(T_g) = \frac{1}{3} n_1(T_g) \tag{5.30}$$

The Treanor distribution is used to compute these stoichiometric coefficients, the results are given in Table 5.8 and Figure 5.22. It is easy noted that the stoichiometric coefficients of the symmetric levels decrease as the bulk gas temperature increase. However, this does not imply that VT relaxation is decreasing, indeed, it is always increasing since the rate constant increases faster with the bulk gas temperature. The latter is shown at the end of this subsection.

Table 5.8: Stoichiometric coefficients for reaction (RV2)

T_g [K]	ν_{l2}	ν_{s2}	T_g [K]	ν_{l2}	ν_{s2}
300	0.177	0.274	1000	0.363	0.212
400	0.226	0.258	1100	0.375	0.208
500	0.262	0.246	1200	0.386	0.205
600	0.290	0.237	1300	0.395	0.202
700	0.313	0.229	1400	0.404	0.199
800	0.333	0.222	1500	0.412	0.196
900	0.349	0.217			

A logarithm fitting of these coefficients is also possible, although it is not proposed in this kinetic model since the software used for the validation does not allow variable stoichiometric coefficients. Average values are used instead and it will be shown in the results that the impact of this assumption is small for bulk gas temperature changes around 200 [K].

The total averaged rate constant of reaction (RV2), for a specific collision partner M, is computed by adding the averaged rate constants of reactions (V2a,b,c) for the same collision partner M. The averaged rate constants for reactions (V2b,c) are computed by following the same steps as for reaction (V2a) (see equations 5.18 to 5.37), although the anharmonicity coefficients are taken from [9] (see Table 4.4). Thus, the total averaged rate constant is

$$k_M(Tg) = k_{M,a}(Tg) + k_{M,b}(Tg) + k_{M,c}(Tg) \tag{5.31}$$

For each colliding partner M, the calculations are done for the whole temperature range in steps of 100 [K], $T_g = 300, 400, \ldots, 1500$ [K]. The results for M = CO_2, CO and O_2 are shown in Figure 5.23, where it is seen that the rate constants of reaction (RV2) increase at a higher rate than the rate constants of dissociation reactions (RN1) and (RN2) (see Figures 5.17 and 5.19). For each of the (RV2) reactions the rate constant is fitted to a modified Arrhenius equation to obtain the temperature dependent expressions given in Table 5.6

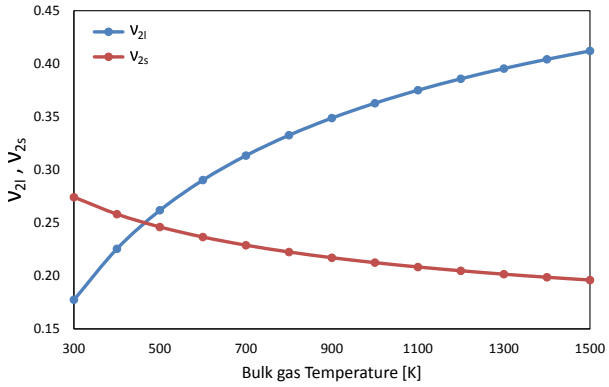

Figure 5.22: Stoichiometric coefficients of reaction (RV2) as a function of the bulk gas temperature.

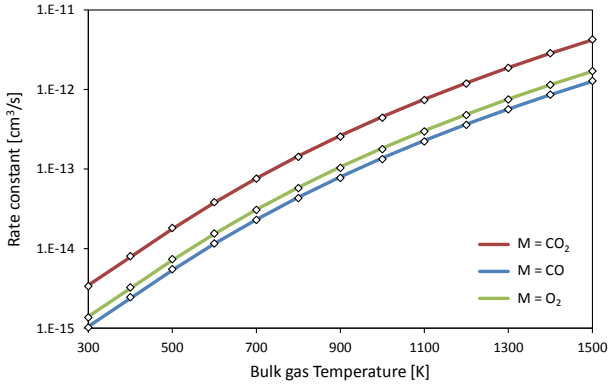

Figure 5.23: Rate constant of reaction (RV2) as a function of the bulk gas temperature, for M = CO_2, CO and O_2.

5.8.2. RATE CONSTANT FOR REACTION (RV3)

The calculation process in this case is very similar to the one previously explained for (RV2). This reaction is the "lumped" version of the VV' relaxation reactions (V5a,b) of Table 4.4. In these reactions, the vibrational energy is transferred between different vibrational modes, namely, the asymmetric and the symmetric modes in this case.

Reactions (V5a,b) are collisions between a purely asymmetric vibrational level v and a CO_2 molecule ($v = 0$), in which the asymmetric vibrational level relaxes to a lower asymmetric level $v-1$ with a symmetric sublevel b or a, respectively. In addition, the CO_2 molecule gets vibrationally excited to a symmetric level a or b. This is,

$$\begin{aligned} CO_2(0\,0\,v) + CO_2 &\rightarrow CO_2(0\,2\,v-1) + CO_2(0\,1\,0) \qquad \text{(V5a)} \\ &\rightarrow CO_2(0\,1\,v-1) + CO_2(0\,2\,0) \qquad \text{(V5b)} \end{aligned}$$

It is assumed, as it is also for reactions (V2a,b,c), that the symmetric sublevels are rapidly relaxed through additional VT relaxation. Thus, for simplicity, reactions (V5a,b) for vibrational levels $v > 1$ scale as follows

$$\begin{aligned} CO_2(0\,0\,v) + CO_2 &\rightarrow CO_2(0\,0\,v-1) + CO_2(0\,1\,0) \qquad \text{(V5a)} \\ &\rightarrow CO_2(0\,0\,v-1) + CO_2(0\,2\,0) \qquad \text{(V5b)} \end{aligned}$$

As explained for reactions (V2a,b,c), these are not direct processes and the rate limiting step is assumed to be the first process [48]. Hence, although for vibrational levels $v > 1$ the reactions are scaled as shown above, the symmetric sublevels must be considered for computing the energy change in the reactions.

The rate constants are also scaled by using expressions derived from the SSH theory. Therefore, the energy change in the reactions should be fitted to diatomic anharmonic oscillator models to compute the anharmonicity coefficient. However, the values of these anharmonicity coefficients are given in [9] (see Table 4.4) and are used herein for the calculations.

The approach used for the calculation of the rate constants is the same approach used for reactions (V2a,b,c) (see equations 5.18 to 5.37). However, in equation 5.21, the energy change in the reaction must also include the vibrational excitation of CO_2, e.g. for reaction (V5a)

$$\Delta E_v = E_{(0\ 0\ v)} - E_{(0\ 2\ v-1)} - E_{(0\ 1\ 0)} \tag{5.32}$$

The calculations are done for both reactions and all the asymmetric vibrational levels v. The results for selected bulk gas temperatures are shown in Figure 5.24, where it is seen that VV' relaxation increases with the vibrational level and the bulk the temperature. The rate constants for 300 [K] are in agreement with those reported in [9].

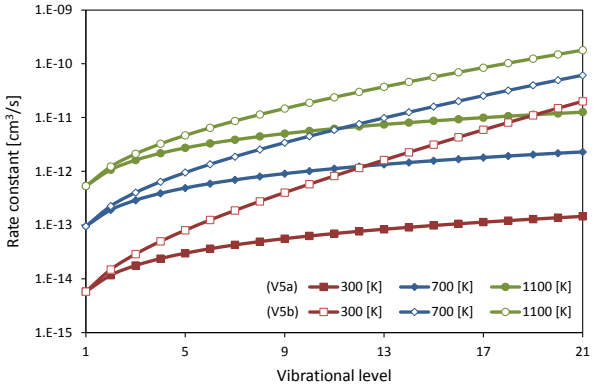

Figure 5.24: Rate constants of reactions (V5a,b), as a function of the asymmetric vibrational level, at bulk gas temperatures of $T_g = 300, 700, 1100$ [K].

By adding the VV' relaxation reactions (V5a) of the excited states within CO_2^*, as done for (V2a) in subsection 5.8.1, the following reaction is obtained

$$\sum_{i=1}^{21} (n_i CO_2\, v_i + n_i CO_2) \rightarrow \sum_{i=2}^{21} (n_i CO_2\, v_{i-1} + n_i CO_2\, v_a) + n_1 CO_2\, v_b + n_1 CO_2\, v_a \tag{5.33}$$

which added together with the analogous reaction obtained for (V5b) and further considering the approximation of equation 5.27, gives the reaction (RV3) that is included in the reduced kinetic model

$$CO_2^* + CO_2 \rightarrow \nu_{l3} CO_2^* + \nu_{s3}(CO_2\, v_a + CO_2\, v_b) \tag{5.34}$$

where the stoichiometric coefficients ν_{l3} and ν_{s3} are functions of the first asymmetric vibrational level population density, which is computed for specific bulk gas temperatures by using the Treanor distribution

$$\nu_{l3}(T_g) = 1 - n_1(T_g)\,, \quad \nu_{s3}(T_g) = \frac{1}{2}\left(n_1(T_g) + 1\right) \tag{5.35}$$

These stoichiometric coefficients are computed for the temperature range of interest, the results are given in Table 5.9 and Figure 5.25. From the results it is seen that the stoichiometric coefficient for the symmetric levels decrease as the bulk gas temperature increase. Nevertheless, the VV' relaxation is always increasing with he bulk gas temperature since the rate constant increases at a faster rate. As in the reaction (RV2), average values are used for the bulk gas temperature of the discharge.

The total averaged rate constant of reaction (RV3) is computed by adding the averaged rate constants of reactions (V5a,b), this is

$$k(T_g) = k_a(T_g) + k_b(T_g) \tag{5.36}$$

where the averaged rate constants of reactions (V5a,b) are computed as

$$k_a(T_g) = \sum_{v=1}^{21} n_v(T_g) k_v(v, \Delta E_v, T_g) \tag{5.37}$$

The calculations are done for the whole temperature range in steps of 100 [K], $T_g = 300, 400, \ldots, 1500$ [K]. The results are shown in Figure 5.26, where it is seen that the rate constants are comparable to those of reaction (RV2) and also increase at a higher rate than the rate constants of dissociation reactions (RN1) and (RN2).

Table 5.9: Stoichiometric coefficients for reaction (RV3)

T_g [K]	ν_{l3}	ν_{s3}	T_g [K]	ν_{l3}	ν_{s3}
300	0.177	0.911	1000	0.363	0.819
400	0.226	0.887	1100	0.375	0.813
500	0.262	0.869	1200	0.386	0.807
600	0.290	0.855	1300	0.395	0.802
700	0.313	0.843	1400	0.404	0.798
800	0.333	0.834	1500	0.412	0.794
900	0.349	0.826			

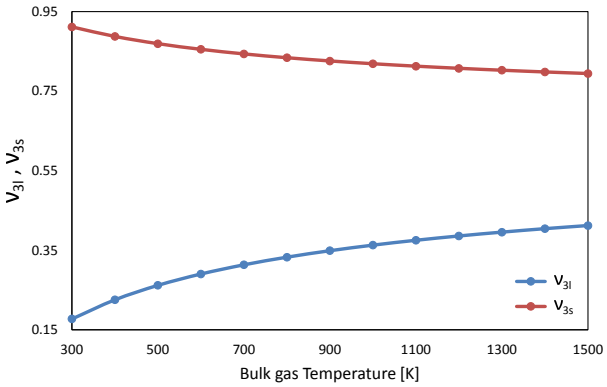

Figure 5.25: Stoichiometric coefficients of reaction (RV3) as a function of the bulk gas temperature.

Lastly, the rate constant is also fitted to a modified Arrhenius equation to obtain temperature dependent expression given in Table 5.6

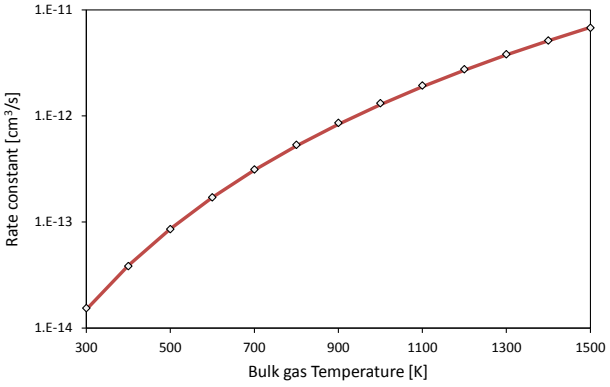

Figure 5.26: Rate constant of reaction (RV3) as a function of the bulk gas temperature.

5.9. SURFACE REACTIONS

These reactions take place in collisions between gas phase species and surfaces, their rate coefficients for the case of a single gas phase reactant species can be computed by the following expression [52]

$$k_s = \left(\frac{1}{1-\gamma/2}\right)\frac{\gamma}{(\Gamma_{\text{tot}})^s}\left(\frac{1}{4}\right)\sqrt{\frac{8k_B T_g}{\pi m}} \tag{5.38}$$

where γ is the sticking coefficient of the reaction, which is the probability that the collision results in a reaction. Γ_{tot} is the total surface site density in $[1/\text{m}^2]$, the exponent s is the sum of the stoichiometric coefficients of the surface reactants. The square root term is the mean thermal speed of the colliding species, computed from the Boltzmann constant k_B, the bulk gas temperature T_g and the mass of the specie m. It

is to be noted that the first term inside the parenthesis is the Motz-Wise correction, which is only included when the sticking coefficient is large, i.e. close to 1 [52].

Different surface reactions can take place inside the reactor, although in this case most of them can be neglected. For a mixture of O and CO the main surface reactions between neutrals species were identified to be the recombination of O to form O_2 and the recombination of O and CO to form CO_2. The sticking coefficients of these recombination reactions are strong functions of the surface material, they are very difficult to determine and the few of them available are not always in agreement [53].

These recombination reactions are not included in the reduced kinetic model since they were not included in the STS kinetic model [8, 9], which is the benchmark. In [8], the STS kinetic model is used to describe the reaction kinetics in the axis of a reactor and all variables are assumed radially uniform. Besides, for the conditions of the study, the characteristic diffusion time is orders of magnitude smaller than the residence time of the reactor [8].

Vibrationally excited states can be de-excited in collisions with surfaces, although the data for the de-excitation probabilities is very scarce or not available at all. A common practice is to assume a sticking coefficient of 1 for the total de-excitation of these states. However, for pressures around 100 [Torr], the collision frequency is high enough to ensure a dominant vibrational de-excitation through the VT relaxation process [30].

The charged species, electrons and ions, diffuse together to the walls by effect of ambipolar diffusion. On the wall they recombine and the neutral charge is restored in the ion. This surface reaction of recombination or neutralization is the only process considered to take place on the surface. Furthermore, it is also required to avoid the accumulation of ions in the reactor. Figure 5.27 shows the surface reactions included in the reduced kinetic model.

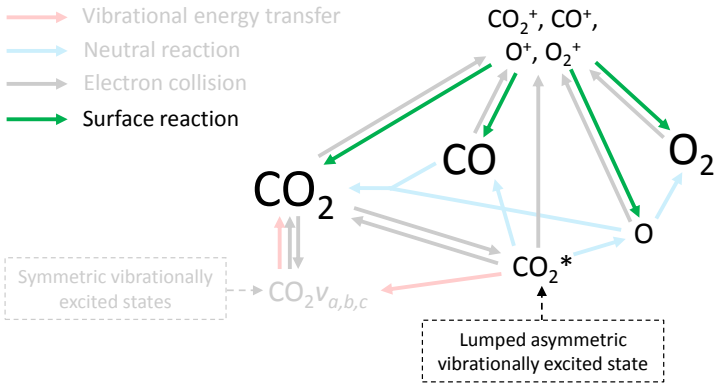

Figure 5.27: Schematic of the surface reactions included in the reduced kinetic model.

A neutralization surface reaction is included for each ion, obtaining a total of 4 surface reactions, which are listed in Table 5.10. For all of them a sticking coefficient of 1 is assumed and since no surface species are involved in the reactions, the rate coefficient expression reduces to

$$k_s = \left(\frac{\gamma}{1-\gamma/2}\right)\sqrt{\frac{k_B T_g}{2\pi m}} \quad [\mathrm{m/s}] \tag{5.39}$$

Table 5.10: Surface reactions included in the reduced kinetic model

No.	Process	Reaction	Sticking Coeff, γ
(RS1)	CO_2^+ Neutralization	$CO_2^+ \rightarrow CO_2$	1
(RS2)	CO^+ Neutralization	$CO^+ \rightarrow CO$	1
(RS3)	O^+ Neutralization	$O^+ \rightarrow O$	1
(RS4)	O_2^+ Neutralization	$O_2^+ \rightarrow O_2$	1

6

RESULTS AND DISCUSSION

In this chapter, the reduced kinetic model described in Chapter 5 is validated against the STS kinetic model [8]. In addition, the effects of the reduced kinetic model's parameters and the process conditions are also studied. Figure 6.1 shows the computed rate constants for the main reactions involving the lumped excited state CO_2^*. These are the result of the simplification process described in Chapter 5.

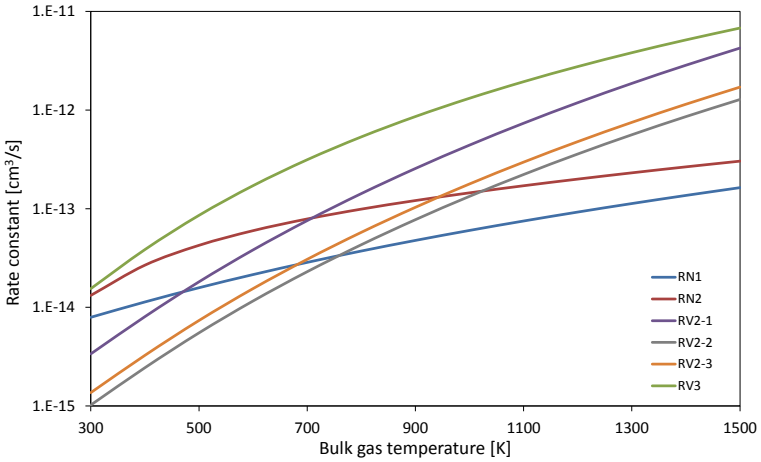

Figure 6.1: Rate constants of the main reactions involving the lumped excited state CO_2^*, as presented in Chapter 5. RV2-1,2,3 makes reference to the reaction (RV2) when M=CO_2, CO, O_2, respectively.

These reactions proceed mainly through collisions of CO_2^* with CO_2, CO and O_2. Therefore, it is clearly seen in the figure that an efficient CO_2 dissociation is achieved at bulk gas temperatures lower than ~700-800 [K]. Around this temperature, the reactions in which the vibrational energy is lost become comparable to the dissociation reactions, and at higher temperatures, the energy loss reactions dominate. Nevertheless, this conclusion may not apply to kinetic models developed with different k factor functions, see Chapter 5.

COMSOL Multiphysics software is used for the simulations of the reduced kinetic model. A two dimensional reactor model as described in Appendix A is built for this purpose. In this model, a spatially uniform quasi-neutral plasma is assumed throughout the reactor volume. The plasma conditions are specified by the electron density and the mean electron energy. In multidimensional models, these are the result of solving the conservation equations and the Boltzmann equation for the electrons, however, this is beyond the scope of this thesis.

The process conditions are specified by the pressure and the bulk gas temperature. Considering the low pressure (100 [Torr] = 0.13 [bar]) and the reactor's size, the viscosity effects are neglected and the pressure is considered constant inside the reactor. No energy equation is included in the reactor model and the temperature profile is specified as an input according to the results of [8]. Multicomponent diffusion equations are included, although the spatial variation of the species densities is of no interest and the results are given as volume average densities. Diffusion was indeed neglected in [8], since its characteristic time is larger than the residence time of the reactor (see section 5.9).

In brief, the inputs are the electron density, electron temperature, bulk gas temperature and pressure. The purpose of the model is to validate the reduced kinetic model, i.e. the reactions and their rates, not to perform self-consistent 2D simulations of a plasma reactor for CO_2 dissociation, which indeed is an extremely complex task that has not yet been done.

To properly compare the results of the reduced kinetic model to those of the STS kinetic model, the simulation is divided in two phases, the plasma zone and the afterglow. In the former, a constant electron density and an increasing electron temperature profile are specified to describe a plasma activated zone in which radicals and excited states are produced. In the latter, the electron density is set to 0 and a decreasing electron temperature profile is specified to describe the zone after the plasma, usually called afterglow, where excited states relax back to equilibrium and radicals recombine. This simple approach is used in [8], even though in reality the electron density is not constant, it gradually increases to a maximum value at the plasma zone and gradually decreases again in the afterglow.

The total simulation time is 0.1 [s], which is enough for the relaxation processes and is divided for the two phases. The plasma zone has a duration of the reactor's residence time t_r, whereas the afterglow lasts for the remaining time of the simulation. The residence time given in [8] is used in the simulations, so that the same conditions are also specified here.

Plasma conditions are specified differently in [8] and the electron energy is computed by solving the Boltzmann equation for a given value of the reduced electric field. Furthermore, the evolution of the bulk gas temperature in the discharge is also computed with the energy equation. The results for these variables are fitted to specific functions of time and given as inputs to the 2D COMSOL model. The average computation time of the simulations is lower than 25 minutes.

6.1. VALIDATION

The validation of the reduced kinetic model is done by comparing results at the same conditions of the time dependent analysis of [8]. The discharge takes place at a pressure of 100 [Torr], reduced electric field of 50 [Td], electron density of 10^{13} [1/cm^3], specific energy input of 0.6 [eV/molecule], the frequency of the electromagnetic field is 2.45 [GHz] and the residence time is 1.4×10^{-5} [s]. The initial composition is 100% groundstate CO_2, the initial bulk gas temperature is 300 [K] and the initial electron temperature is 4500 [K].

It is first required to fit the electron and bulk gas temperatures to functions of time that can be included as inputs in COMSOL. Figure 6.2 shows the time evolution of the bulk gas temperature T_g and the electron temperature T_e.

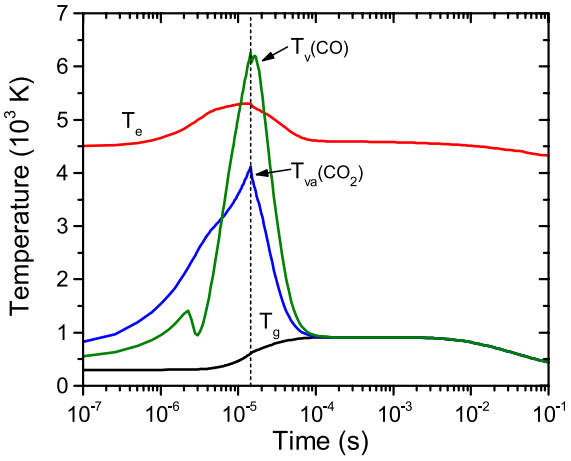

Figure 6.2: Evolution of the bulk gas temperature T_g, the electron temperature T_e, the vibrational temperature of the asymmetric mode of CO_2 $T_{va}(CO_2)$ and the vibrational temperature of CO $T_v(CO)$. Residence time is indicated by the dashed line. Taken from [8].

With temperatures in [K] and time in [s] the fitted functions for the first phase ($10^{-7} \leq t \leq 1.4 \times 10^{-5}$) are

- Bulk gas temperature T_g

$$T = \sum a_i t^i \tag{6.1}$$

With the coefficients a_i given in Table 6.1.

- Electron temperature T_e

$$T = \sum b_i \ln(t)^i \tag{6.2}$$

  With the coefficients b_i given in Table 6.1.

and with the same units, for the second phase ($1.4 \times 10^{-5} \leq t \leq 0.1$)

- Bulk gas temperature T_g

  Equation 6.2 with the coefficients c_i given in Table 6.1.

- Electron temperature T_e

  Equation 6.2 with the coefficients d_i given in Table 6.1.

Table 6.1: Coefficients for the fittings of equations 6.1 and 6.2

i	a_i	b_i	c_i	d_i
0	3.026×10^{2}	1.139×10^{7}	7.880×10^{2}	-1.842×10^{3}
1	-1.046×10^{7}	5.173×10^{6}	7.401×10^{2}	-1.051×10^{4}
2	4.082×10^{12}	9.738×10^{5}	3.916×10^{2}	-7.606×10^{3}
3	-1.442×10^{17}	9.721×10^{4}	7.535×10^{1}	-3.031×10^{3}
4		5.428×10^{3}	6.402	-7.214×10^{2}
5		1.608×10^{2}	2.038×10^{-1}	-1.051×10^{2}
6		1.974		-9.180
7				-4.405×10^{-1}
8				-8.907×10^{-3}

Assuming a mean bulk gas temperature of 500 [K] in the discharge, the values of the stoichiometric coefficients ν_l and ν_s for reactions (RV2) and (RV3), as well as the value of the scaling factor ϕ for the vibrational excitation cross section are constant during the simulation. It will be shown in the following section the effects of assuming a different mean temperature. The results of the simulation are shown in Figure 6.3b, while the results of the STS kinetic model are given in Figure 6.3a for comparison.

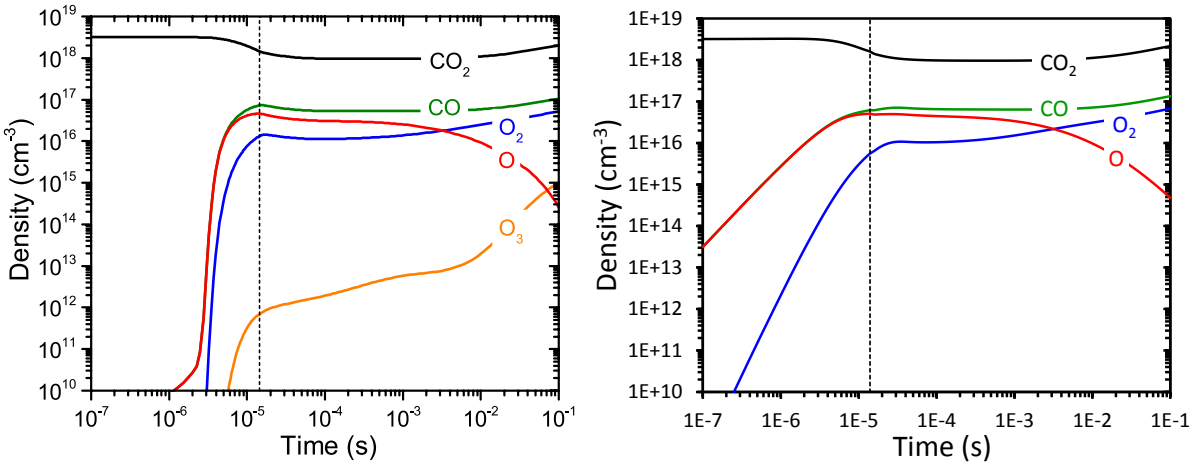

(a) STS kinetic model [8]

(b) Reduced kinetic model

Figure 6.3: Densities of the most important neutral species. Residence time is indicated by dashed lines.

The good agreement obtained with the reduced kinetic model is evident by comparing the figures. As expected, CO_2 dissociation mainly takes place in the plasma zone, while recombination processes are present in the afterglow, although they proceed at a slower rate and the variation of the densities is smaller than in the plasma zone. The following is also noticed for the reduced kinetic model

- At high densities the results resemble those of the STS kinetic model. The densities at the end of the reacting phase, as well as during the afterglow, are in agreement. Their time evolution follow the expected trends, with dissociation in the plasma zone and recombination in the afterglow. The best results are obtained for the CO_2 density, whose evolution is virtually exact to the STS kinetic model, whereas for the CO and O_2 densities, errors around ~10% and ~20% are obtained at the end of the simulation, respectively.

- The results can be improved by tuning the assumed value of the k factor at the initial temperature and the high temperature in which equilibrium is assumed (see section 5.4). However, the steep slope seen in Figure 6.3a for $t < 10^{-5}$ [s] won't be attained with the assumed temperature dependence of the k factor. It is important to remark, though, that the purpose of this study is not to fit the results of [8] and obtain very accurate results, but to demonstrate that by using the Treanor distribution it is possible to develop a kinetic model that captures the dissociation and vibrational kinetics of non-equilibrium regimes in a reduced set of reactions. Furthermore, the STS kinetic model qualitatively predicts experimental results and it would be very difficult to adjust thousands of reactions to improve the agreement. On the contrary, the reduced kinetic model can be adjusted to experimental results by tuning the k factor.

- There are notable differences in the densities of CO, O and O_2 for $t < 10^{-5}$ [s]. Firstly, these differences arise at the very beginning of the plasma zone, at times that are extremely small if compared with the total time of the simulation, and it becomes smaller at the end of the plasma zone. The steep slopes seen in Figure 6.3a are the result of the state to state vibrational kinetics. The energy is transferred from the electrons to the lower levels of the vibrational ladder and it is progressively transferred by VV relaxation to higher levels, of which only the highest dissociate at high rates.

  Thus, from Figure 6.3a it is seen that it takes around $\sim 10^{-6}$ seconds to excite the highest vibrational levels. After this time, the whole vibrational ladder is excited and the highest vibrational levels dissociate after being produced. This mechanism continues until $\sim 10^{-5}$ seconds, when VT relaxation increases and the dissociation declines. The rate constants for the dissociation of the highest vibrational levels are very high, since the activation energy is lowered by the vibrational energy. This combined effect of rapid VV relaxation and dissociation of high levels leads to a very fast dissociation process, which explain the steep increase in the densities of CO and O. The steep increase in the O_2 density is mainly caused by O recombination.

  In the reduced kinetic model it is assumed that at low bulk gas temperatures the lumped excited state CO_2^* includes high populations of the high vibrational levels, therefore, the dissociation starts taking place as soon as CO_2^* is produced by electron collisions. This explains the slower dissociation process that takes place in the reduced kinetic model between $\sim 10^{-6}$ and $\sim 10^{-5}$ seconds. For $t > \sim 10^{-5}$ [s] the densities of CO and O are in agreement with the results of [8].

- A subtle peak in the CO density is observed at $t \approx 3 \times 10^{-5}$, when the temperature is almost 800 [K] (see Figure 6.2). This means that up to that time the dissociation rate is slightly higher than the energy loss rate. This is in agreement with Figure 6.1, as it shows that efficient CO_2 dissociation takes place at temperatures lower than ~ 700-800 [K] in this reduced kinetic model. Nevertheless, it is also seen that this peak does not affect the results and if it is to be fixed the assumed bulk gas temperature at which $k = 1$ should be decreased.

- At the end of the plasma zone the larger difference in the results is seen in the O_2 density. This is caused by the different behavior in the rate constant of reaction (N2) at high vibrational levels (see Figure 5.18 and compare to Figure 5.16). This difference is dealt with the correction of equation 5.17 and although the obtained rate constant seems to be slightly lower, there is no big impact in the O_2 density in the afterglow, where it is produced mainly by O recombination. Moreover, in the afterglow the densities of O and O_2 are slightly higher since O_3 is not included in the reduced kinetic model.

It is not possible to perform a second validation like this at different process conditions with the results reported in [8], until the electron dynamics and the energy equation are included in the model.

6.1.1. EFFECTS OF ϕ AND STOICHIOMETRIC COEFFICIENTS ν_l, ν_s

The results shown in Figure 6.3b were computed with constant values of the scaling factor $\phi = 1.12$ and stoichiometric coefficients $\nu_{l2} = 0.262$, $\nu_{s2} = 0.246$, $\nu_{l3} = 0.262$ and $\nu_{s3} = 869$, which correspond to an assumed

mean bulk gas temperature of 500 [K] (see Tables 5.3, 5.8 and 5.9). As explained before, COMSOL Multiphysics does not support variable cross sections or stoichiometric coefficients.

Nonetheless, it is required to evaluate the impact of keeping these values constant and not as functions of the bulk gas temperature, as derived in Chapter 5. The largest impact should be expected in the plasma zone, where electron impact vibrational excitation and vibrational energy transfer reactions are more important. In this first phase of the simulation the bulk gas temperature rises from 300 [K] to ~560 [K] (see Figure 6.2), therefore, a simulation at a mean bulk gas temperature of 300 [K] is performed with the corresponding values of ϕ, ν_l, ν_s.

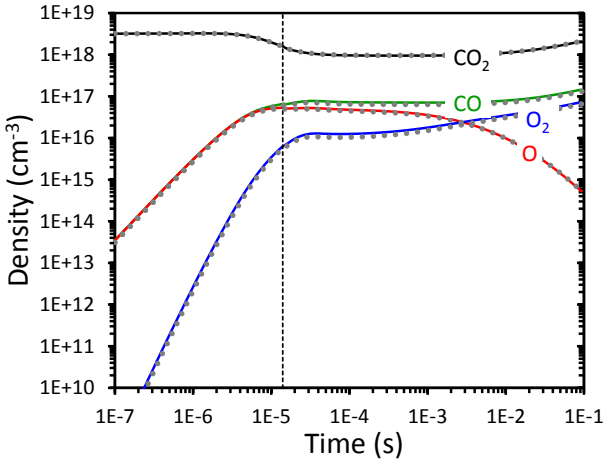

Figure 6.4: Densities of neutral species for different values of the mean bulk gas temperature. Solid line: 500 [K], dots: 300 [K].

Figure 6.4 shows the results of the simulations in solid lines for 500 [K] and in dots for 300 [K]. It is seen that the variation in the results is barely noticeable for a change of 200 [K] in the assumed mean bulk gas temperature. Furthermore, it is concluded from Figures 5.14, 5.22 and 5.25 that at higher temperatures the variation is even smaller for the same $\Delta T_g = 200$ [K]. This is, if the simulations were performed at 700 [K] the variations would have been even smaller. It is then concluded that no large errors are induced if these values are kept constant during the simulation. Besides, it is not required to specify them with high accuracy and an approximate value of the mean bulk gas temperature is good enough for the calculations ($\pm \sim 200$ [K]).

6.1.2. EFFECTS OF THE k FACTOR

The k values used in the calculation of Treanor distributions were obtained with a fitted function of the form given in equation 5.4. Two values are required to perform such fitting, an initial k factor, which indicates the maximum degree of non-equilibrium reached with the initial conditions, and $k = 1$ at a estimated temperature in which it is assumed that thermal equilibrium is attained. For the reduced kinetic model a value of $k = 6$ is assumed at $T_g = 300$ [K] and $k = 1$ at $T_g = 5070$ [K], see section 5.4.

If any of these values is to be changed, a new function for k must be fitted. With this function the Treanor distributions are computed and finally the rate constants, the scaling factor ϕ and the stoichiometric coefficients ν_l and ν_s. The effect of changing the initial k value is shown in Figure 6.5. These results correspond to reduced kinetic models built with initial k values of 5.8, 6 and 6.2 at $T_g = 300$ [K], and a final k value of 1 at $T_g = 5070$ [K].

The initial k value can also be seen as a dissociation potential, since a higher value indicates that more vibrational energy is stored in high levels and therefore a high dissociation rate is achieved. This is clearly seen in Figure 6.5, where for a higher k value the dissociation increases and the opposite is true for a lower k value. It is also seen that it alters the dissociation from the beginning of the plasma zone and the effects last for the whole simulation.

On the other hand, the final k value is closely bound to the evolution of the VT relaxation process, i.e. the energy lost in heating the bulk gas. Hence, it is related to the efficiency of the dissociation process and the residence time, which should be set to the moment when the dissociation is no longer efficient. A good approximation for this can be obtained by computing the characteristic VT relaxation process, as done in [8]. The effect of changing the bulk gas temperature at which thermal equilibrium is assumed ($k = 1$) is shown in Figure 6.6. These results correspond to reduced kinetic models built with an initial k value of 6 at $T_g = 300$ [K]

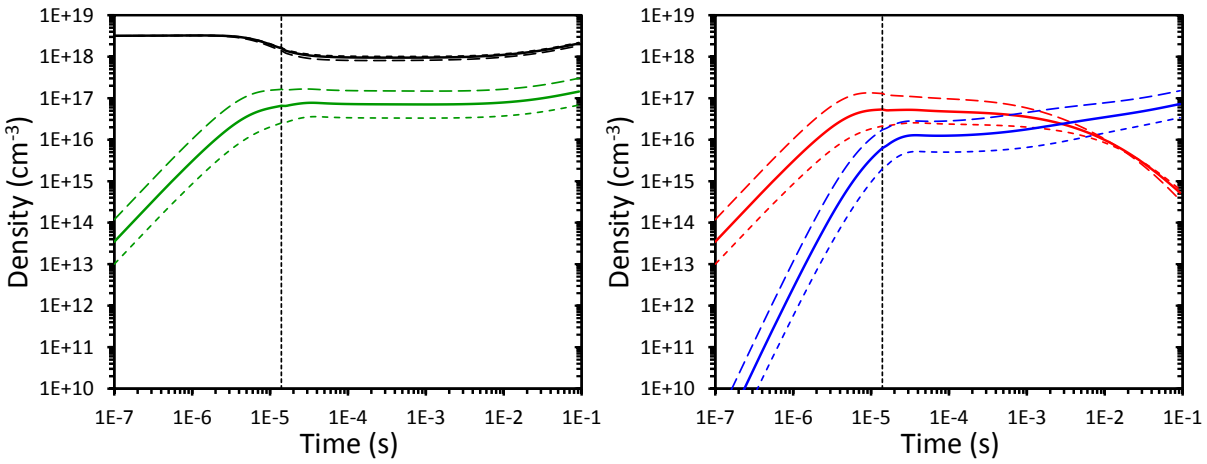

(a) CO_2 and CO densities (b) O and O_2 densities

Figure 6.5: Densities of neutral species for different values of the k factor at a bulk gas temperature of 300 [K]. Solid line: $k = 6$, short dash: $k = 5.8$, long dash: $k = 6.2$.

and a final k value of 1 at $T_g = 5070$ [K], $T_g = 4500$ [K] and $T_g = 5500$ [K].

Increasing this temperature implies that at lower bulk gas temperatures the vibrational energy is used in dissociation reactions instead of bulk gas heating. The dissociation process extends further, since higher bulk gas temperatures are required for VT relaxation to take place. This effect is seen in Figure 6.6, where a higher dissociation is obtained at the end of the plasma zone. The opposite is true for a lower temperature of the final k value. In both cases the effects are only present at the end of the plasma zone and they last for the remaining time of the simulation.

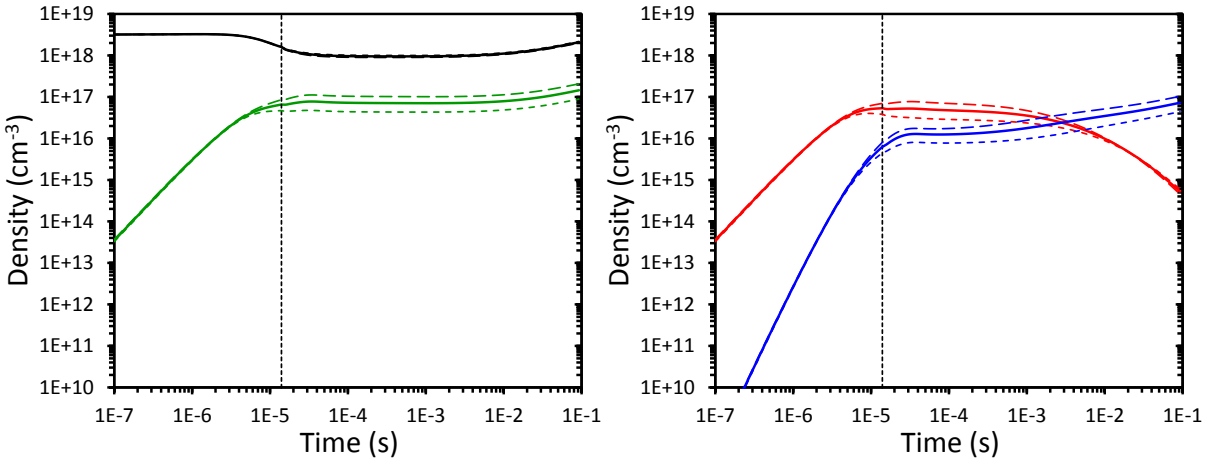

(a) CO_2 and CO densities (b) O and O_2 densities

Figure 6.6: Densities of neutral species, assuming different bulk gas temperatures for $k = 1$. Solid line: $T_g = 5070$ [K], short dash: $T_g = 4500$ [K], long dash: $T_g = 5500$ [K].

6.1.3. EFFECT OF ELECTRON DENSITY AND ELECTRON TEMPERATURE

As stated before, the inputs to the reduced kinetic model are the electron density, electron temperature, bulk gas temperature and gas pressure. The first two are the plasma conditions and are computed by solving the electron dynamics of the plasma. The last two are the process conditions and are mainly determined by the conservation equations of heavy species.

However, all these parameters are interrelated and a variation in one of them affects the others. For instance, an increase in the electron temperature leads to higher ionization rates, hence, the electron density

increases. An increase in the electron density causes an increase in the rate of the electron impact reactions, increasing the density of excited species and therefore the rates of all reactions, including VT relaxation (bulk gas heating). For constant gas pressure and volume an increase in the bulk gas temperature causes a decrease in the densities, including the electron density, however, it also leads to an increase in the VT relaxation rate, which is the main cause of the bulk gas heating. On the other hand, higher densities are obtained at higher pressures, electron collisions increase since the mean free path decreases, consequently, the electron temperature decreases (higher collision loses). These relations are some evident ones, since indeed, the involved physics are far more complex. Therefore, the process of finding the optimal conditions for a reactor is very challenging without a self consistent model.

A thorough validation of the reduced kinetic model is not possible until the electron dynamics and the energy equation are included in the model. Nonetheless, it is possible to make qualitative validations to check how the model behaves at different conditions. For this purpose, multiple simulations are performed with one parameter changed at a time while the others are kept constant at the values used in section 6.1.

Figure 6.7 shows the densities of neutral species for three different values of the electron density. The CO_2 density is very similar in all cases, yet, its dissociation can also be inferred from the CO density, which looks different in all cases. It is seen that for a low electron density, the CO_2 dissociation decreases as a consequence of lower electron impact vibrational excitation rates. On the other hand, an interesting effect is seen for a high electron density. In this case, a higher CO_2 dissociation is obtained until 2×10^{-6} seconds, when it ceases due to a saturation of the symmetric vibrational levels.

A higher electron density at fixed neutrals density implies higher ionization rates, which are achieved at higher electron temperatures. Furthermore, at higher electron temperatures the vibrational excitation of the symmetric modes decrease [3]. Hence, in the case under study, CO_2^* and $CO_2\,v_{a,b}$ are produced at a higher rate. The CO_2^* dissociates through reactions (RN1,2) and produces $CO_2\,v_{a,b}$ through reactions (RV2,3), at high rates. The symmetric levels $CO_2\,v_{a,b}$ relax to CO_2 through reaction (RV1) at a lower rate. Therefore, after second 2×10^{-6} the discharge is saturated of the symmetric modes and the dissociation ceases. Naturally, this effect is a consequence of not having the electron dynamics and the energy equations included in the model. The dissociation should indeed be higher [8].

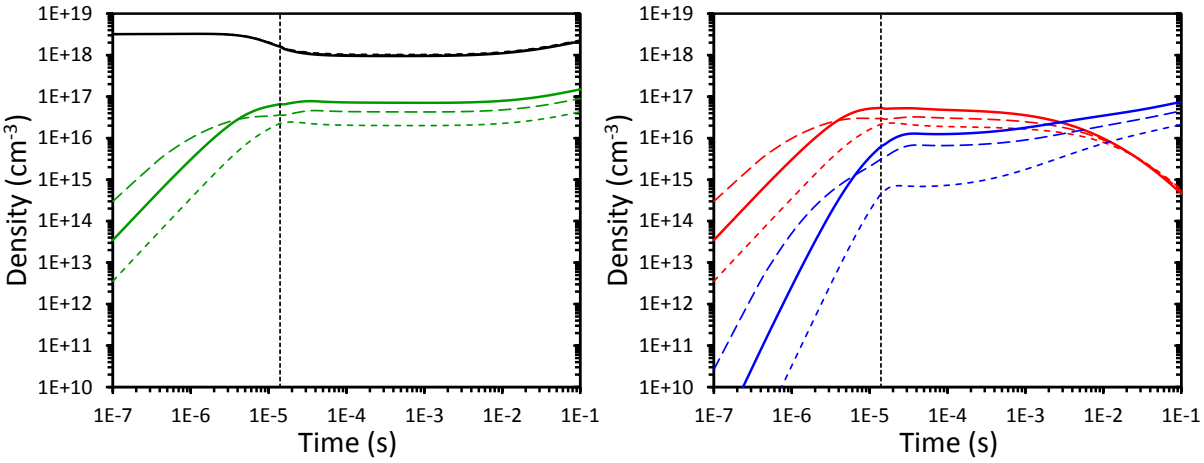

(a) CO_2 and CO densities

(b) O and O_2 densities

Figure 6.7: Densities of neutral species for different values of the electron density. Solid line: $n_e = 10^{13}$ [1/cm^3], short dash: $n_e = 10^{12}$ [1/cm^3], long dash: $n_e = 10^{14}$ [1/cm^3].

The results of changing the electron temperature are shown in Figure 6.8. The main reason for the small variations is that the electron density is assumed constant, although it changes with the electron temperature. As the electron temperature increases, the EEDF broadens and shifts to higher energy collisions, where ionization collisions are located (see Figure 2.2). The electron dynamics must be included in the model in order to compute the electron density.

The slight variations in the neutral's densities are also a consequence of the lumping process. The electron impact vibrational excitation cross section was broadened and its sensitivity to the EEDF was reduced. This is clearly seen by comparing $\sigma_{0,1}$ with σ_V in Figure 5.12. Further validations as the one presented in section 6.1 are required to evaluate the impact of this reduced sensitivity.

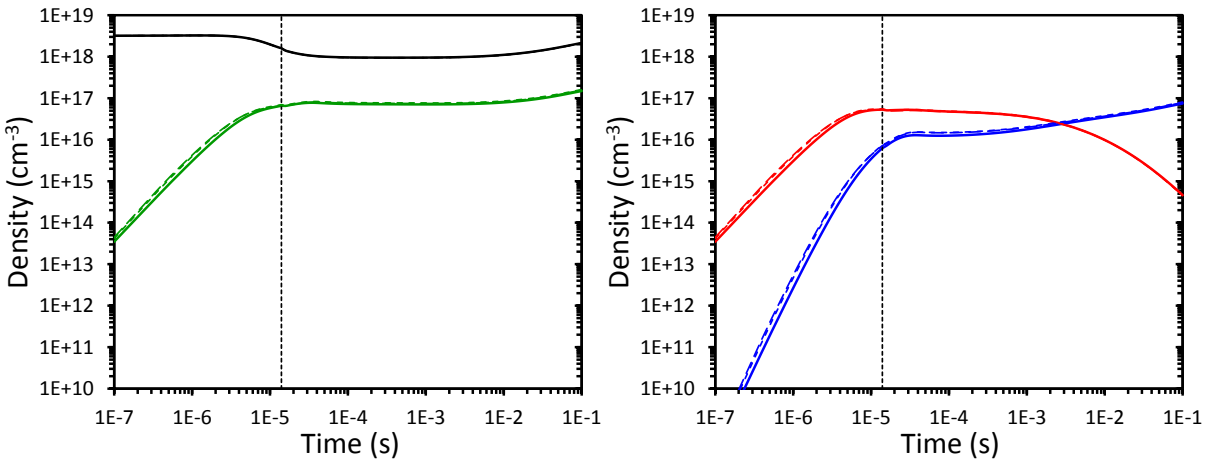

(a) CO_2 and CO densities (b) O and O_2 densities

Figure 6.8: Densities of neutral species for different values of the maximum electron temperature. Solid line: $T_e \approx 5300$ [K], short dash: $T_e \approx 9200$ [K], long dash: $T_e \approx 13000$ [K].

6.1.4. EFFECT OF BULK GAS TEMPERATURE AND PRESSURE

The results of increasing the initial bulk gas temperature are shown in Figure 6.9. The expansion that takes place for higher bulk gas temperatures (ideal gas, $p = nk_bT$) is noted for the whole simulation. In addition, at higher temperatures, lower CO_2 dissociation is seen by comparing the difference between the initial and final values of CO_2, or by comparing the nT_g products. The cause of the lower dissociation is the increase of VT relaxation rates, see reactions (RV2,3) in Figure 6.1. For this qualitative validation the same profile of section 6.1 is assumed, however, this should be the result of an energy conservation equation.

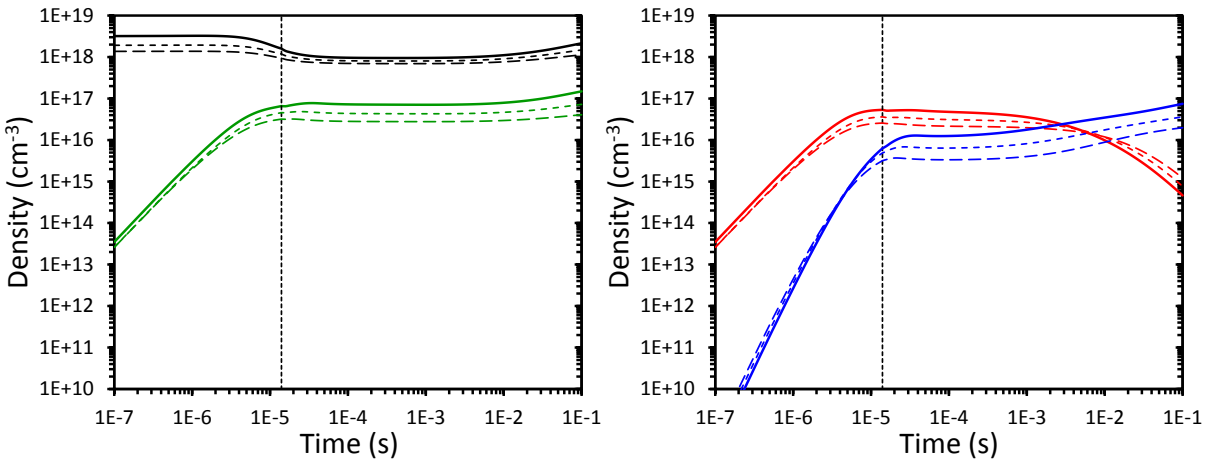

(a) CO_2 and CO densities (b) O and O_2 densities

Figure 6.9: Densities of neutral species for different values of the initial bulk gas temperature. Solid line: $T_g = 300$ [K], short dash: $T_g = 500$ [K], long dash: $T_g = 700$ [K].

Figure 6.10 shows the densities of neutral species for three different values of the gas pressure. The variation of the total neutrals density is noted for the whole simulation ($p = nk_bT$). At higher pressures the CO_2 dissociation rate slightly increases, this is verified by comparing the n/p quotient at the end of the simulation and is caused by the large difference between the dissociation and recombination kinetics, i.e. between rate constants of reactions (RN1,2) and (RN3,4). One should avoid using Le Châtelier's principle, which is formulated for chemical equilibrium and leads to the erroneous conclusion that recombination increases (RN3,4).

The effects of higher pressures in the plasma conditions are usually more important and can lead to lower dissociation and plasma instabilities. However, this could not be evaluated in the reduced kinetic model since the electron dynamics are not included.

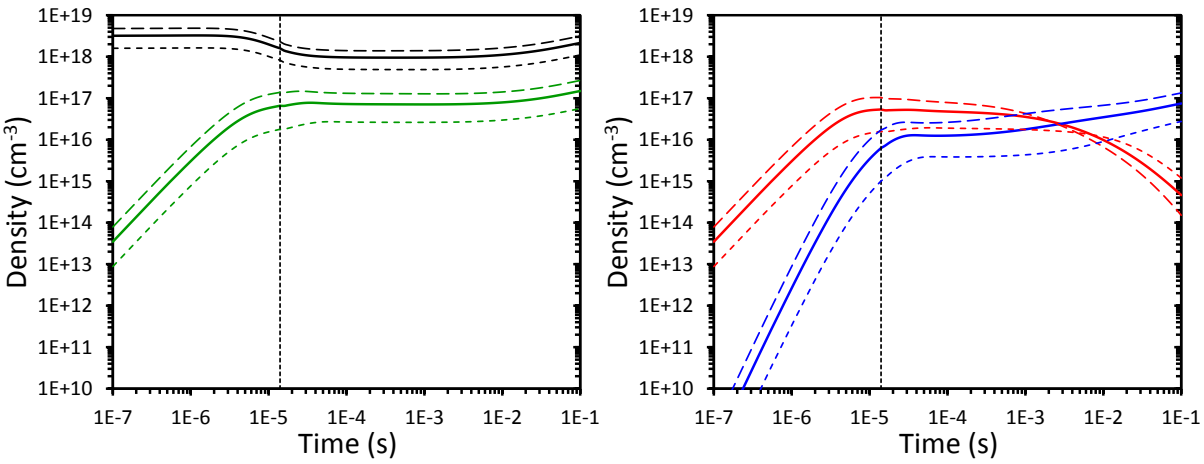

(a) CO_2 and CO densities

(b) O and O_2 densities

Figure 6.10: Densities of neutral species for different values of gas pressure. Solid line: $p = 100$ [Torr], short dash: $p = 50$ [Torr], long dash: $p = 150$ [Torr].

6.2. PROSPECTIVES

It was shown in the previous sections that the electron dynamics and the energy equation for heavy species must be included in the reactor's model to obtain consistent results. Indeed, this is the next step towards the development of a self-consistent model for a CO_2 plasma reactor. In such model, the electron dynamics and energy equation must be solved simultaneously with the reaction kinetics and the mass conservation equations for heavy species. However, as a first approximation the electron dynamics can be calculated in a preprocessing step, in which the time or space evolution of the plasma conditions are obtained.

At different process conditions the residence time should be modified to keep a high dissociation and energy efficiency. For instance, at higher electron densities the dissociation is faster and the VT relaxation increases at a higher rate. Once the VT relaxation dominates, the power given to the plasma is wasted in heat instead of being used in the dissociation process, hence, the efficiency drops. In these cases, the residence time should be smaller to avoid higher rates of VT relaxation. The residence time can be computed from the specific energy input or estimated from the collision frequency of VT relaxation [8].

The approach of dividing the simulation in phases would not be required in a self-consistent 2D model, since the electron density and electron temperature are not uniform throughout the reactor. The residence time is then computed as usual by defining the gas flow and the reactor's size.

It is worth to mention that the reduced kinetic model can also be adjusted to experimental results by changing the initial and final k values. The initial value can be obtained experimentally by determining the vibrational temperature from Optical Emission Spectroscopy. For instance, initial k values in the range from 5.6 to 8.3 are obtained for the $CO_2 + N_2$ pulsed microwave discharge discussed in [14]. The final k value must be adjusted according to the type of discharge and the process conditions, although presumably it is only determined by the species. The type of discharge and process conditions most likely influence the time in which the thermal equilibrium is reached.

Limited information is available regarding the full transition from a non-equilibrium regime to a thermal equilibrium regime. Besides, the rate constants given in [8] have a temperature range of validity usually lower than 2000 [K]. Therefore, calculations at higher temperatures would mostly lead to erroneous conclusions.

It might be possible to implement additional simplifications. The symmetric vibrational levels considered in this study are coupled by the Fermi resonance, i.e. the energy levels of $CO_2\,v_c$ and $CO_2\,v_b$ are three and two times the energy level of $CO_2\,v_a$. Therefore, one additional simplification could be the grouping of these vibrational levels into a single symmetric group, for which a Boltzmann equilibrium distribution could be assumed. This simplification would eliminate 2 species and 8 reactions, leaving the reduced kinetic model with 11 species and 36 reactions. Besides, for a Maxwellian EEDF it is possible to compute the convolution of the EEDF and the cross sections to obtain the rate constants as a function of the mean electron energy. By fitting these rate constants to Arrhenius type equations it is possible to compute all reactions by algebraic expressions instead of cross sections.

Finally, the simplification process proposed in this study could also be used to simplify other state-to-state kinetic models of interest. For instance, a reaction kinetics model for a Hydrogen microwave plasma at moderate pressures comprises around 1000 reactions. If this kinetic model is reduced by the proposed approach it is possible to obtain a similar reduced kinetic model, which coupled with the reduced kinetic model of CO_2 lead to the reduced kinetic model of the reverse water gas shift in non-thermal microwave discharges.

7

CONCLUSIONS AND FUTURE WORK

A reduced kinetic model for the CO_2 dissociation in a non-thermal microwave reactor was developed. This reduced kinetic model can be used to qualitatively predict the influence of different parameters in the CO_2 dissociation process. For the reduction, only the dominant reactions were included and the asymmetric vibrationally excited states of CO_2 were grouped into a fictitious species CO_2^*. It was further assumed that the excited states within CO_2^* followed the Treanor non-equilibrium distribution and their populations were used to compute the rate constants of the reactions involving CO_2^*.

It was shown that it is possible to capture the dissociation and vibrational kinetics in a reduced set of reactions by following the proposed simplification process. The number of species was reduced from 110 to 13, and the number of reactions was reduced from more than 10000 to only 44. For the validation of this reduced kinetic model, a 2D reactor model was developed in COMSOL. The computation time for each of the performed simulations did not exceed 25 minutes.

Additional simplifications are possible, although their implementation should be evaluated beforehand, since the effort and time needed for their implementation could easily outweigh the benefits of having almost the same number of species and reactions. Besides, as mentioned before, it was proved that reasonable computation times are obtained when the reduced kinetic model is implemented in simplified 2D reactor models.

The validation showed that the densities of the neutral species are in good agreement with those of the STS kinetic model, specially at the end of the plasma zone and the afterglow. The end of the afterglow can be considered the outlet composition of the reactor and therefore a good approximation for the steady state solution. It was not possible to perform additional validations with the reported results of the STS kinetic model, therefore, the effects of changing the simplification parameter (k), the plasma conditions (n_e, T_e) and the process conditions (p, T_g) were analyzed through qualitative validations. The results proved that the energy conservation for heavy species and the electron dynamics must be included in the reactor's model.

Indeed, this is the next step towards the development of a self-consistent multidimensional model of a non-thermal plasma reactor. The energy equation for heavy species must be solved simultaneously with the mass conservation equation, whereas the electron dynamics could be implemented in a preprocessing step as a first approximation.

The qualitative validations also showed that the reduced kinetic model can be adjusted to experimental results by changing the initial and final k values, the former one being easily obtained experimentally by Optical Emission Spectroscopy. This is an important feature of the reduced kinetic model, considering that adjusting the STS kinetic model to experimental results could be an extremely demanding task, if possible at all.

Finally, the simplification process could be used to reduce other relevant state-to-state plasma kinetic models, which coupled together yield the reduced kinetic model of gas mixtures. This can be used in multidimensional simulations of non-thermal plasma reactors, which have been hindered by the complexity of the chemical processes that take place in the discharge. These models will facilitate the outlining of design and operation guidelines to optimize the conversion and energy efficiency, speeding up the transition of this technology to larger scale industrial applications.

A

REACTOR MODEL IN COMSOL

The 2D reactor model used for the validation of the reduced kinetic model was built with the Heavy Species Transport interface of the Plasma Module in COMSOL 4.4 [16]. The Heavy Species Transport interface can be coupled with the Driff Diffusion Interface for future development of self-consistent reactor models.

The Heavy Species Transport interface solves the following multicomponent diffusion equation for the species of the model [16]

$$\rho \frac{\partial}{\partial t}(w_k) + \rho(\mathbf{u} \cdot \nabla) w_k = \nabla \cdot \mathbf{j}_k + R_k \tag{A.1}$$

where ρ denotes the density of the mixture, w_k is the mass fraction of the kth species, $\mathbf{u}$ is the mass averaged fluid velocity vector, $\mathbf{j}_k$ is the diffusive flux vector of the kth species and R_k is the rate expression for the species k. They additional equations are needed for calculating these variables are found in [16].

It is to be noted that there are no driving forces for the diffusion of neutral species, only the ions diffuse to the walls by the effect of surface reactions. This is due to the assumptions made for developing the reduced kinetic model and the adopted modeling approach. The ions diffusion cause a charge imbalance inside the reactor, since the electrons density is assumed constant and ambipolar diffusion is not considered. Nevertheless, neither the diffusion nor the charge imbalance affect the dissociation kinetics, as mentioned in Chapter 4. This effect won't take place is a self-consistent model.

The diffusive flux vector depends on the chosen diffusive model. From the two available options, the Mixture average diffusive model is chosen since it is more accurate than the simpler Fick's law.

The validation is done to compare the results of the reduced kinetic model with those reported in [8]. Therefore, their same modeling approach is used here, no convection is considered and time dependent simulations are performed based on the residence time value. The details are explained in Chapter 6.

The migration in electric field is neglected since the electrons density must be constant in space and time during each of the two simulation phases. A Maxwellian EEDF is used as required by the reduced kinetic model. The remaining configurations for the interface are left in their default values: Stabilization is included, the equations are solved in logarithmic form and linear space discretizations are used. The calculation of thermodynamic properties, the full expression for diffusivity and the ion transport properties tensor are not required.

The following is also specified in the model

- Domain

  The reactor is the only domain needed for the model. A rectangle with a length of 10[cm] and a height of 2 [cm] is used to represent the reactor. The size of the reactor in this model does not influence the results, since the concentration of the neutral species is uniform. The walls of the reactor are defined in view of the recombination surface reactions.

- Parameters

  The ϕ scaling factor is the only parameter defined for the model. It takes a value according to the mean temperature of the discharge. See Table 5.3.

- Variables

  Three variables are specified for the model. The electron density takes a constant value depending on the phase of the simulation. The mean electron energy and the gas temperature are specified by the fitted equations 6.1 and 6.2 and the values of Table 6.1, depending on the phase of the simulation.

- Electron impact reactions

  All electron impact reactions are imported from a cross section data file with the format required by COMSOL. It is practical to specify in the data file that the cross sections for the reverse processes must be computed by using the detailed balancing principle. The cross sections of vibrational excitation and de-excitation of CO_2^* must be multiplied by the ϕ parameter.

- Reactions of neutral species

  They are included as reactions with the kinetic expressions given in Table 5.4. It is necessary to multiply by the Avogadro number to convert the units to the specified by COMSOL.

- Vibrational energy transfer reactions

  They are included as reactions with the kinetic expressions given in Table 5.6. It is necessary to multiply by the Avogadro number to convert the units to the specified by COMSOL. The stoichiometric coefficient must be specified according the Tables 5.8 and 5.9 at the mean temperature of the discharge.

- Surface reactions

  They are included for the defined walls and are specified by sticking coefficients, according to Table 5.10. The Motz-Wise correction is included and secondary emission is neglected.

- Species

  The species are automatically included by COMSOL. The electrons density and the mean electron energy must be specified with the variables defined before. CO_2 is computed from the mass balance constraint and CO_2^+ initial value is computed from the electroneutrality constraint. The initial condition for each of the neutrals is set to a mole fraction of 1×10^{-16}, whereas for each of the ions a number density of 100 is specified.

- Process conditions

  The temperature is specified with the variable defined before. Considering the low pressure the ideal gas equation of state is chosen. The pressure must be specified as well.

- Mesh

  Since no large gradients are present it is possible to build a simple mesh. A mapped mesh for general physics with an extremely fine predefined size is chosen. Although a coarser mesh could be used, it is desired to evaluate the computational time of a finer mesh. In the future, extremely fine meshes could be required to solve the electron dynamics, whose gradients are known to be extremely large. Boundary layers with default parameters are also included for the walls,

- Method of solution

  The simulations are divided in two phase and both make use of the time dependent solver.

  The first phase of the simulations (plasma zone) is performed between 1×10^{-8} and 1.4×10^{-5} seconds, with 50 points of data equally distributed. Before running the simulations the following must be done

  - The ϕ scaling factor and stoichiometric coefficients are updated according to the mean temperature of the discharge
  - The functions of the mean electron energy and the bulk gas temperatures are specified for the first phase
  - Electron impact reactions are enabled
  - The reaction rate constants are updated if needed
  - The simulation time is specified for the first phase

  - The initial values of the variables solved for are set to the mole fractions and number densities specified for the species

  The second phase of the simulations (afterglow) is preformed between 1.4×10^{-5} and 0.1 seconds, with approximately 200 points of data. Before running the simulations the following must be done

  - The ϕ scaling factor and stoichiometric coefficients are updated according to the mean temperature of the discharge
  - The functions of the mean electron energy and the bulk gas temperatures are specified for the second phase
  - Electron impact reactions are disabled
  - The simulation time is specified for the second phase
  - The initial values of the variables solved for are set to the solution of the first phase.

  The results must be obtain after each simulation if only one solution data set is included, otherwise they will be overwritten in the following simulation.

- Solver configuration

  For the time dependent solver the default Backwards Differentiation Function is used with a maximum order of 2. The initial step is set to 1×10^{-17} and the maximum step to 0.001.

  The fully coupled PARDISO linear solver is used with the default relative tolerance of 0.01 and an absolute tolerance of 0.001.

- Results

  The number densities of the species are obtained as surface average values of the domain. Excited states are included for the calculation of the CO_2 number density. The electron and bulk gas temperatures are also obtained for their validation.

BIBLIOGRAPHY

[1] J. Amouroux and P. Siffert, *CO2: a future chemical fuel: key questions about this project,* in *SPIE Eco-Photonics 2011: Sustainable Design, Manufacturing, and Engineering Workforce Education for a Green Future*, Vol. 8065, edited by P. Ambs, D. Curticapean, C. Emmelmann, W. Knapp, Z. T. Kuznicki, and P. P. Meyrueis (2011) pp. 80650E–80650E–7.

[2] R. Engeln, S. Welzel, F. Brehmer, S. Ponduri, M. Creatore, and M. C. M. V. D. Sanden, *Plasma-assisted CO 2 processing for energy storage,* in *XXI Europhysics Conference on the Atomic and Molecular Physics of Ionized Gases* (2012).

[3] A. Fridman, *Plasma chemistry* (Cambridge University Press, 2008).

[4] J. Amouroux and P. Siffert, *Carbon dioxide: a raw material and a future chemical fuel for a sustainable energy industry,* IOP Conference Series: Materials Science and Engineering **19**, 012001 (2011).

[5] C.-j. Liu, G.-h. Xu, and T. Wang, *Non-thermal plasma approaches in CO2 utilization,* Fuel Processing Technology **58**, 119 (1999).

[6] A. Fridman and L. A. Kennedy, *Plasma Physics and Engineering* (CRC Press, 2011).

[7] T. Van Gerven and A. Stankiewicz, *Structure, Energy, Synergy, Timeî—¸The Fundamentals of Process Intensification,* Industrial & Engineering Chemistry Research **48**, 2465 (2009).

[8] T. Kozák and A. Bogaerts, *Evaluation of the energy efficiency of CO 2 conversion in microwave discharges using a reaction kinetics model,* Plasma Sources Science and Technology **24**, 015024 (2015).

[9] T. Kozák and A. Bogaerts, *Splitting of CO 2 by vibrational excitation in non-equilibrium plasmas: a reaction kinetics model,* Plasma Sources Science and Technology **23**, 045004 (2014).

[10] M. A. Lieberman and A. J. Lichtenberg, *Principles of Plasma Discharges and Materials Processing* (John Wiley & Sons, Inc., Hoboken, NJ, USA, 2005).

[11] M. Capitelli, C. M. Ferreira, B. F. Gordiets, and A. I. Osipov, *Plasma Kinetics in Atmospheric Gases*, Springer Series on Atomic, Optical, and Plasma Physics, Vol. 31 (Springer Berlin Heidelberg, Berlin, Heidelberg, 2000).

[12] Y. Itikawa, *Molecular Processes in Plasmas*, edited by Y. Itikawa, Springer Series on atomic, optical, and plasma physics, Vol. 43 (Springer Berlin Heidelberg, Berlin, Heidelberg, 2007).

[13] G.-b. Zhao, X. Hu, M.-c. Yeung, O. a. Plumb, and M. Radosz, *Nonthermal Plasma Reactions of Dilute Nitrogen Oxide Mixtures: NO x in Nitrogen,* Industrial & Engineering Chemistry Research **43**, 2315 (2004).

[14] T. Silva, N. Britun, T. Godfroid, and R. Snyders, *Optical characterization of a microwave pulsed discharge used for dissociation of CO 2,* Plasma Sources Science and Technology **23**, 025009 (2014).

[15] G. J. M. Hagelaar and L. C. Pitchford, *Solving the Boltzmann equation to obtain electron transport coefficients and rate coefficients for fluid models,* Plasma Sources Science and Technology **14**, 722 (2005).

[16] COMSOL, *Plasma Module User's Guide* (COMSOL 4.4, 2013).

[17] K. Anzai, H. Kato, M. Hoshino, H. Tanaka, Y. Itikawa, L. Campbell, M. J. Brunger, S. J. Buckman, H. Cho, F. Blanco, G. Garcia, P. Limão-Vieira, and O. Ingólfsson, *Cross section data sets for electron collisions with H2, O2, CO, CO2, N2O and H2O,* The European Physical Journal D **66**, 36 (2012).

[18] C. E. Treanor, *Vibrational Relaxation of Anharmonic Oscillators with Exchange-Dominated Collisions,* The Journal of Chemical Physics **48**, 1798 (1968).

[19] V. Rusanov, A. Fridman, and G. Sholin, *The physics of a chemically active plasma with nonequilibrium vibrational excitation of molecules,* Uspekhi Fizicheskih Nauk **134**, 185 (1981).

[20] L. F. Spencer and a. D. Gallimore, *CO 2 dissociation in an atmospheric pressure plasma/catalyst system: a study of efficiency,* Plasma Sources Science and Technology **22**, 015019 (2013).

[21] M. Tsuji, T. Tanoue, K. Nakano, and Y. Nishimura, *Decomposition of CO2 into CO and O in a Microwave-Excited Discharge Flow of CO2/He or CO2/Ar Mixtures,* Chemistry Letters **1**, 22 (2001).

[22] S. Dobrea, I. Mihaila, V. Tiron, and G. Popa, *Optical and mass spectrometry diagnosis of a CO2 microwave plasma discharge *,* Romanian Reports in Physics **66**, 1147 (2014).

[23] A. Vesel, M. Mozetic, A. Drenik, and M. Balat-Pichelin, *Dissociation of CO2 molecules in microwave plasma,* Chemical Physics **382**, 127 (2011).

[24] T. Oberreuther, C. Wolff, and A. Behr, *Volumetric plasma chemistry with carbon dioxide in an atmospheric pressure plasma using a technical scale reactor,* IEEE Transactions on Plasma Science **31**, 74 (2003).

[25] W. a. Bongers, S. Welzel, D. C. M. V. D. Bekerom, G. Frissen, G. J. V. Rooij, a. P. H. Goede, and M. F. Graswinckel, *Developments in CO 2 dissociation using non-equilibrium microwave plasma activation for solar fuels,* in *ISPC 22* (2015).

[26] A. Lebouvier, S. a. Iwarere, P. D'Argenlieu, D. Ramjugernath, and L. Fulcheri, *Assessment of Carbon Dioxide Dissociation as a New Route for Syngas Production: A Comparative Review and Potential of Plasma-Based Technologies,* Energy & Fuels **27**, 2712 (2013).

[27] I. Suzuki, *General anharmonic force constants of carbon dioxide,* Journal of Molecular Spectroscopy **25**, 479 (1968).

[28] R. Aerts, T. Martens, and A. Bogaerts, *Influence of Vibrational States on CO 2 Splitting by Dielectric Barrier Discharges,* The Journal of Physical Chemistry C **116**, 23257 (2012).

[29] K. Peerenboom, A. Parente, T. Kozák, A. Bogaerts, and G. Degrez, *Dimension reduction of non-equilibrium plasma kinetic models using principal component analysis,* Plasma Sources Science and Technology **24**, 025004 (2015).

[30] K. Hassouni, A. Gicquel, M. Capitelli, and J. Loureiro, *Chemical kinetics and energy transfer in moderate pressure H 2 plasmas used in diamond MPACVD processes,* Plasma Sources Science and Technology **8**, 494 (1999).

[31] T. E. Magin, M. Panesi, A. Bourdon, R. L. Jaffe, and D. W. Schwenke, *Coarse-grain model for internal energy excitation and dissociation of molecular nitrogen,* Chemical Physics **398**, 90 (2012).

[32] A. Indarto, N. Coowanitwong, J.-W. Choi, H. Lee, and H. K. Song, *Kinetic modeling of plasma methane conversion in a dielectric barrier discharge,* Fuel Processing Technology **89**, 214 (2008).

[33] H. Zheng and Q. Liu, *Kinetic Study of Nonequilibrium Plasma-Assisted Methane Steam Reforming,* Mathematical Problems in Engineering **2014**, 1 (2014).

[34] A. Rutscher and H. E. Wagner, *The Model of Macroscopic Kinetics in Non-Equilibrium Plasma Chemical Reactions I. General Considerations and Basic Relations,* Beiträge aus der Plasmaphysik **25**, 337 (1985).

[35] A. H. Markosyan, A. Luque, F. J. Gordillo-Vázquez, and U. Ebert, *PumpKin: A tool to find principal pathways in plasma chemical models,* Computer Physics Communications **185**, 2697 (2014).

[36] R. Lehmann, *An Algorithm for the Determination of All Significant Pathways in Chemical Reaction Systems,* Journal of Atmospheric Chemistry **47**, 45 (2004).

[37] G. Colonna, I. Armenise, D. Bruno, and M. Capitelli, *Reduction of State-to-State Kinetics to Macroscopic Models in Hypersonic Flows,* Journal of Thermophysics and Heat Transfer **20**, 477 (2006).

[38] G. Colonna, L. D. Pietanza, and M. Capitelli, *Recombination-Assisted Nitrogen Dissociation Rates Under Nonequilibrium Conditions,* Journal of Thermophysics and Heat Transfer **22**, 399 (2008).

[39] A. Guy, A. Bourdon, and M.-Y. Perrin, *Consistent multi-internal-temperatures models for nonequilibrium nozzle flows,* Chemical Physics **420**, 15 (2013).

[40] H. P. Le, A. R. Karagozian, and J.-L. Cambier, *Complexity reduction of collisional-radiative kinetics for atomic plasma,* Physics of Plasmas **20**, 123304 (2013).

[41] Y. Itikawa, *Cross Sections for Electron Collisions With Carbon Dioxide,* Journal of Physical and Chemical Reference Data **31**, 749 (2002).

[42] K. Kameta, N. Kouchi, and Y. Hatano, *4 Cross sections for photoabsorption, photoionization, neutral dissociation of molecules,* in *Interactions of Photons and Electrons with Molecules*, Vol. 17C (Springer-Verlag, Berlin/Heidelberg, 2003) pp. 4001–4061.

[43] A. Zecca, G. P. Karwasz, and R. S. Brusa, *One century of experiments on electron-atom and molecule scattering: A critical review of integral cross-sections,* La Rivista del Nuovo Cimento **19**, 1 (1996).

[44] R. R. Laher and F. R. Gilmore, *Updated Excitation and Ionization Cross Sections for Electron Impact on Atomic Oxygen,* Journal of Physical and Chemical Reference Data **19**, 277 (1990).

[45] Y. Itikawa, *Cross Sections for Electron Collisions with Oxygen Molecules,* Journal of Physical and Chemical Reference Data **38**, 1 (2009).

[46] S. J. Buckman, J. W. Cooper, M. T. Elford, M. Inokuti, Y. Itikawa, and H. Tawara, *Interactions of Photons and Electrons with Atoms*, edited by Y. Itikawa, Landolt-Börnstein - Group I Elementary Particles, Nuclei and Atoms, Vol. 17A (Springer-Verlag, Berlin/Heidelberg, 2000).

[47] R. D. Levine and R. B. Bernstein, *Thermodynamic Approach to Collision Processes,* in *Dynamics of Molecular Collisions* (Springer US, Boston, MA, 1976) pp. 323–364.

[48] T. Kozák, *Private communication,* (2015).

[49] R. N. Schwartz, Z. I. Slawsky, and K. F. Herzfeld, *Calculation of Vibrational Relaxation Times in Gases,* The Journal of Chemical Physics **20**, 1591 (1952).

[50] R. N. Schwartz and K. F. Herzfeld, *Vibrational Relaxation Times in Gases (Three-Dimensional Treatment),* The Journal of Chemical Physics **22**, 767 (1954).

[51] J. Keck and G. Carrier, *Diffusion Theory of Nonequilibrium Dissociation and Recombination,* The Journal of Chemical Physics **43**, 2284 (1965).

[52] R. J. Kee, M. E. Coltrin, and P. Glarborg, *Chemically Reacting Flow* (John Wiley & Sons, Inc., Hoboken, NJ, USA, 2003).

[53] A. Vesel, R. Zaplotnik, J. Iacono, M. Balat-Pichelin, and M. Mozetic, *A Catalytic Sensor for Measurement of Radical Density in CO2 Plasmas,* Sensors **12**, 16168 (2012).